RECONSTRUCTING THE COMPLEX HISTORY OF A SMALL-VOLUME BASALTIC VOLCANO (NGATUTURA VOLCANIC FIELD, NEW ZEALAND): THE ROLE OF SUBSURFACE PROCESSES AND IMPLICATIONS FOR DIATREME FORMATION.

A thesis presented in partial fulfilment of the requirements for the degree of

Master of Science

in

Earth Science

at Massey University, Palmerston North, New Zealand.

Rickus van Niekerk

2016

ABSTRACT

Monogenetic volcanism is very common on continents and often occur very close to civilisation. Limiting the ability of volcanologists to predict the location and extent of future eruptions at monogenetic volcanic fields is the lack of knowledge about subsurface processes at small basaltic volcanoes. This research aims to utilize exceptional exposures of subsurface volcanic structures at a coastal section in the upper North Island of New Zealand to investigate the role of subsurface processes in the development of a small basaltic volcano. Exposures include dykes, lava flows, peperite and hyaloclastite deposits, a lava pond, and diatreme. Along with detailed mapping, K-Ar age dates reveal the complex history of the Ngatutura Bay Volcanics as syn-sedimentary volcanism in a shallow marine environment. Volcanism at Ngatutura Bay is shown to have occurred in two phases, the first around 3.34-3.22 Ma, and the second at c. 1.81-1.72 Ma. Subsurface processes documented include magma-country rock interactions, the role of groundwater, magma ascent, and thermal alteration of country rock. The importance of tectonics and rock structure at small basaltic centres is also demonstrated. Moreover, deposits of the diatreme were analysed for grain size and lithic componentry. The local stratigraphy is composed of well-defined lithologies, each with unique textural and visual properties, enabling the identification of lithics in the diatreme. The diatreme deposits are described as five distinct lithofacies, and together with grain size and componentry data, the series of events by which the diatreme formed is constrained. A conceptual model is drawn for the formation of the diatreme, which is compared to current models and theories.

ACKNOWLEDGEMENTS

I would like to thank the following people for their prodigious efforts in assisting with my research. Without this team I simply would not have been able to produce even part of a thesis. A heartfelt thanks to each of you.

Gert Lube, Karoly Németh – As my supervisors you have guided me through each step of the way. Your wisdom and knowledge have helped to vastly improve all of my ideas. Thank you for your enthusiasm and patience.

Bob Stewart, Clel Wallace – As veteran researchers you have tirelessly shared with me your vast reservoir of knowledge. Thank you for all the inspiring and insightful conversations and help along the way. Bob, thank you also for accompanying me in the field and for your assistance in the XRD lab.

Anja Moebis – I have thoroughly enjoyed all the hours I spent in your lab. You have taught me so much. Thank you for your hard work maintaining and setting up equipment, particularly the microprobe, which took up hours of your time for many days.

Peter Lewis – Thank you for keeping and maintaining the microprobe. I have been told that you are a miracle worker.

Eric Breard – I don't have the words to thank you for your efforts in the field. You have climbed to heights that no-one thought possible, and retrieved samples from places where no human has ever been. You should be very proud of what you have done, although I'd strongly advise not to do it again!

Goldie Walker – You deserve the title of field technician. Abseiling from a fence post was terrifying, but you managed to keep me safe. Thank you for your hard work in doing so.

Szabolcs Kósik, Gabor Kereszturi – Thank you both for accompanying me in the field. You have worked unremittingly to gather samples and take thousands of very valuable photographs.

TABLE OF CONTENTS

LIST OF FIGURES

LIST OF TABLES

CHAPTER 1 – INTRODUCING THE RESEARCH

1.1 INTRODUCTION

Monogenetic basaltic volcanoes are the most abundant volcano types on continents (Valentine & Gregg, 2008). They are commonly a feature of volcanic fields where tens to thousands of small volcanoes have developed in close proximity (Németh, 2010). Monogenetic volcanic fields can grow to extend over enormous areas (thousands of km^2, table 1) and are often heavily populated areas, for example Auckland City (Cassidy & Locke, 2004). While hazards associated with this type of volcanism have received lots of attention over the past decade (Murcia et al., 2015; Lorenz, 2007, Németh et al., 2012, Lindsay & Leonard, 2007, etc.), much remains to be learned about the way in which these volcanoes develop.

Attention has been drawn to the influence of subsurface processes on the emplacement and eruption of small basaltic volcanoes, and the fact that relatively little is known about these processes (e.g. Németh, 2010, Valentine, 2012; Németh et al., 2012; Kereszturi & Németh, 2012). Processes such as magma ascent, degassing and fragmentation take place almost exclusively in the subsurface, as does the interaction between magma and country rock/groundwater, none of which can ever be observed in nature. Explosions and effusion of magma that occur in the subsurface have similarly obscure dynamics.

Good exposures of subsurface structures at these volcanoes are rare, and often very poorly preserved. The research presented in this thesis is structured around a remarkable outcrop of a small basaltic volcanic centre in a cliff face on the Waikato Coast, New Zealand. The outcrop is located at Ngatutura Bay (figure 1.1) and includes extraordinarily detailed three-dimensional exposures of a diatreme, subaqueous lava flows, hyaloclastites and fault-bounded dykes.

These features are described in detail from field observations and process-form relationships are investigated, pertaining to the formation of a diatreme in particular.

While maar-diatreme volcanoes are the second most common type of volcano (White & Ross, 2011), no consensus has been reached about their formation mechanisms. The research presented here explores the similarities and differences between the Ngatutura Diatreme and current models or theories of diatreme formation. The outcrop at Ngatutura Bay offers the opportunity to study nearly complete vertical transects of a diatreme. Much of the exposure is inaccessible and samples were obtained by way of photography and the secondment of a fearless Frenchman (Eric Breard, see acknowledgements).

This research also explores magma-country rock interactions in a number of settings, as well as the development (and longevity) of the volcanic centre at Ngatutura Bay. Through detailed mapping of the outcrop a paleoenvironmental history is interpreted. Implications of these findings are discussed in the context of global research.

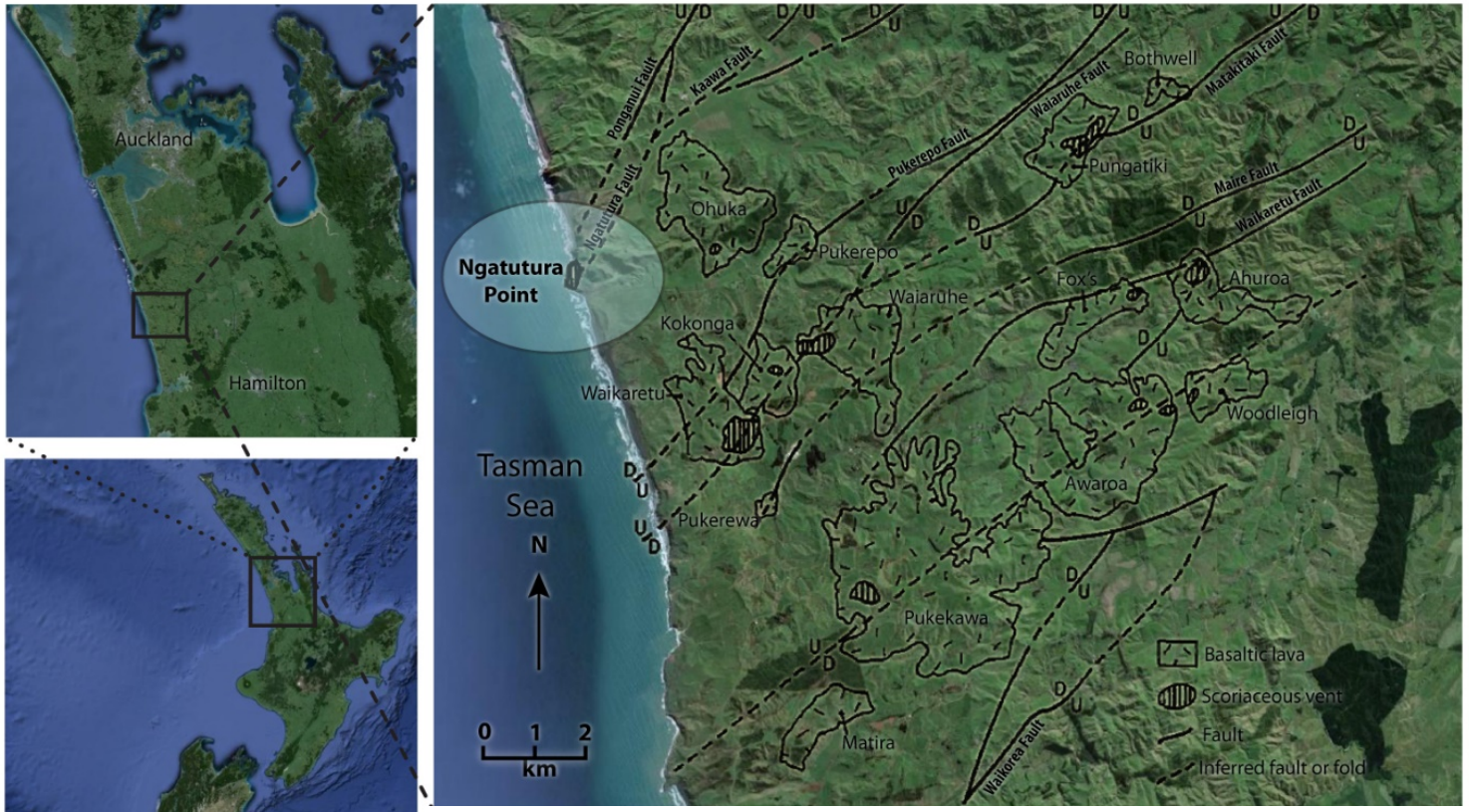

Figure 1.1 – The study site is located at Ngatutura Point, one of at least 16 volcanic centres within the Ngatutura Volcanic Field (NVF). Ages of the various centres vary from 1.54 to 1.83 Ma (Briggs et al., 1989). The NFV belongs to a series of alkali-basalt volcanic fields including the Northland, Auckland, South Auckland, and Alexandra Volcanic Fields (Table 1; Briggs et al., 1989).

Geographical and structural data of the Ngatutura Volcanic Field have been obtained from Briggs et al. (1990; references therein). Satellite imagery sourced from Google Earth.

1.2 OBJECTIVE AND STRUCTURE

The first objective of this research is to illustrate the influence of subsurface processes on volcano development, in light of a paleoenvironmental reconstruction. This part of the research draws on the physical volcanology of various subsurface features, alongside geochemical, thermal and mineralogical data and radiometric age constraints.

The second research objective is to characterise a well-exposed diatreme in terms of geomorphic and sedimentary features in order to relate its formation to current theories, models and experiments.

Therefore, three research questions are posed:

1. How did the subsurface influence the development of the volcanic features at Ngatutura Bay?

2. What was the paleoenvironment at the time the eruption took place?

3. Are the processes interpreted for the evolution of the diatreme consistent with current theories and models?

In the remainder of Chapter 1 an introduction to the study area outlines the geologic setting and includes descriptions of the various volcanic features that are investigated in this research.

Chapter 2 provides literature reviews, which discuss the *status quo* of current research on monogenetic volcanism and the formation of diatremes respectively. The significance of subsurface processes is highlighted and current theories, models and results from scaled experiments on the formation of diatremes are discussed in detail.

Chapter 4 introduces the research that explores the role of subsurface processes at the Ngatutura Volcanic Centre – a typical monogenetic volcano

consisting of lava flows and hyaloclastite piles, a diatreme, and associated dykes. These features are deeply incised but preserved in an extraordinarily detailed exposure in a cliff face at the coast. Data are presented from various lines of investigation, which aim to address the research questions outlined above. Methods are described in chapter 3 and include detailed field observations, radiometric dating, componentry and grain size analyses, scanning electron microscopy and microprobe analysis.

Results are discussed in chapter 5. The discussion consists of a critical evaluation of the data, as well as links to the literature. The aim of this chapter is to address the research questions by testing results against established theories and other real world examples in the literature.

Table 1.1 – Selected examples of continental volcanic fields

Volcanic Field	Location	Age (Ma)	Area (km^2)	Number of Centres	Composition of Basalt	References
Kaikohe-Bay of Islands	New Zealand	9-0.04	2,500	>20	Hawaiite, Alkali Basalt, Olivine Tholeiite	Smith et al. (1993), Shane (2012)
Auckland	New Zealand	0.25-200yr	360	49	Alkali Basalt, Basanite	Cassidy & Locke (2010), Shane & Sandiford (2003)
South Auckland	New Zealand	1.56-0.51	190	>70	Basanite, Alkali Basalt, Tholeiite	Rafferty & Heming (1979)
Ngatutura	New Zealand	1.83-1.54	170	16	Hawaiite	Briggs et al. (1989, 1990)
Alexandra	New Zealand	2.74-1.6	450	>40	Hawaiite, Alkali Basalt, Basanite	Briggs (1983) Briggs et al. (1989, 1990)
West Eifel	Germany	0.7-0.011	600	240	Basanite, Nephelinite	Schminke (2007), Mertes & Schminke (1983)
Michoacán-Guanajuato	Mexico	2.78-recent	34,500	1894	Alkali Olivine-Basalt, Basanite, Basaltic-andesite	Connor (1987) Hasenaka & Carmichael (1985)
Lunar Crater	Nevada, USA	~5-0.04	1,600	>100	Alkali Basalt, Hawaiite	Valentine & Cortés (2013), Cortés et al. (2015)
Calatrava	Spain	3.7-0.7	5,500	>200	Alkali Basalt, Basanite, Olivine Nephelinite	Gonzalez-Jimenez et al. (2014)
La Garrotxa	Spain	0.1-0.01	600	>50	Alkali Basalt, Basanite	Araña et al. (1983) Marti et al. (1992)
Lake Natron-Engaruka	Tanzania	~0.13-recent	2500	~200	Olivine-melilite, Nephelinite, Basanite	Mattsson & Tripoli (2011) Hillaire-Marcel et al. (1986)
Sierra Chichinautzin	Mexico	0.04-recent	2400	>220	Basalt, Basaltic trachy-andesite	Márquez et al. (1999) Marquez & De Ignacio (2002)
Harrat Rahat	Saudi Arabia	10-recent	20,000	>950	Alkali-basalt	Murcia et al. (2015) Runge et al. (2014)

1.3 THE STUDY AREA: NGATUTURA POINT

1.3.1 GEOLOGIC SETTING

The Ngatutura Volcanic Field (NVF) is one of several Pliocene-Quaternary basalt fields of the upper North Island, including the Alexandra, South Auckland, Auckland, and Northland Volcanic Fields (Briggs et al., 1989; Rafferty & Heming, 1979). The NVF is located in a back-arc continental intraplate setting and Briggs et al. (1989) describe these volcanoes as being dominantly alkalic in composition. The NVF consists of scoria cones, lava flows, dykes and volcanic breccias forming at least 16 small monogenetic volcanic centres (Utting, 1986).

Regional faults typically strike in a north-easterly direction (Utting, 1989; Briggs et al., 1990). These faults were mostly active during the Kaikoura Orogeny in the late Miocene (Kear, 1959), while some faulting continued into the Pliocene up to, and during, the deposition of the Kaawa Formation (Spratt, 1971). A striking feature of the NVF is the alignment of volcanic centres with these regional faults. Most volcanoes in the field are centred directly over a fault (figure 1), implying that the fault plane formed conduits favourable for magma ascent. The tectonic influence on the Ngatutura Volcanic Field is also evident on a smaller scale at Ngatutura Bay where two dykes have intruded into the planes of extensional faults on either side of a diatreme structure.

Briggs et al. (1989) reports K-Ar ages of 1.83-1.54 Ma for the NVF, placing the volcanism at the Pliocene-Pleistocene boundary. The volcanic eruptive features are emplaced upon a thick sequence of Miocene-Oligocene marine strata (figure 1.2) which overlies the Mesozoic Basement.

The local Mesozoic basement comprises Late Jurassic marine strata of the Murihiku Supergroup (Edbrooke, 2005; Mortimer et al., 2014), which extend from near Port Waikato ~140km southward to the Awakino area (Challinor, 2001). The lowermost unit to outcrop in the area is the Puti Siltstone (Fleming & Kear, 1960), consisting of two members: Upper and Lower Puti Siltstone,

comprising fine-grained, thin sandstone beds, and dominant siltstone and mudstone of up to ~800m in total (Challinor, 2001). The c. 45-75m Ruakiwi Sandstone intermittently divides the two Members (Fleming & Kear, 1960; cf. Waiharakeke Conglomerate: Waterhouse, 1978). Thin and deformed tuff beds are found throughout (Challinor, 2001; Edbrooke, 2005), as well as abundant belemnites and other marine fossils in places (Kear, 1966; Challinor, 2001). The Puti Siltstone unit is generally blue-grey in colour, non-calcareous, fossiliferous and closely jointed, displaying spheroidal fractures (Kear, 1987; Edbrooke, 2005). The weakly bedded siltstone also contains concretions in places (Edbrooke, 2005).

Overlying the Puti Siltstone is the Coleman Conglomerate, belonging to the Late Tithonian substage of the Latest Jurassic (Challinor, 2001). The Coleman Conglomerate is distinguished by sandstones, siltstones and conglomerates up to 220m thick (Challinor, 2001) with the conglomerate containing volcanic and calcareous tuff pebbles, as well as greywacke pebbles (Kear, 1987). Marine fossils, i.e. *Buchia plicata* & *Belemnopsis aucklandica* are common but small (Kear, 1987).

The Waikorea Siltstone overlies the Coleman Conglomerate. It consists of blue-grey siltstone, very similar to the Puti Siltstone, as well as some grey silt- and sandstone, and hard carbonaceous sandstone (rare) in upper parts (Challinor, 2001; Kear, 1987). Rare plant material is also present in some strata (Kear, 1987). The Waikorea Siltstone is up to 600m thick in the south but decreases to ~250m in the north (Kear, 1987; Challinor, 2001). The Waikorea Siltstone also displays close jointing with spheroidal fracturing (Kear, 1987).

The thicknesses of Mesozoic basement rocks are highly variable in the area due to their location on a major fold belt which includes the Kawhia Regional Syncline (Edbrooke, 2005).

The Waikato Coal Measures (Hutton, 1871; Kear & Schofield, 1959), while extensively present in up to 200m thick accumulations in the region, are largely absent from western areas, particularly west of the Waipa Fault (Tripathi et al., 2008) and is inferred to also be absent from the study location at Ngatutura Bay.

Overlying the Mesozoic basement at the Ngatutura Volcanic Field is the Waka Supergroup, consisting of marine strata of the Taranaki Basin (Mortimer et al., 2014; Kamp et al., 2014). The basal constituent of the Waka Supergroup is the Elgood Limestone of the Glen Massey Formation (part of Te Kuiti Group; Kear & Schofield, 1959), which has an average thickness of 6-10 m (Nalin et al., 2008; Kear & Schofield, 1959, 1978). It is present as lenses which formed in low-lying topography during a marine transgression (Nalin et al., 2008; Hood et al., 2005).

The Elgood Limestone is rich in calcium carbonate containing 85-95 wt% in much of the unit, however some interflag-beds have a calcium carbonate content as low as 36 wt% (Kamp et al., 2008). Tripathi et al. (2008) describe its main lithofacies as "medium to coarse biocalcarenite" while Kear & Schofield (1959) note the presence of up to three constituents, including a glauconitic shelly sandstone at the base, a flaggy limestone which is very glauconitic at its top, and a shelly greensand which grades into the additional two members of Glen Massey Formation: Dunphail Siltstone Member and Ahirau Sandstone Member (Kear & Schofield, 1959, 1978; White & Waterhouse, 1993).

The Dunphail Siltstone was found to be largely absent from western areas near the coast (Kear & Schofield, 1959) and is likely to be absent from the study location at Ngatutura Bay. It is a calcareous siltstone, sandy in places, with a blue grey colour and massive to coarsely bedded structure (Kear & Schofield, 1959; Kear, 1987). The Dunphail Siltstone is up to 15 m thick at its type location (Kear & Schofield, 1959).

The Ahirau Sandstone Member, formerly Glen Massey Sandstone (cf. White & Waterhouse, 1993; Kear & Schofield, 1959), is a calcareous, silty sandstone with a thickness of 15-35m (Kear, 1987). The sandstone is blue-grey to yellow in colour, massive to weakly bedded, and contains silt lenses in places (Kear & Schofield, 1959; Kear, 1966).

The Te Kuiti Group is continued by the Aotea Formation (Kear, 1966), represented locally by the Waimai Limestone Member (Kear, 1966). The limestone is described by Kear (1966, 1987) as flaggy, glauconitic, sandy, and up to 15 m thick.

The Carter Siltstone (Te Akatea Formation) uncomformably overlies the Waimai Limestone. The Carter Siltstone, (formerly the Te Akatea Siltstone of Kear & Schofield, 1959), is a highly calcareous, sandy siltstone with a thickness of 60-100m (Kear, 1987; White & Waterhouse, 1993). The sandy siltstone is light grey to white in colour and massive to weakly bedded. The lithology is uniform throughout, apart from some sandstone beds at the top in some places and a hard, very calcareous siltstone at the base where the Raglan Limestone Member is absent (White & Waterhouse, 1993).

The Papakura Limestone was first described by Hochstetter (1864) and later included in the Waitemata Series (Balance, 1976). Hayward & Brook (1984) identified three distinguishable Members of the Papakura Limestone: The Motuketekete Member in the north, the Te Akau Member in the south, and the Purser Member in central parts, with its type section at Ngatutura Bay. The Purser Member is here referred to, after its parent lithology, as the Papakura Limestone. At Ngatutura Bay the limestone is up to 4m thick and comprises zones of variable cementation (Balance & Nelson, 1969) with well-cemented beds containing up to 75% calcium carbonate, while poorly cemented beds contain about 40% calcium carbonate.

The Waikawau Sandstone was first mapped by Henderson & Grange (1926) and is described by Kear (1961) as a grey calcareous sandstone of Otaian age. At Ngatutura Bay the Waikawau Sandstone comprises alternating, decimetre-thick beds of clay/siltstones and sandstones of blueish-green (Henderson & Grange, 1926) colour with some calcareous bands and coarse greensand in places. The section at Ngatutura Bay is c. 15 m thick. In thin section the Waikawau Sandstone is much coarser grained than the Ahirau Sandstone and is composed of detrital quartz and minor feldspar, glauconite and mica in a silty matrix.

The Kaawa Formation is the youngest sequence implicated in the formation of the diatreme, and is also the stratigraphic location of other volcanic features such as a lava pond. It is composed of a basal shell bed and a soft sandstone 15 - 20 m thick at its type locality at Kaawa Beach, adjacent to Ngatutura Bay. The basal shell bed is blue-grey in colour and the overlying pumiceous sandstone has a prominent yellow-grey colour. The sandstone is silty and friable, and weakly bedded to massive. The Kaawa Formation is described in detail by Henderson & Grange (1926) and Kear & Schofield (1978).

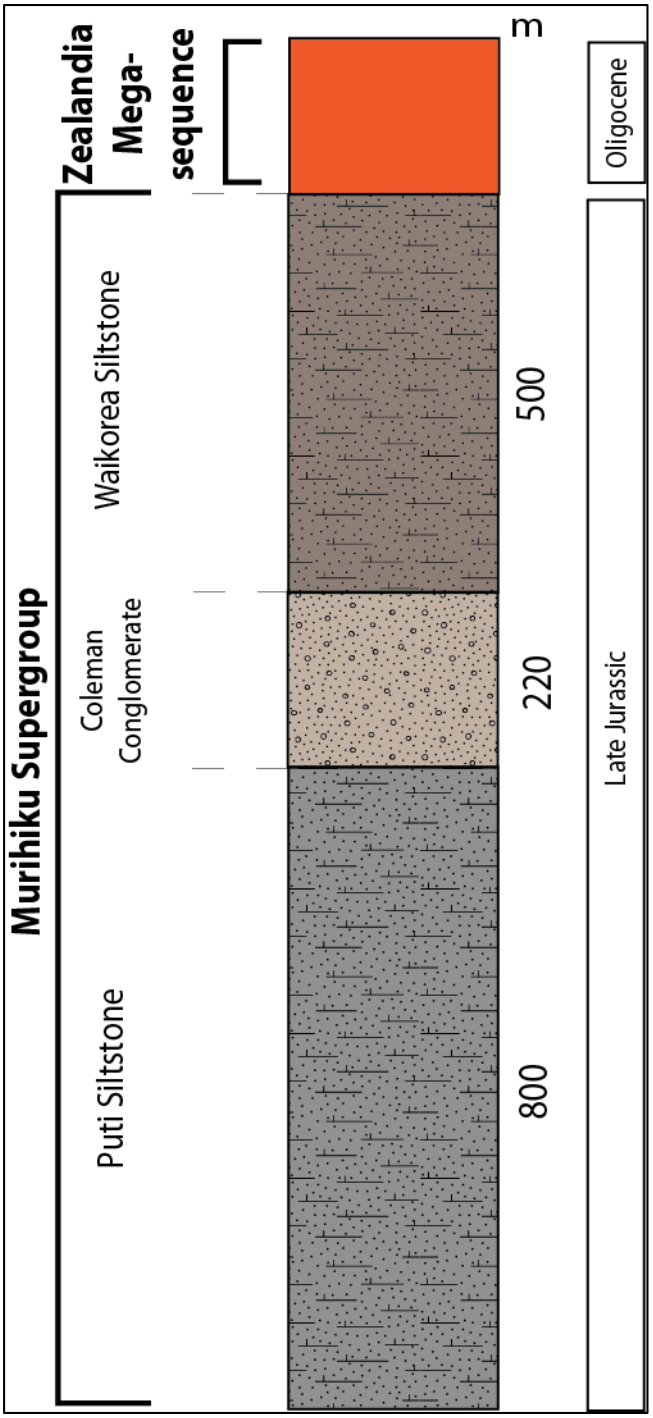

Figure 1.2 – The lithostratigraphy at Ngatutura Bay. Thicknesses measured in outcrop are shown in bold. The thicknesses of subsurface units have been obtained from literature (*see main text for references*). The presence of lower units is inferred from regional stratigraphic exposures, and assumed due to their presence in diatreme-matrix as accidental lithics in the Ngatutura Diatreme.

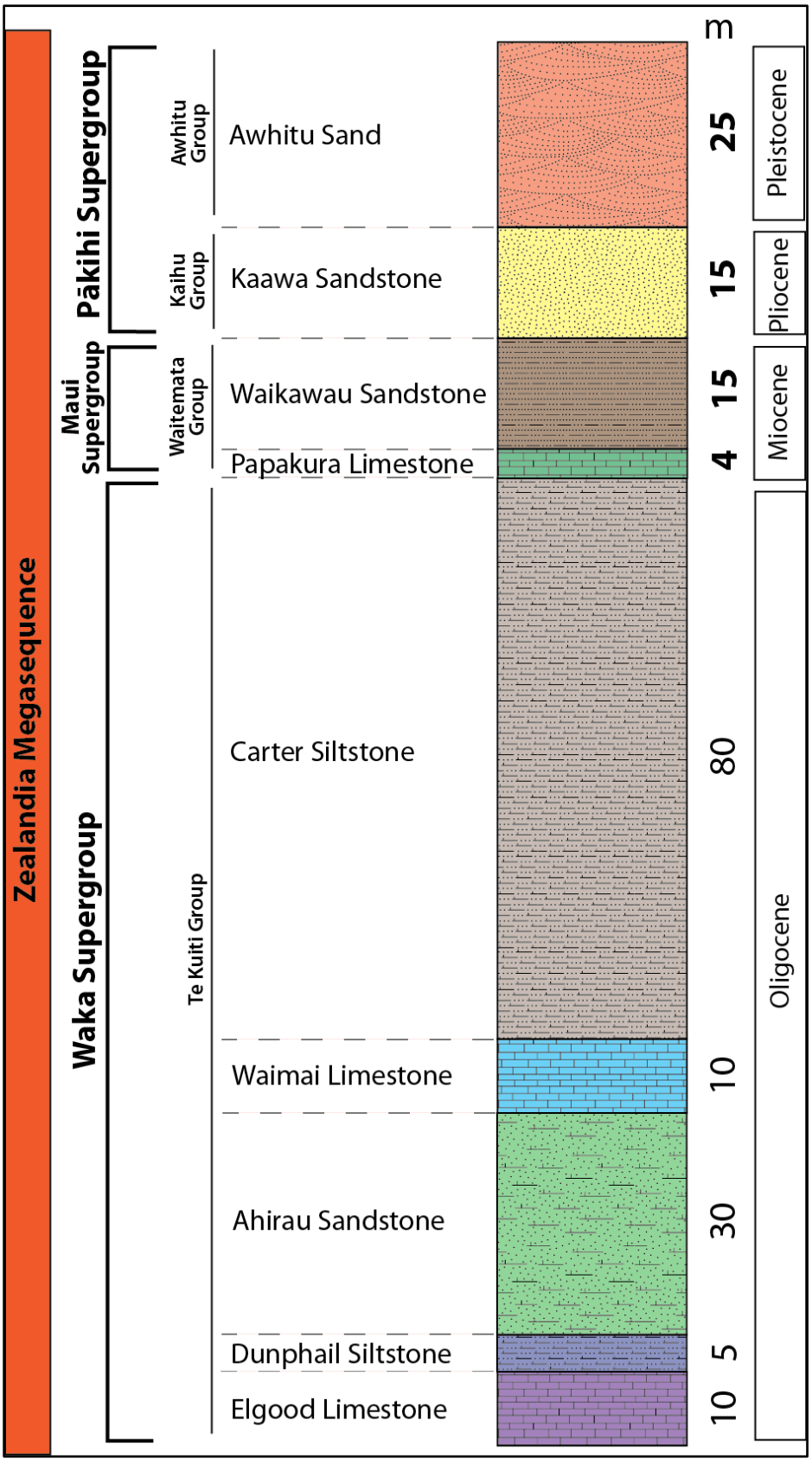

Figure 1.2 continued.

1.3.2 NGATUTURA BAY VOLCANICS AT A GLANCE

Ngatutura Point lavas

The Ngatutura Point lava flows comprise a steep vertical exposure, which is continued in Shag Rock, a small island immediately adjacent to the main exposure (figure 1.3). The basal parts of the flows are exposed at beach level and comprise a pillow lava facies up to c. 8-10 m in height. Pillows are 30-50 cm in diameter. The pillows have an irregular contact to the overlying colonnade-jointed flows (cf. Long & Wood, 1986; Forbes et al., 2014) of c. 4 - 6 m thickness at the Shag Rock exposure. At the main exposure the basal pillows are overlain by entablature-jointed flows which comprise a large portion of the exposure. This portion of the exposure displays complex cooling patterns with hackly fractures throughout and irregular contacts to the surrounding colonnades and pillows, as well as rosette-shaped columnar jointing.

Figure 1.3 – Ngatutura Point lava flows. Field of view: 50 m.

Dykes & sills

Two major dykes have been described by Spratt (1975) whom had designated the names *Dyke A*, located at the northern fault, and *Dyke B*, located at the southern fault at Ngatutura Bay. The fault-bounded dykes are found on either side of a diatreme and are intruded into the Waikawau Sandstone and the Carter Siltstone respectively. Dyke A is about 1.5 m wide and consists of a variably vesicular core with a border of peperite. Shallow dykes associated with maar-diatreme volcanism commonly have peperitic margins where the magma interacted with water-rich and/or friable host rock (Martin & Németh, 2002a,b; 2004; 2005; 2007; Dadd & Van Wagoner, 2002). Dyke B is approximately 10 m wide and has baked margins in the Carter Siltstone, which are more than 1.5 m wide (figure 1.4). Dyke B also has a variably vesicular basaltic core and is surrounded by peperite.

Figure 1.4 – Dyke B (lower left) with a baked margin in the calcareous Carter Siltstone and its location on a fault plane. Field of view: 25 m.

Volcanic breccias

A lava pond above dyke A extends for at least 10 m along the upper Kaawa boundary, with a hyaloclastite veneer along the top and in basal parts peperitic intrusions into the soft substrate.

In the southern cliff face near the Ngatutura Point lavas is a volcanic breccia, which appears to be a submarine debris flow deposit emanating from the overlying lava flows (figure 1.5). The breccia contains palagonatized basalt as well as blocks of country rock and redeposited breccia blocks.

Figure 1.5 – Debris flow below the Ngatutura Point lava flows containing large blocks of basalt suspended in a fine-grained palagonitic matrix which also contains abundant country rock lithics. Field of view: 15 m.

The Ngatutura Diatreme

The exposure of the Ngatutura Diatreme is more than 40 m in height and protrudes laterally from the cliff face up to 8 m (figure 1.6). The diatreme has a complex facies architecture consisting of massive deposits in some lower areas while other lower deposits have well-developed, steeply dipping beds. Central and upper parts have moderately to well-bedded deposits with variable bed thicknesses and dipping angles varying from sub-vertical to sub-horizontal. The deposits are composed of a mixture of basaltic and country rock fragments. The walls of the diatreme are cut into Tertiary marine strata and are subvertical, becoming more horizontal near the top. Lower deposits are well-indurated while higher deposits become more friable towards the top of the structure. The base of the diatreme consists of agglomerate of highly vesicular basalt and welded spatter. The base has a sharp, undulating contact with the overlying breccia. The feeder dyke(s) is not exposed and the top of the diatreme appears to be truncated and is overlain by late Quaternary Awhitu Sand.

Figure 1.6 – Southern view of the Ngatutura Diatreme showing the pipe-like form of the structure which is filled with volcaniclastic sediment.

CHAPTER 2 – THE LITERATURE

2.1 SUBSURFACE PROCESSES IN MONOGENETIC VOLCANISM

Monogenetic volcanic fields typically consist of a variety of landforms, from scoria cones to maar-diatremes and tuff rings to lava flows, scattered over a relatively large area, usually hundreds to thousands of square-kilometres (Walker, 2000; Kereszturi & Németh, 2012; Németh, 2010; etc.). Volcanism at monogenetic volcanic fields are typically mafic in composition, but other magma compositions can also be involved. Monogenetic volcanism is distinguished from four other types of basaltic volcanism: Lava shield volcanoes, stratovolcanoes, flood basalts, and central volcanoes (Walker, 2000).

It is inferred that monogenetic volcanoes are supplied by small and/or transient magma sources which only send magma to the surface periodically. In such a scenario a magma pathway would cool sufficiently before the next eruption so that this ascent route is no longer the preferred pathway of the magma (Walker, 2000). However, most of the recent publications recognize that monogenetic volcanoes are in most cases not monogenetic in the sense that they have erupted more than once and their landforms are the result of a series of events as part of a short-lived eruptive sequence lasting hours to months (Németh & Kereszturi, 2015; Fornaciai et al., 2012; Tchamabe et al., 2015; Brenna et al., 2010; Schminke, 1989; etc.)

Some monogenetic volcanic fields are entirely basaltic in composition (e.g. Ngatutura and Auckland), while others contain centres which are composed of more evolved magmas like tephrite, phonolite, or even rhyolite and trachyte where volcanic fields have developed on thick continental crust (e.g. Eifel; Schminke et al., 1983).

Irrespective of the composition of the volcanism, many workers recognize the significance of the subsurface environment on the volcanic activity that takes place in monogenetic volcanic fields. Recent large-scale experiments and other studies have demonstrated that the initial crater geometry is an important aspect of volcano development and that crater geometry is largely dependent on subsurface processes and pre-eruptive subsurface conditions (Németh et al., 2001; Graettinger et al., 2015; Valentine et al., 2015; Lorenz, 1973, 1986; Self et al., 1980; Kienle et al., 1980; Auer et al., 2007).

Prior to an eruption a rising batch of magma will encounter a complex interplay of internal and external factors (Kereszturi et al., 2011) on its journey from the mantle (e.g. Huang et al., 1997) through the lithosphere. When magma rises through the lithosphere, it not only undergoes intrinsic physical changes, but also responds to conditions imposed by the environment through which the body of magma is travelling (Kereszturi et al., 2011). Regardless of these processes a threshold looms which determines whether the magma will erupt effusively or be fragmented and erupt explosively (Dingwell, 1996), either within the subsurface (Lorenz, 1986; Sparks et al., 2007; Re et al., 2015), or at the surface (Kereszturi & Németh, 2012). Factors influencing this threshold include magma flux rate, temperature, viscosity, and volatile content (Gonnermann, 2015; Fisher & Schmincke, 1984).

These factors, together with environmental conditions, also influence the effectiveness of fragmentation. Magma fragmentation is therefore an intrinsic process in the formation of monogenetic volcanoes. The mechanisms of magma fragmentation are discussed below:

2.1.1 MAGMA FRAGMENTATION

Without the input of external water, magma fragmentation can occur with the rapid exsolution of volatiles (Cashman et al., 2000). This is the dominant process of fragmentation in silicic eruptions where it can produce extensive ash clouds (Sparks, 1978), and occurs during decompression of magma, where vesicles nucleate as volatiles exsolve. This is followed by continued bubble growth and disruption of the magma (Sparks, 1978; Gonnerman, 2015).

Basalt is typically of lower viscosity than silicic magmas, which inhibits the fragmentation of magma during volatile exsolution and therefore ash is not a major product of "dry" basaltic eruptions (Schmincke, 2004; Namiki & Manga, 2008; cf. Berghuijs & Mattson, 2013). However, at monogenetic fields, which are typically mafic, phreatomagmatic processes (involving magma and water) are an important mechanism of fragmentation.

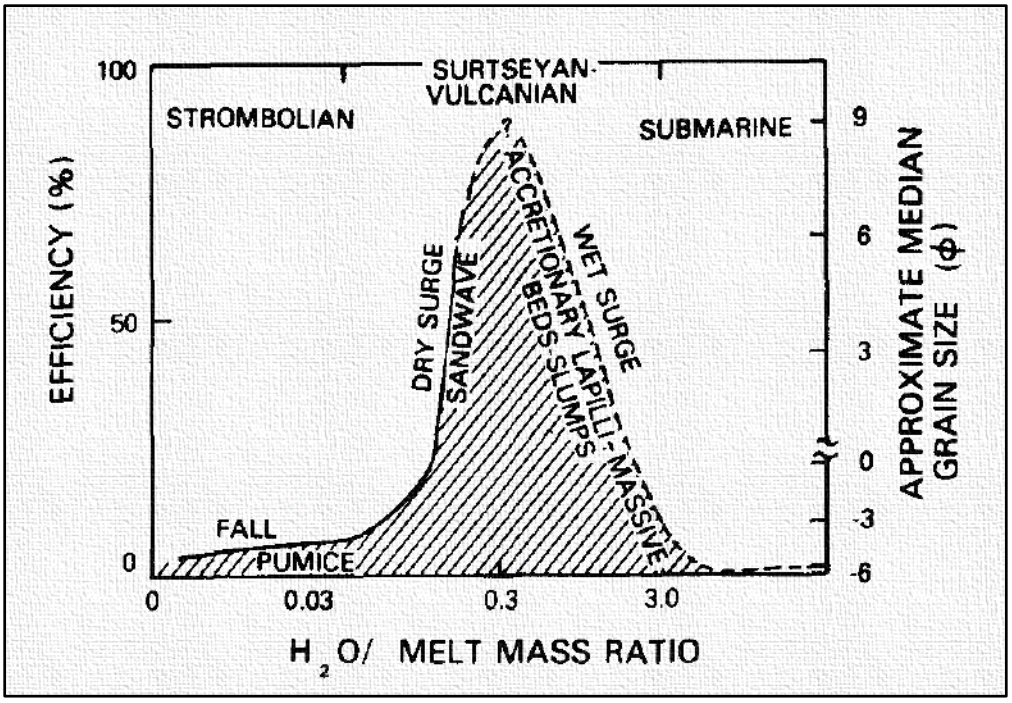

Figure 2.1 – The conversion of thermal energy to explosive kinetic energy. Depending on the water to melt ratio, various kinds of deposits can result from a volcanic eruption. The degree of fragmentation is dependent on the amount of water available, and in turn the degree of thermal energy conversion into explosive kinetic energy. The amount of water present also influences the behaviour of the fragments created e.g. the formation of accretionary lapilli and dry vs. wet surges (Schminke, 2004; Fischer & Schminke, 1984). From (Wohletz, 1983).

In fact, Walker (1973) showed that magmatic pyroclasts have a much smaller degree of fragmentation than phreatomagmatic pyroclasts. In cases where water is not involved in the fragmentation process, landforms such as scoria cones and spatter cones form through "dry" eruptive processes (Schminke, 2004; Kereszturi & Németh, 2012). Magma pathways often terminate in subaqueous environments (e.g. Rangitoto, Shane et al., 2013) or intrude into aquifers (Németh et al., 2012) where magma can come into direct contact with water. External water input is central to the nature of eruption processes in phreatomagmatic volcanism. Figure 2.1 shows the spectrum of volcanic processes that result from varying ratios of water to melt. The diagram illustrates that the efficiency of fragmentation, and therefore the median grain size of deposits, is strongly dependent on the amount of water present during a magmatic event.

The interaction between magma and water has been likened to that of molten fuel-coolant interactions (MFCIs) which have been studied extensively in industrial settings (Wohletz, 1983; Sheridan & Wohletz, 1983; MFCI: Buchanan, 1974; Schipper et al., 2013; Zimanowski et al., 1991, 1997; White, 1996; Kokelaar, 1986). Wohletz (1983) conducted an extensive analysis on the grain morphology of pyroclasts produced in hydrovolcanic settings by comparing hundreds of samples of hydrovolcanic ash with experimentally produced ash.

Wohletz considers a wide range of volcanic processes in explaining the different kinds of pyroclasts that are found at volcanoes; strombolian explosions occur where limited amounts of water are involved in an eruption, while more violent eruptions of Surtseyan and Vulcanian style occur in the presence of more abundant (but not excessive) amounts of environmental water (cf. Blackburn et al., 1976; Kokelaar, 1983), the latter resulting in very effective fragmentation of magma to produce vast quantities of ash. Wohletz focuses on grain morphology to explain the different kinds of phreatomagmatic fragmentation mechanisms.

Rising magma can come into contact with external water either within an aquifer or where water is present along faults or fractures. In other cases, magma encounters water at the surface when it erupts under glaciers, in lakes or the ocean (cf. Schminke, 2004; Lorenz, 1987). When magma comes into contact with environmental water, a small film of water vapour forms at the interface when water flashes to steam by the processes of superheating and homogeneous nucleation. Water becomes superheated when it is heated above boiling point without vaporization. In a superheated state water is metastable and can vaporize instantly when nucleation sites are introduced (i.e. sedimentary pollutants; White, 1996).

What happens after the initial interaction depends largely on the nature of the magma (i.e. viscosity, pressure conditions), surface area involved, and the amount of water available. Porosity of magma is also said to have significant effects on the efficiency of magma-water interactions (Trigila et al., 2007). Other environmental controls on magma-water interactions include the pollution of water i.e. muddy water in country rock (White, 1996).

The models in figures 2.2 & 2.3 (Wohletz, 1983) elucidate two mechanisms of phreatomagmatic fragmentation. In MFCI phreatomagmatic explosions can occur either by flashing of superheated water, or pressure detonation. The former results in rapid expansion of a superheated water mass when it becomes unstable via homogeneous nucleation and flashes to steam. Pressure-induced detonation relies on the rapid heating of water and subsequent pressure waves generated when the water is vaporized (Sheridan & Wohletz, 1983).

After initial contact, a thin vapour film is formed at the magma-water interface, which subsequently collapses. This is usually a violent reaction which creates a shock wave. The propagation of the shock wave into the melt drives the formation of Raleigh-Taylor (and Kelvin-Helmholtz) instabilities at the water-melt interface. The instabilities driving the vapour film collapse occur because of the different densities of magma and water (Buchanan, 1974).

This process leads to cavitation of the melt and subsequent brittle or ductile fragmentation, depending on the viscosity and strength of the melt.

In the stress wave fragmentation model (figure 2.2) a superheated vapour film is formed when magma contacts water. In this model the collapse of a superheated vapour film results in fractures in the melt near the interface. Fracturing of the melt occurs as brittle deformation, requiring either high viscosity (Houghton & Gonnerman, 2008) or rapid quenching (Mastin, 2007) - for example, a batch of magma may undergo fractional crystallisation where up to 90% of the magma crystallises to form a mush (Houghton & Gonnermann, 2008). This mush will have a viscosity up to several orders of magnitude higher than the crystal-poor magma from which it originated (Houghton & Gonnermann, 2008).

Fractures developing near the interface are found to propagate at angles less than 45^{o} from the principle direction of extension or compression and occur when the energy of the shockwave (which results from vapour film collapse) exceeds the tensile strength of the melt, resulting in angular, blocky and equant grains. Wohletz (1983) reports increases in specific surface area of the melt up to nearly 6000x after magma had been fragmented to sub-millimetre-size particles. The increase in surface area provides positive feedback in the cycle of recurring explosions, each becoming more energetic as surface area increases. Fragments are then dispersed by vapour expansion and turbulent mixing.

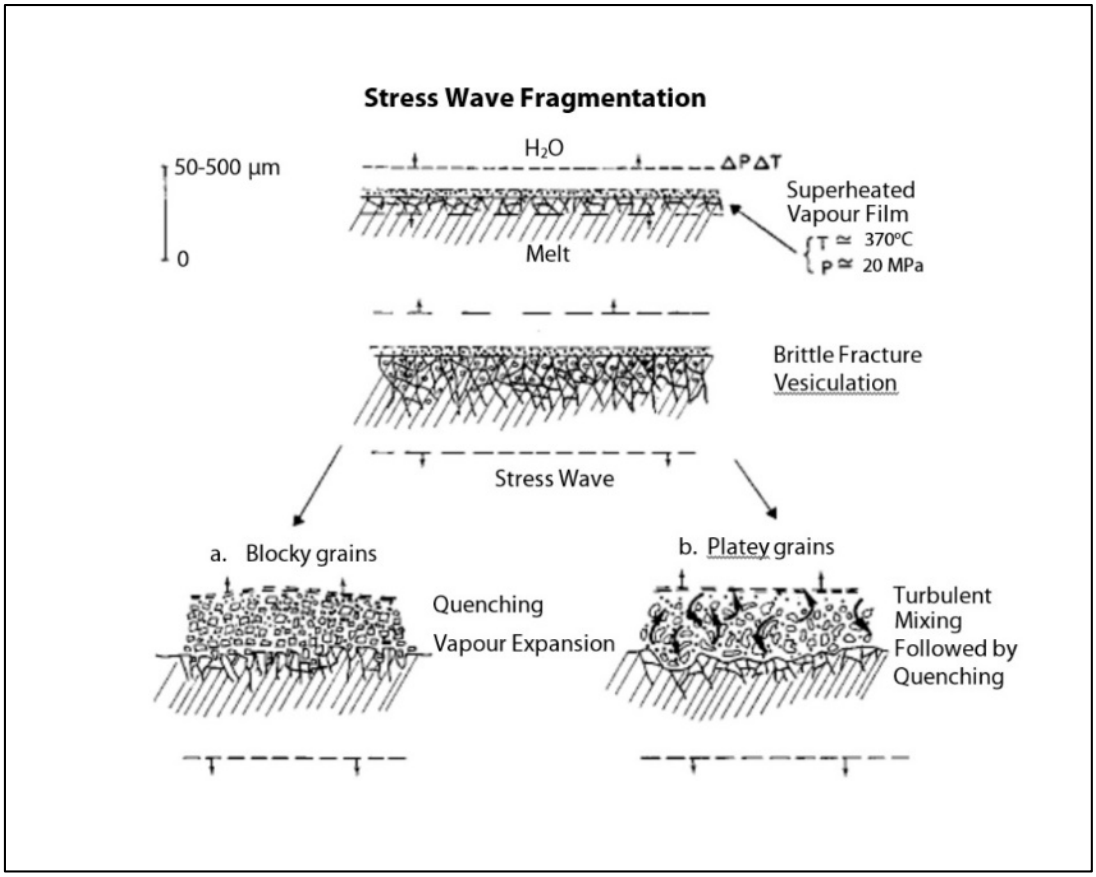

Figure 2.2 – The Stress Wave Fragmentation model. From (Wohletz, 1983).

The same process can also take place in less viscous magma where brittle deformation does not occur. Figure 2.3 illustrates the processes that take place during fluid instability fragmentation in a ductile environment. In this case, a vapour film also develops after initial water contact with the melt. However, when the vapour film collapses, droplets of water can impact the melt and together with rheological instabilities (Raleigh-Taylor & Kelvin-Helmholtz types) initiate the process of melt fragmentation by causing small plumes or undulations to form on the melt surface, these structures being only a few microns in diameter. Water or steam jets cause the fractured particles to be removed from the explosion site, along with shock waves and gas expansion. The process is repeated as a positive feedback loop with conductive surface area of the melt increasing after each MFCI.

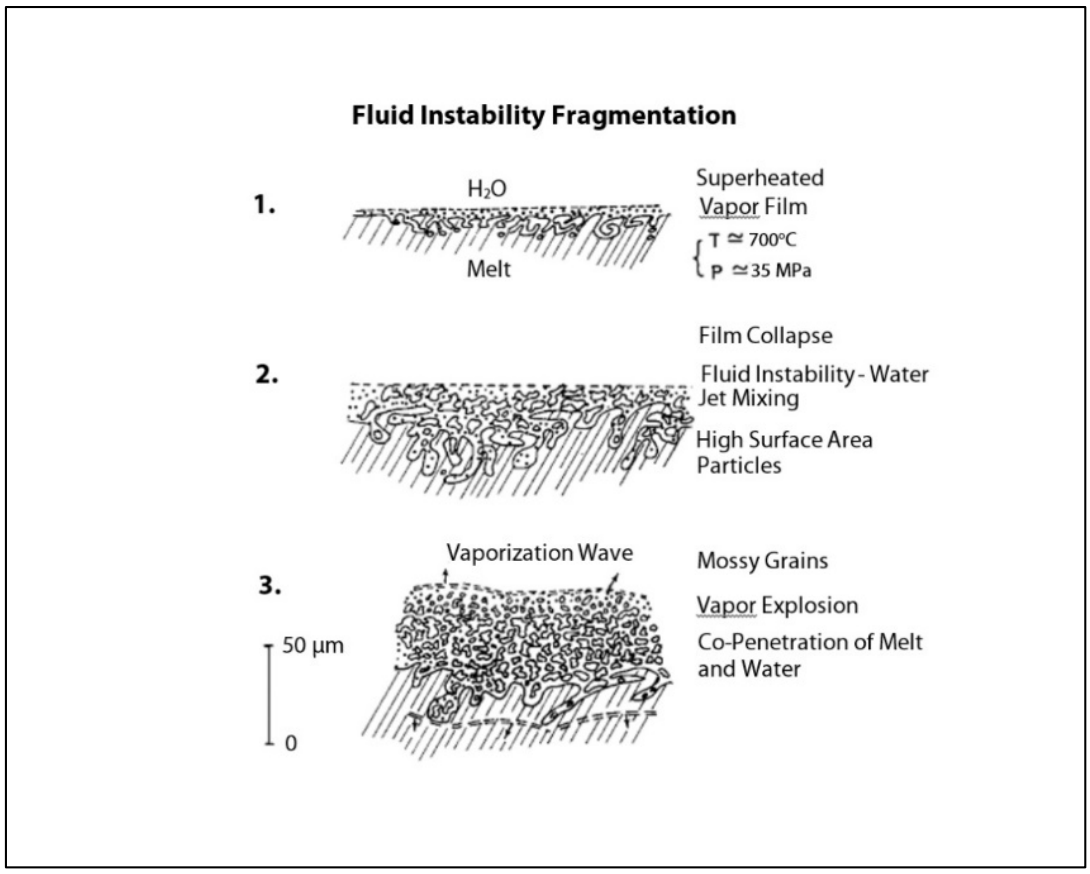

Figure 2.3 – The Fluid Instability Fragmentation model. From (Wohletz, 1983).

Water droplets can also become encapsulated, which can cause further disruption of the melt interface when a critical overpressure is reached, causing the water vapour bubbles to burst. This ductile mode of fragmentation leads to particles with fluidal textures and potentially some vesicles, as well as mossy grains with intricate surface textures as a result of rapid quenching (Wohletz, 1983).

Mastin (2007) proposed an additional mechanism of fragmentation, which is related to the model above. In his investigation, Mastin found evidence for the disintegration of glassy rinds of rapidly cooling pyroclasts. This occurs when molten pyroclasts are deformed during turbulent expulsion and a glassy rind forms due to rapid cooling. With the centres of pyroclasts still molten, they become deformed during the turbulent pathway to deposition, resulting in the fracturing of the glassy rinds and the formation of very angular, platy clasts,

microns to millimetres in diameter. The process is termed "turbulent shedding" (Mastin, 2007).

To validate Wohletz's attribution of particle morphology to primary processes, Zimanowski et al. (1997) used laboratory experiments to determine that fine ash (32-130 μm) is exclusively generated by MFCI, as described by Wohletz (1983). Further results of Zimanowski et al.'s experiments include the distinction between aerodynamic, hydrodynamic and brittle fragmentation processes (cf. Mastin et al., 2009). Aerodynamically fragmented particles form when droplets of magma are ejected while molten and solidifies before landing. Such particles are often referred to as achneliths (Walker & Croasdale, 1972) and may form during less energetic MFCI, when magma has low viscosity, or during magmatic explosions.

Hydrodynamically fragmented particles, according to Zimanowski et al. (1997) are formed during early stages of MFCI, prior to the generation of shock waves in response to vapour collapse. Brittle fragmentation occurred almost exclusively in MFCI – only with the involvement of water and subsequent shockwaves can the critical stresses be achieved that are required for brittle fracturing of low viscosity magma.

The applicability of the MFCI theory to phreatomagmatic volcanism has been questioned by Kokelaar (1986) and White (1996). Exceptions to textbook processes are also documented (e.g. Houghton & Nairn, 1991). Kokelaar (1986) deems the MFCI models of Wohletz (1983) grossly oversimplified. Kokelaar emphasises the highly variable nature of pyroclast morphology, as well as the relative abundances of pyroclasts versus country rock. This variability is likely due to a number of different processes, some of which can only be loosely explained by MFCI models, according to Kokelaar (1986). In his paper, the differences between deep and shallow marine environments in terms of phreatomagmatism are considered, as well as explosive and non-explosive magma-water interactions in shallow water environments. Kokelaar points out that in some cases Surtseyan or Ultra-Surtseyan volcanism occurs at

emergent volcanoes in shallow water environments, while in the same kind of environment pillow lavas are widely documented. In both cases magma interacts directly with water, but pillow lavas are emplaced non-explosively with fragmentation only occurring very proximally to the magma-water interface in a much more subdued manner than Surtseyan explosions.

Houghton & Nairn (1991) documents the historic phreatomagmatic and Strombolian eruptions of White Island (1976-1982). From their investigation, Houghton & Nairn speculate that much of the water involved in the phreatomagmatic explosions were in the vicinity of the "boiling-point-for-depth" curve, being heated by the local hydrothermal system. This would mean for a much different energy-budget than in cases where cold water is involved (as assumed in phreatomagmatic fragmentation models).

In addition, the authors found that much of the fine deposits that resulted from the explosions were not primary fragmentation products but rather were entrained near or at the explosion site where loose and fine material (often hydrothermally altered deposits) predated these explosions. In light of these findings, Houghton & Nairn (1991) concluded that the phreatomagmatic explosions in this case had not been effective in fragmenting the melt. Little juvenile pyroclasts formed and much of the deposited material had in fact been recycled.

The explosions witnessed at White Island are said to be steam explosions involving magma and water, or sometimes just water. It is thus illustrated that environmental factors can have a significant impact on the style of phreatomagmatic volcanism and may not always be according to magma-water interaction models (White & Nairn, 1991).

White (1996) provides extensive criticism for the MFCI models and their importance to phreatomagmatism. This criticism stems mainly from the fact that these models, as outlined above, assume pure water only to be part of the reaction with magma and do not necessarily allow for any kind of impurity,

whether it be dissolved substances or suspended sediment, or both. As pointed out by White (1996), instances of pure water contacting magma in nature is extremely rare if they occur at all.

Impurities in coolants can alter factors such as thermal conductivity, coolant density, heat capacity, and viscosity. The process of superheating water and subsequent homogeneous nucleation would also be adversely affected (cf. Wohletz, 1986). However, with lower contact wetting angles achieved in impure coolants, vaporization potential is increased. This process, together with heterogeneous nucleation strengthens the propensity for vaporisation and therefore provides a different means for vast quantities of water vapour to form rapidly and resulting in explosions of sorts.

While the frequency of explosions can increase in this way, other factors have a dampening effect on MFCI. For instance, White (1996) explains that higher sediment content in water increases the density and viscosity of the coolant and therefore inhibits explosions by increasing the detonation energy needed for MFCI to occur. The extent to which the impacts of impure coolants affect phreatomagmatic volcanism is uncertain, but this study provides an alternative view on the essence of magma-water interactions. Reviewing some other landforms that result from magma-water interaction in subsurface environments enables a more holistic perspective on the development of small basaltic volcanoes.

Some of the hypotheses of White (1996) were tested experimentally by Schipper et al (2011). Their main conclusions are that the addition of sediment in water will slow heat transfer rates during non-explosive magma-water interactions, potentially explaining the occurrence of globular peperite in such environments.

2.1.2 SUBMARINE VOLCANIC DEPOSITS

Hyaloclastite is described by van Otterloo et al. (2015) as a subaqueous volcaniclastic deposit that forms as a result of super-cooling-induced quench fragmentation. Hyaloclastite is described from a number of contexts, including subglacial volcanism (Fisher & Schminkce, 1984), on the submerged flanks of seamounts (Smith & Batiza, 1989; Staudigel & Schminke, 1984), deep sea volcanism (Schminke et al., 1978; White & Busby-Spera, 1987) and maar volcanoes (Fisher & Waters, 1970; Heiken, 1972).

Hyaloclastites are characteristically glassy volcaniclastic breccia deposits; the shape and form of individual deposits being highly varied, reflecting a wide range of depositional environments. Hyaloclastite was originally described by Rittman (1960) as sand-sized basaltic breccia which formed *in situ* by the breakage of glassy pillow rims. While the definition and applicability of the term hyaloclastite has remained a contentious subject (Honnorez & Kirst, 1975; Fisher & Schminke, 1984 p. 233; etc.), the fundamental concept in all instances is that hyaloclastite results from the interaction between magma and water in subaqueous settings, the resultant deposit being a vitroclastic breccia.

The rapid quenching of magma by water introduces thermal stresses which can readily shatter magma into fine angular fragments (Heiken, 1972). In submarine environments this process can lead to thick deposits of volcaniclastic breccia, often at the margins of pillow lavas where magma has come into direct contact with water (e.g. Batiza et al., 1984). This form of MFCI is generally non-explosive (Peckover et al. 1973), but fragmentation of hyaloclastite particles can also occur via steam explosions (McBirney, 1963) or spalling of pillow rinds (Schminke et al., 1978).

Vesiculation can also aid fragmentation processes by producing thin bubble walls in the melt, which can fracture easily (Batiza et al., 1984; Fisher & Schminke, 1984), however, vesiculation can have a number of influences on the stress regime of the magma and can either result in dispersal or concentration of certain stresses (van Otterloo et al., 2015). Batiza et al. (1984)

investigated the origins of differently shaped clasts in hyaloclastite on a seamount near the East Pacific Rise. It was speculated that blocky, equant clasts are formed through steam explosions in the manner described by Wohletz (1983; figure 3). Batiza et al. found that flakes and slivers of very thin glass most likely form due to thermal shock as a result of rapid quenching.

These findings are corroborated by Schminke et al. (1978) who also found that blocky shards could form by thermal shock, but that these types of clasts are rare in comparison with thin flakes. In contrast, van Otterloo et al. (2015) explains that it is possible for large amounts of blocky, equant shapes to form as a result of thermal shock. Their explanation is that such clast shapes can result from self-organisation of fractures in an isotropic medium, whereby an intricate network of fractures propagate successively in a body of magma, generally perpendicular to each other. This process is said to take place much slower than the rapid (possibly explosive) quenching of magma which results in the thin slivers and flakes described by Batiza et al. (1984).

An additional clast type is identified by Batiza et al. (1984) that is jig-saw puzzle shaped and appears to have been formed in situ shortly after emplacement of the magma. They propose that these clasts formed by the mechanism described by Carlisle (1963), where droplets of melted basalt remained whole when dropped into a beaker of water until the steam film gave way and the basalt contacted the water directly, resulting in rapid quenching and shattering of the clasts to produce a jigsaw-like texture. Such textures provide evidence for hot deposition of hyaloclastite, although this is not a defining criterion.

In many of the case studies describing hyaloclastite deposits, emphasis is placed on the non- to poorly-vesiculated nature of the clasts. In shallow marine environments the lack of vesiculation has been attributed to volatile-poor magma (Honnorez & Kirst, 1984) or high hydrostatic pressure (Jafri et al., 2010). In deep marine hyaloclastite deposits vesiculation can be almost completely absent (Schminke et al., 1978; Heiken, 1972). It is also common for

hyaloclastite to be thinly bedded. In these cases, the deposits have been redeposited, for instance, in submarine valleys (Smith & Batiza, 1989) or in submerged seamount craters (Van Otterloo et al., 2015).

Peperite is another kind of volcaniclastic deposit found in subaqueous settings. The term peperite is defined by White et al. (2000) as "*a genetic term applied to a rock formed essentially in situ by the disintegration of magma intruding and mingling with unconsolidated or poorly consolidated, typically wet sediments. The term also refers to similar mixtures generated by the same processes operating at the contacts of lavas and other hot volcaniclastic deposits with such sediments*". This definition, like that of hyaloclastite, is contentious in the sense that some workers apply the term in a genetic sense, while others base their definition on physical characteristics of the deposit (Brown & Bell, 2007).

The formation of peperite is through processes of magma fragmentation or disintegration and subsequent mixing or mingling of the magma fragments with a sediment host (Skilling et al., 2002). In forming peperite, magma fragmentation can occur in a number of different ways, whether through brittle or ductile deformation, resulting in a range of clast morphologies. Important fragmentation processes include autobrecciation, quench-fracturing and fuel-coolant-interactions (Skilling et al., 2002; Zimanowski & Buettner, 2002). Magma can also be fragmented by fluid-fluid shear processes when flowing into or over liquefied sediment (Skilling et al., 2002).

The mingling of fragmented magma with host sediment is an intrinsic process in peperite formation. Previous studies have focused on the spatial relationships between magma and host sediment, as well as rheological implications and process-form relationships (e.g. Busby-Spera & White, 1987; Kokelaar, 1982; Delaney, 1982; Hanson & Hargrove, 1999). Fluidisation is an important process which allows magma to permeate soft sediment. Fluidisation can occur on variable space- and timescales; one mechanism is proposed by Kokelaar (1982) as the heating of pore-fluid with the consequent expansion causing fluidisation potentially over large areas as magma flux

progresses. For fluidisation to occur, sufficient water content is needed to support sediment grains, as well as high pore connectivity and good sorting of host sediment (Skilling et al., 2002). Temperature, density and viscosity differences between magma and host sediment can lead to fluid instabilities (e.g. Raleigh-Taylor or Kelvin-Helmholtz), which can further aid mingling of magma and sediment (Kokelaar, 1986; Leat, 1985).

In addition, hydromagmatic explosions can significantly contribute to mingling of sediment and magma. Such explosions can only occur where confining pressures are suitably low, i.e. below the critical pressure for sediment-free water (Skilling et al., 2002). Hydromagmatic explosions are suspected to be most common during intrusion-phases when heat transfer and volatile release are at a maximum (Busby, Spera & White, 1987; Skilling et al., 2002).

Finally, mingling of magma and sediment can occur via liquefaction of host sediment, induced by shear stresses, seismic activity and physical jostling of sediment when magma is intruded and/or explosions take place (Skilling et al., 2002).

In a case study of a phreatomagmatic volcano in the Snake River Plain volcanic field (USA), Németh & White (2009) documented peperite deposits associated with feeder dykes in a complex basaltic system which produced extensive phreatomagmatic deposits. The peperite here is found as intra-vent deposits. The host sediment is muddy, sandy siliciclastic sediments that had been wet when magma was emplaced. The dykes are described as being 5-10 m in thickness and they have strongly chilled margins. The preserved interface between the dykes and surrounding sediment is irregular and form protrusions of up to 1 m. The peperite found adjacent to the dykes is mostly globular in texture, with blocky clasts only occurring in the >1m size fraction. Globules of decimetre-millimetre size are proposed to have formed due to shear stress where bits of magma were torn from the main body during intrusion and subsequently intermingled with and shaped by surrounding

sediment, a process described by Doyle (2000). Németh & White (2009) further suggest that blocky-shaped clasts formed due to fuel-coolant interactions and/or quench fragmentation.

Németh & White (2009) also document peperite forming within lapilli tuffs and tuff breccias near the top of the same volcanic succession. These volcaniclastic deposits have formed at an earlier stage and their unconsolidated nature provided a suitable environment for the formation of peperites during magma intrusion. This study illustrates the complexity of peperite formation with regard to paleoenvironment.

It is suggested that the presence of peperites preserve the primary processes by which they formed and this property is useful to determine spatio-temporal relationships of volcanism and its host sediment (McClintock & White, 2002; references therein). McClintock & White (2002) describe peperites as "frozen" fuel-coolant interactions, implying that magma fragmentation by FCI is preserved in situ within the newly formed volcaniclastic deposit. Indeed, this case study of the Coombs Hills volcanics in Antarctica reveal the impacts of time- and space-dependent behaviour of host sediment during the formation of peperite. McClintock & White (2002) found that thermal and rheological properties of both the magma and hosts sediment involved, can be altered rapidly to affect, in turn, processes of peperite formation i.e. fragmentation and dynamic mingling of fragmented magma and sediment. This complex interplay between, often multiphase, flows and syn-depositional fragmentation processes can result in an intricately mingled deposit, but can also lead to the arrest of certain process-forms and thereby preserve parts of the deposit that were formed by primary peperite-forming processes (McClintock & White, 2002).

In addition to dykes and other types of syn-volcanic intrusion, peperite is also associated with lava flowing over soft and/or wet sediment (e.g. Waichel et al., 2007) and a range of other settings (Skilling et al., 2002; references therein).

The behaviour of lava when flowing into subaqueous environments depends largely on magma flow rates and consequent cooling regimes (Sanchez et al. 2012). The flow rate of magma can determine if lava will be emitted as sheet flows or pillow lavas. Submarine lava flows are subject to rapid and sustained cooling by water. This can result in cooling patterns such as columnar jointing in flows. Such columns usually form perpendicular to the flow direction and can terminate in a cooling front at the terminal of the flow. Pillow lavas form as tubes with equidimensional flow sides, resembling pillow-like shapes in cross section (Sanchez et al., 2012). Pillow lavas often form at the front of lava flows where the flow becomes thinner and slower, causing lava to propagate as narrow tubes rather than a sheet. Accompanying these processes are the formation of peperite and hyaloclastite at the margins, and breccia at the cooling front (Sanchez et al., 2012).

2.1.3 PLUMBING SYSTEMS OF MONOGENETIC VOLCANOES

Basaltic volcanism on the continents is most commonly emplaced via dykes (Rivalta et al., 2015; Parker et al., 1990). Dyke propagation is the subject of complex physics in terms of stress regimes, nature of country rock, and a range of other processes like dyke-induced seismicity, magma-country rock interactions, and magma rheology (Rivalta et al., 2015). The pathways of dykes are one of the most curious subjects about dyke emplacement in the literature. For instance, fault boundaries are well-documented as preferred pathways for magma in propagating dykes (Re et al., 2015; Rivalta et al., 2015), more so in hard-rock environments where lithologies are well indurated and have low permeability. Established faults preferentially accommodate the propagating tip of a dyke, followed by widening of the crevice which can occur in a number of ways. In such a scenario the dyke structure is likely to have a thickness much less than its breadth and length and would have a similar aspect ratio to that of sills (Rivalta et al., 2015). The pathways of dykes are also determined by magma-country rock interaction. Brittle vs. ductile deformation of host

rock can lead to changes in dyke propagation (Rubin, 1993) and can also affect the rheology of the magma, altering heat transfer rates and changing viscosity (Skilling et al., 2002). The paths of dykes can be altered during syn-eruptive changes in shallow stress fields surrounding a volcano. Re et al. (2015) found that the excavation of deep maar craters and the emplacement of a scoria cone caused the local stress fields in the shallow subsurface to become unstable at a small mafic volcano. Altering the stress field in such a way had caused dykes to initially follow sub-vertical paths but when the stress field was altered, *en echelon* dyke and sill emplacement became more favourable.

Dyke propagation is important because dykes play influential roles in the style of eruptions. Not all dykes in subvolcano plumbing systems are necessarily involved in an eruption and the connectivity of dykes and conduits driving eruptions has been an important consideration in recent studies (Galindo & Gudmundsson, 2012; Németh & Martin, 2007; Geshi et al., 2010; etc.) While it is often assumed that monogenetic volcanoes erupt from a single batch of magma, which rises rapidly through the crust (Thordarson & Self, 1993; Sparks et al., 1977), research has shown that small mafic volcanoes are often underlain by complex plumbing systems comprising networks of dykes, sills and even small domes. Németh & Martin (2007) investigated a case of a shallow sill and dyke complex in western Hungary. They state that density rise of magma is dependent on the regional stress field within the lithosphere, and in some cases the rising magma may pond in thick, low-density sedimentary successions to form a sill and dyke complex.

Geshi et al. (2010) also investigated the relationship between feeder and non-feeder dykes i.e. those that drive an eruption versus those that are accessory and stall before reaching the surface. They found that the geometry of the two types of dykes is largely the same, with the most variation occurring in the very upper part of the subsurface igneous succession. It is concluded that feeders propagate in the same way as non-feeders and that they only become geomorphically distinct when buoyancy-related stress in the magma body

cause expansion in a free surface setting (Geshi et al., 2010; references therein), and with the erosion of conduit walls.

2.1.4 SUBSURFACE CONTROLS ON VOLCANO MORPHOLOGY

Five types of monogenetic volcanoes are recognized (Kereszturi & Németh, 2013; references therein): lava spatter cones, scoria or cinder cones, maars or maar-diatremes, tuff rings, and tuff cones. The variability in volcano morphology and eruption style is controlled not only by the nature of magma and its ascent, but also by an array of environmental factors which strongly influence the behaviour of magma in terms of its interactions with surroundings.

The interplay of magma with the near-surface environment and the various processes and variables that abide is shown in Figure 2.4. Kereszturi & Németh (2013) provide a detailed account of how internal and external parameters govern the style of an eruption, and consequently the morphology of a volcano. It is, however, important to consider that not all eruptive processes are represented geomorphically in an edifice when overprinting of geomorphic signatures occur.

An example of how the environment might control the style of volcanism is provided by Kereszturi et al. (2011) of monogenetic volcanism at a Mio/Pleistocene continental volcanic field in western Hungary. Here, the environment had profound effects on volcanism in a number of ways. First, the tectonic setting and local stress field was shown to govern the distribution of vents, whether phreatomagmatic or "dry". Secondly, Kereszturi et al. found that the pre-volcanic topography likely affected eruption styles of some centres by causing heterogeneities in groundwater availability for phreatomagmatic explosions.

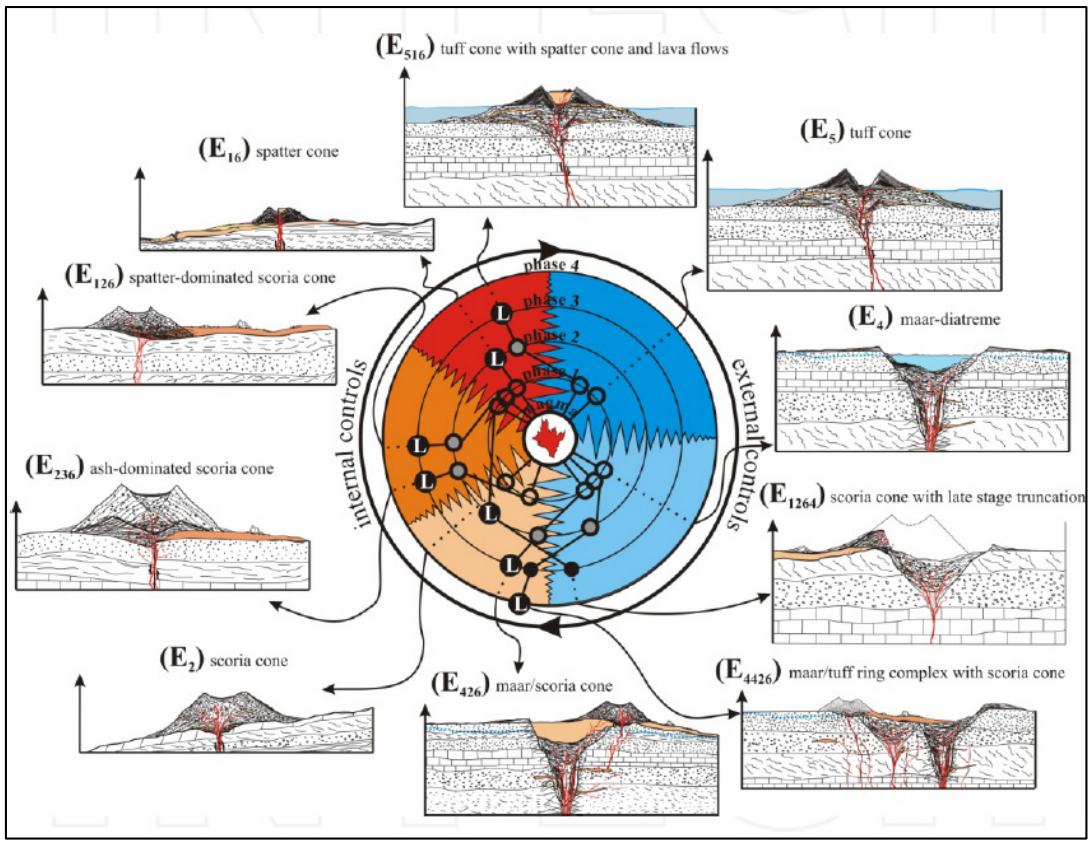

Figure 2.4 – The development of small basaltic volcanoes: internal and external controls. *"Eruption history (E) defined by a spectrum of eruptive processes determined by internal and external parameters at a given time. The initial magma (in the centre of the graph in red) is fragmented by the help of internal and external processes which determine the magma fragmentation mechanism and eruption style (phase 1). If a change (e.g. sudden or gradual exhaustion of groundwater, shift in vent position or arrival of new magma batch) occurs, it will trigger a new phase (phases 2,3,4,…, n); moving away from the pole of the diagram until the eruption ceases. Note that black circles with white "L" mean lava effusion. If the eruption magma is dominantly basaltic in composition, the colours correspond to Surtseyan (dark blue), phreatomagmatic (light blue), Strombolian (light orange), violent Strombolian (dark orange) and Hawaiian (red) eruption styles."* From (Kereszturi & Németh, 2013).

In the north the topography is elevated with an affinity for larger volcanoes, which are more magmatically-evolved, while in the south where the topography is basin-like, groundwater is more abundant and the fragmentation processes here are mostly phreatomagmatic and are distinct from that found in the north. Thirdly, the paleoclimate is proposed to have influenced the eruption style by causing hydrological variability due to climate change on a timescale of several thousands of years. Kereszturi et al. reports instances of aridification in the climate record which would have led

to a depletion of groundwater and therefore more magmatic or "dry" eruptions.

The subsurface features of dry volcanism are very different to phreatomagmatic eruptions. Phreatomagmatic volcanism often result in excavation of the conduit walls by country rock fragmentation and/or collapse into an explosion crater. This can develop complex subsurface structures, many of which are poorly understood. As illustrated in Figure 2.4, diatremes and other types of synvolcanic sedimentation form in the light blue phreatomagmatic field where the interaction of magma with water is an important process.

2.2 THE ENIGMA OF DIATREMES

2.2.1 WHAT ARE DIATREMES?

Diatremes are conical-shaped structures filled with debris composed of country rock and juvenile igneous clasts (Lorenz, 1986; Valentine & White, 2012). Diatreme structures are cut into country rock below the pre-eruptive surface and usually underlie a maar crater with a surrounding tuff ring at the surface (White & Ross, 2011). Maar-diatreme systems are most commonly mafic in composition and are associated with monogenetic volcanic fields where they are very common (White & Ross, 2011), although, diatremes with other compositions have been reported e.g. carbonatite (Stoppa, 1996; Lorenz & Kurszlaukis, 1997). These systems have a strong resemblance, in terms of architecture, to kimberlite pipes (Cas et al., 2008), but their genesis can be very different (Kurszlaukis & Lorenz, 2008; White & Ross, 2011)).

For decades, the mechanisms behind the formation of diatremes have mystified researchers. A diatreme typically consists of domains with distinct sedimentological characteristics. Some domains are massive and contain chaotic mixtures of juvenile and country rock lithics, while others are well-

bedded. Some domains show evidence for significant subsidence within a diatreme structure. The typical morphology of a well-developed diatreme is shown in Figure 2.5. The sequence of events that result in the formation of a diatreme undoubtedly include numerous phreatomagmatic-style explosions within the subsurface. Neither the exact nature of these explosions, nor the time- and space-relationships of explosions, their effects, and their deposits are constrained in the literature. Both theoretical and empirical models have been developed to explain diatreme formation by a succession of numerous subsurface explosions. These models are reviewed in the following section, which discusses the mechanisms of diatreme formation: excavation, sedimentation and reworking of sediment.

2.2.2 MECHANISMS OF DIATREME FORMATION

Lorenz (1986) proposed the first comprehensive model that set out to explain the growth and formation of maars and diatremes as a result of phreatomagmatic eruptions. The model is based on the concept of multiple small phreatomagmatic explosions, which take place over a period of hours to days. Evidence for multiple small explosions as the mechanism for maar-diatreme formation is found not only in tuff rings which surround maars, where multiple layers of lithic-rich tuff represent individual explosions, (e.g. Lefebvre et al., 2013), notably at the Ukinrek Maars where the birth of a maar and its diatreme was documented through eye witness accounts in 1977 (Kienle et al., 1980; Self et al., 1980). The second assumption of the model is based on the conjecture that diatreme structures grow in size during their eruptive activity (Valentine & van Wyk de Vries, 2014; White, 1991; Lorenz & Kurszlaukis, 2007, etc.).

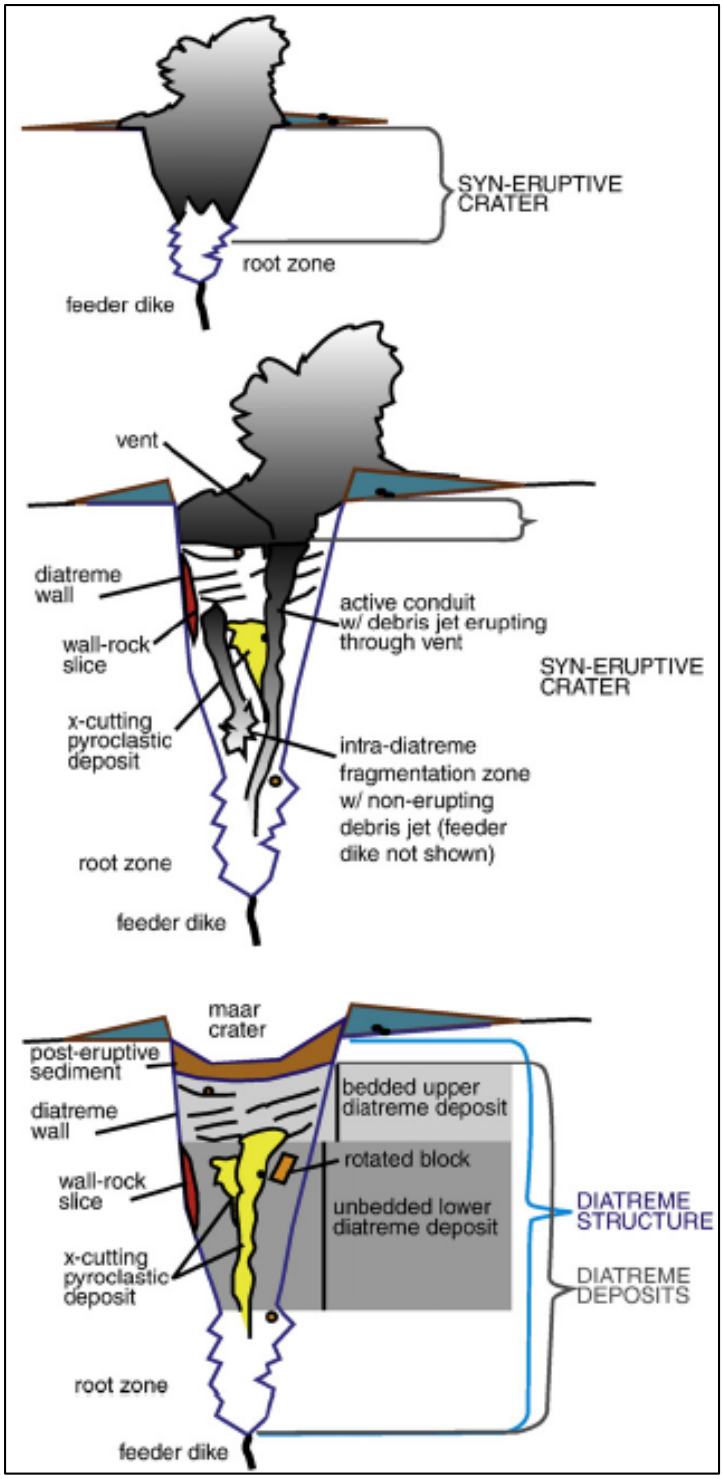

Figure 2.5 – Schematic cross section of the syn- and post-eruption features commonly found at a diatreme. From (White & Ross, 2011).

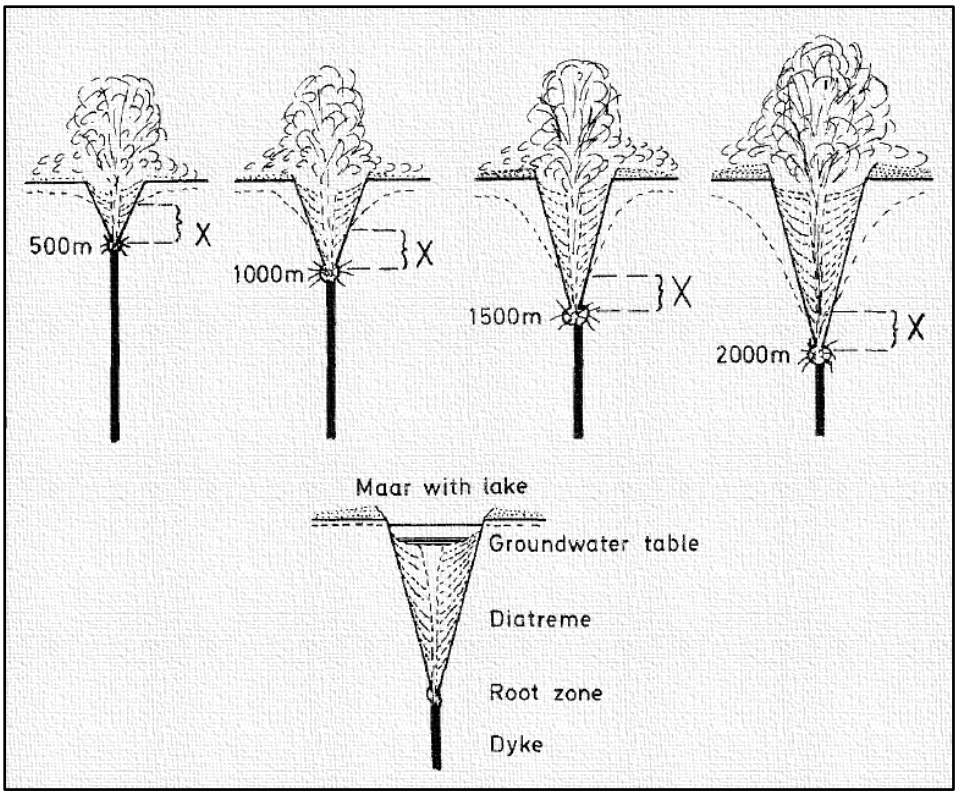

Figure 2.6 – Schematic drawing illustrating diatreme formation according to the Lorenz model. *X* denotes the "*assumed maximum depth of groundwater column on water vapour explosion site*", which is restored to original levels once the eruptions cease, aiding in the formation of a maar lake. From (Lorenz, 1986).

With the presence of abundant groundwater, Lorenz assumes the initial explosion (MFCI) takes place near the surface creating a cone-shaped depression, partially filled with fall-back debris consisting of fractured wall rock fragments and juvenile pyroclasts. Incremental growth of the proto-diatreme takes place in a two-part process: explosions at the bottom of the growing diatreme ejects debris to higher levels thus creating a void at the tip of the downward propagating structure. This is accompanied by subsidence of early pyroclastic beds - and in some cases subsidence of wall rock - which formed during the previous explosion. In the continuation of this process the groundwater supply becomes exhausted, thus leading to less violent explosions and in some cases explosions become "dry" in nature, forming Strombolian-type deposits and lava lakes. With continued explosions at depth, a central pipe is said to form through which debris is ejected to form

more pyroclastic beds and contribute to the tuff ring structure at the surface. This explanation accounts for the preservation of subaerially deposited, well-bedded pyroclastic beds near the bottom of diatreme structures. The mechanism behind the deepening of explosion locales is proposed to be drawdown of the water table in response to groundwater being consumed by phreatomagmatic activity. However, Lorenz also states that explosions deeper in an aquifer are less likely because of increased hydrostatic pressure.

Valentine & White (2012) provides a revised version of the Lorenz model. The revised model addresses weaknesses of the Lorenz model, as identified by the authors, and provides a means of explaining the formation of some diatreme deposits which do not fit the morphologic or sedimentary criteria of the Lorenz model. Similar to the Lorenz model, the Valentine & White model explains the formation of diatremes by multiple phreatomagmatic explosions. In this case the explosions can take place at any level within the diatreme, wherever magma encounters favourable conditions i.e. available water, and water pressure below the critical pressure (Zimanowski et al., 1997).

Even though the model allows explosions to occur at any depth (cf. Buettner & Zimanowski, 2003), the classic conical shape of diatremes is inherent in the process of excavation for three reasons as explained by Valentine & White: a) At lower hydrostatic pressures MFCI are more effective. b) Rock strength generally increases with increasing lithostatic pressure (Jaeger & Cook, 1979 in Valentine & White, 2012), meaning that explosions at shallower depths are likely to cause greater damage to surrounding country rock. c) Near the surface, diatreme and crater walls are prone to collapse.

The Valentine & White model deviates from the standard diatreme morphology (White & Ross, 2011) in that explosions at all levels within the diatreme result in a diatreme which does not necessarily have bedded deposits in upper parts and non-bedded deposits in lower parts. Instead, Valentine & White propose that debris jets are an important process in the sedimentation of the diatreme, leading to chaotic, unbedded domains at any

level within the diatreme structure. Because shallower explosions are more effective and have lower lithostatic pressures they are more likely to erupt at the surface and thereby forming bedded pyroclastic deposits, while deeper explosions are likely to remain buried and result in the formation of debris jets with deposits of this kind being chaotic and unbedded (cf. Ross & White, 2006). With continued explosions within the diatreme, debris is expected to become well mixed at least in the proximity of debris jets and temporary dykes get destroyed.

Some diatremes, for example Rattlesnake Crater (Marshall et al., 2015), conform to the predicted morphology of the Valentine & White model. In the case of Rattlesnake Crater, the underlying diatreme was surveyed using ground penetrating radar and magnetic surveys.

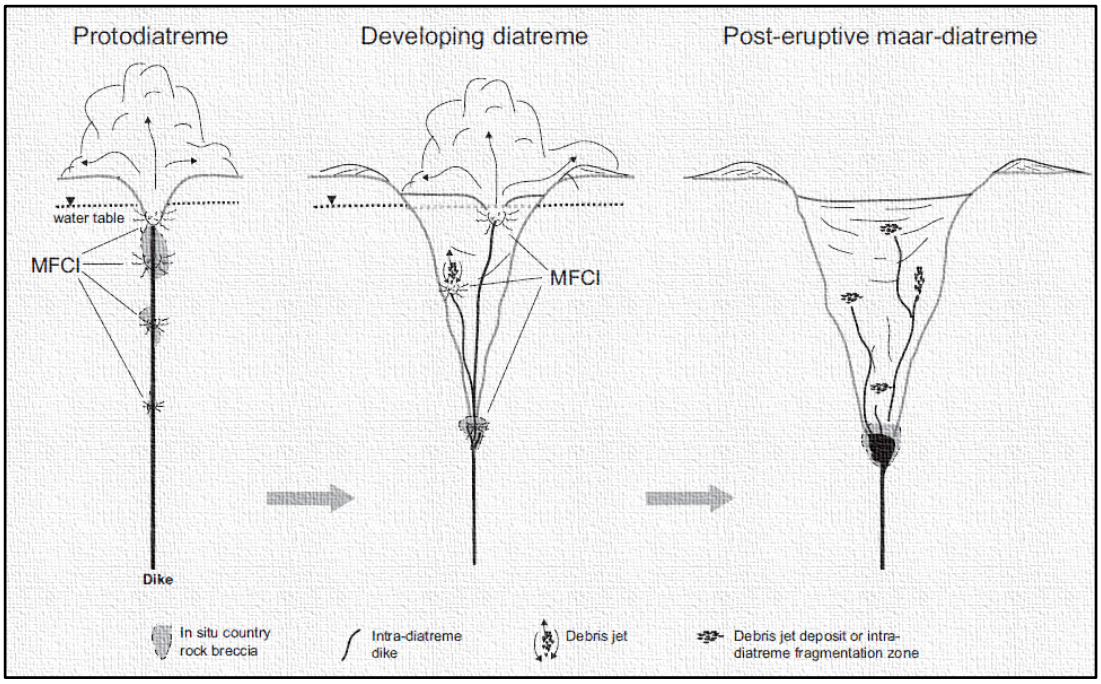

Figure 2.7 – Schematic drawing illustrating the formation of diatremes according to the Valentine & White model. In this model, MFCI-explosions can take place at any level in the diatreme structure. Explosions are most effective at lower depths, meaning the diatreme grows to be wider at the top. Debris jets are an important sedimentation process in this model. From (Valentine & White, 2012).

Marshall et al. (2015) concluded that the diatreme was not uniform in shape, and the diatreme fill not homogeneous but consisting of variably dense material and variable ratios of country rock to juvenile basalt based on the magnetic variability within the diatreme structure. This example is consistent with explosions at varying depths, as described in the Valentine & White model, where explosions closer to the diatreme wall cause uneven excavation while varying ratios of country rock and juvenile material can be explained by the injection of juvenile basalt into different parts of the diatreme, in the proximity of explosion locales.

Attempts have also been made to explain the formation of diatremes empirically via bench- and field-scale experiments (Ross et al., 2013; Valentine et al., 2012; Ross et al., 2008; Andrews et al., 2014; Graettinger et al., 2015; etc). In a recent experimental study (Andrews et al., 2015) diatreme-like structures were created with single and multiple blasts in a bench-scale setup with coloured sand layers. In the multiple-blast runs, differences in sedimentation were documented for ascending and descending blast series. These experiments were designed to be an analogue for natural systems, with the aim being to test current theories of diatreme formation.

The study successfully replicated many aspects of diatreme formation e.g. crater diameter-depth ratios, fallback sedimentation, and the stratigraphy of maar-diatreme systems. The most important findings of this study were the plausibility of single-explosion diatreme formation, and some aspects of debris jet dynamics and their role in the reworking of sediment. Results show that a two-stage process is involved in sediment transportation in debris jets: cavitation and granular fountaining.

2.2.3 MAGMA-COUNTRY ROCK INTERACTIONS

The steep-sided structure of diatremes, according to Valentine et al. (2015), form in both soft- and hard-rock settings. This is because the structure remains at least partly filled with debris during its formation, providing support to host rock walls. Valentine et al. (2015) believe that only explosions in the uppermost diatreme are significantly affected by the mechanical properties of the host rock.

The implications of host rock mechanics on vent geometry have been investigated by Auer et al. (2007) in a case study of the Fekete-hegy maar volcano of Hungary. In hard-rock environments diatremes develop to have steep sides because of the high angle of repose of hard-rock. The shattering of hard host rock is attributed to shockwaves resulting from MFCI's and wall rock collapse after explosions deepen the structure (Auer et al., 2007). In contrast, diatremes that develop in soft-rock environments are found to have broad, bowl shaped structures or form irregular depressions. Auer et al. found that such diatremes grow larger mostly due to substrate collapse in response to liquefaction of unconsolidated material due to shock waves, and slumping when buttressing within the crater is removed during continued explosions.

Valentine & Grove (1996) described deposits resulting from hydrovolcanic eruptions at Alkali Buttes, Lucero Volcanic Field, New Mexico. It is noted by the authors that the entrainment of country rock is strongly dependent on the nature of the rock units involved, as well as that of the magma i.e. velocity, temperature and bulk density. Analysis of tephra deposits surrounding the Alkali Butte vents show that mixing of soft, wet country rock with magma was an important process during phreatomagmatic explosions. Explosions are inferred to have occurred within this silty mudstone and clay shale. Furthermore, this specific lithology is a well-studied aquifer with very low water flux rates due to low permeability.

Thus, for the effectiveness of explosions to be maintained, water needs to be sourced by fragmenting the country rock, rather than seepage of ground water alone. However, this process did not endure the entire eruption sequence with evidence for increasingly drier eruptions of Strombolian type in the surrounding tephra deposits.

2.2.4 SEDIMENTATION IN DIATREMES

Sedimentation in diatremes is a process that occurs parallel to excavation processes which form the diatreme structure. The facies architecture within the diatreme structure is therefore a representation, albeit not necessarily of primary processes, of the mechanism by which a diatreme formed (White & Ross, 2011). Therefore, sedimentation of a diatreme structure is dependent on the style of successive explosions. In cases where a diatreme forms according to the Lorenz model, i.e. progressively deeper explosions, the sedimentary signatures would be very different from that of White & Valentine-diatremes were explosions occur throughout the structure penecontemporaneously or those diatremes that might form through explosions that become progressively shallower (Andrews et al., 2015).

Primary sedimentary signatures are destroyed by a number of processes, for example the lateral or vertical shift of explosion sites during an eruption sequence (Kurszlaukis & Fulop, 2013) or by the propagation of debris jets through the diatreme structure (Valentine & White, 2012). Widespread subsidence of pyroclastic beds within a diatreme, as described by Lorenz (1986) and many others, can also result in the destruction of primary sedimentary signatures. These subsided beds can, however, be found as "rafts" of preserved, but rotated stratigraphy outside of the environment in which it was deposited (White & Ross, 2011).

In diatreme morphology, the main difference between sedimentary domains is bedding. Some deposits are well-bedded with beds of variable thickness, while others are unbedded and form chaotic masses within the diatreme structure and sometimes cutting across bedded deposits, for example in the formation of debris jets (White & Ross, 2011). Bedded deposits are in most cases inferred to represent primary processes, even though the deposits may have been moved in situ, during or after an eruption (White & Ross, 2011). Moreover, sedimentation of a diatreme structure can be described in terms of the morphological classification of the standard diatreme structure, in which different domains are identified, each characterised by a certain type(s) of deposit (figure 2.5).

White & Ross (2011) distinguish between two types of "upper diatreme" deposits. The first type forms during excavation processes and typically subsides as the eruption progresses. The second type only develops in later stages of the eruption, is not deeply subsided, and commonly fills the syn-eruptive crater after major excavation. This type often grades upward into tuff or scoria cones at the surface. White & Ross (2011, and references therein) reports type 1 upper diatreme deposits found up to 1 km below the surface as a result of deep subsidence, yet minimal disruption of beds.

Lower diatreme deposits, as described by White & Ross (2011), are typically unbedded and form "homogenized" or "well mixed" deposits which are usually poorly sorted. These deposits can have different sedimentary relationships with overlying, bedded deposits; domains of different particle populations often cross-cut each other and there are examples of steep, sharp contacts but also gradational contacts between lower and upper diatreme deposits (White & Ross, 2011; Clement & Skinner, 1985; White, 1991; Ross & White, 2006). Rafts of country rock and bedded upper diatreme deposits are also a common feature of lower diatreme deposits (White & Ross, 2011).

2.3 SUMMARY

The diversity of 'monogenetic' volcanism comes from processes that largely occur in the subsurface. Of the plethora of factors that influence magma behaviour in continental settings, the most important are magma viscosity, temperature, volatile and crystal content, and flux rate; as well as environmental factors such as groundwater content, litho-or hydrostatic pressure, different types of country rock, etc. These factors determine if the magma will erupt at the surface or stay in the subsurface as intrusions. These factors also determine whether magma will erupt explosively or effusively.

Magma (and country rock) fragmentation is an intrinsic process in this type of volcanism. Fragmentation can occur on a range of scales and by many different mechanisms. Water is shown to have a profound influence on magma behaviour with respect to explosivity and fragmentation. Further, water can aid in the subsurface mingling of magma and country rock with implications for magma intrusion and early-stage fragmentation. The formation of peperite provides many important clues to the workings of volcanic plumbing systems and provide insights into the mechanisms of dyke emplacement and brecciation of magma and country rock.

Vents at monogenetic volcanic fields can be diverse, depending on the nature of the country rock and whether any water is present. Maar-diatreme volcanoes are the most common at monogenetic volcanic fields. Diatremes form in the presence of groundwater where multiple magma-and-water-explosions lead to the excavation and infilling of a (usually) conical structure which underlies a maar crater and tuff ring at the surface. The exact mechanisms behind diatreme formation is a contested subject and various models are discussed which explain these phenomena.

CHAPTER 3 – METHODS

3.1 INTRODUCTION

The environment of Ngatutura Bay is typical of New Zealand's west coast. The terrain is rugged and steep and exposures of the various volcanic features are scattered among the cliffs. Many key features crop out at beach level, including the two dykes, parts of the Ngatutura Point lavas, and the base of the diatreme. Accessing other parts of the diatreme were far more challenging. Attempts were made to abseil from above to reach upper parts of the diatreme, but 60 metre ropes weren't nearly long enough. Climbing from below was precarious at best, but this allowed for sampling of some of the higher features. The upper half of the diatreme structure was deemed inaccessible, but a good zoom-lens enabled detailed photography of these parts. However, a significant part of the diatreme was accessible for detailed sampling that could be used for characterising the deposits and inferring eruptive styles.

3.2 FIELD WORK

Hand samples were taken from Dyke A & B, and Ngatutura Point lava for K-Ar dating, microprobe analysis and thin sections of the various basalts. The lava pond above Dyke A was sampled from a fresh landslide deposit on the beach. The diatreme was extensively sampled at accessible levels, including juvenile basalt from the lower diatreme and agglutinate from the base. Selected samples were obtained from higher parts of the diatreme which were deemed inaccessible by all previous workers. Sample locations are shown in Figure 3.1.

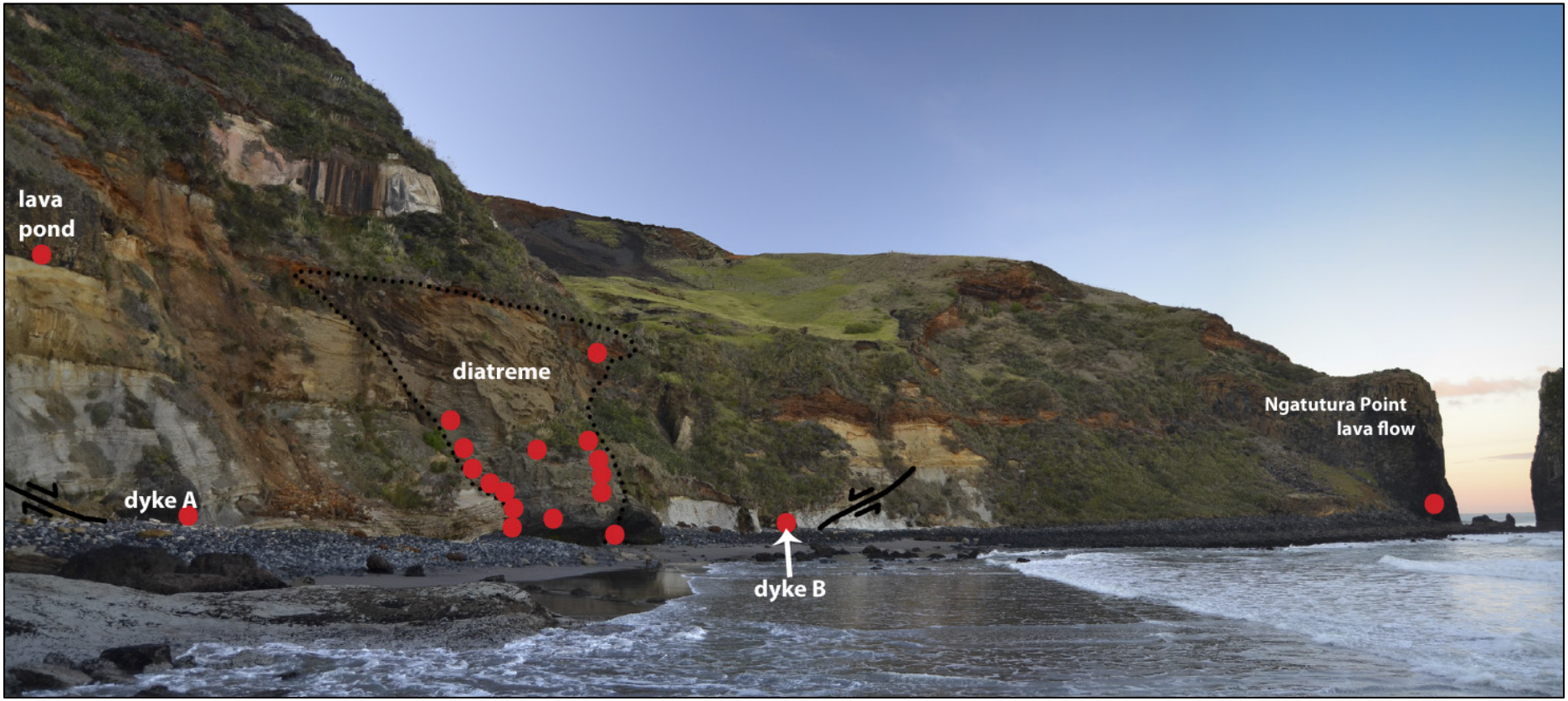

Figure 3.1 – Locations of basaltic samples used for microprobe analysis and K-Ar dating, as well as volcaniclastic samples from the diatreme used for componentry and grain size analyses.

All the features at Ngatutura Bay were photographed and a laser distance meter and clinometer were employed to gather dimension and orientation data. This combination enabled photographs to be corrected for distortion due to obliquity. Photographs of higher parts of the outcrop were scaled by cross-reference to photographs of lower parts where a graduated survey pole was used for scale.

3.3 COMPONENTRY & GRAIN SIZE ANALYSIS

Thin sections were prepared for each of the country rock lithologies, as well as the different kinds of lithics found in the diatreme. The lithics were then matched to their parent country rock according to textural and mineralogical properties. The lithic types were characterised visually for identification in the diatreme fill on photographs. Criteria included colour, texture and shape (including fracture and erosion patterns). These matches were corroborated with field observations.

Photographs were selected to represent two vertical transects within the diatreme. An area was selected in each photograph in which the deposit is well-exposed and grains identifiable down to 8 mm diameter. A grid was placed over the selected area and point counts were completed at intersections, recording lithic type and size. The majority of clasts are blocky in shape and roughly equant. Elongated clasts are rare and there is no observable systematic variation in clast shape. Therefore, it was deemed appropriate to approximate each clast as a circle. The area represented by each phi-size in the range -7Φ - 3Φ was calculated for each type of lithic. The matrix was analysed in thin section, using the same method. Thin sections were only analysed for basalt and Oligocene clasts, and overall grain size. The -2Φ fraction was found to be underrepresented in thin sections. This fraction is too coarse to be representative on small glass slides. These clasts are also too small to be counted on photographs. Instead, results for this fraction were

interpolated using the Cubic Spline method (see www.srs1software.com for details).

The percentage of area for each lithic type was calculated, and normalised to exclude matrix area for each transect.

Country rock lithologies (Fig. 1.2) have been grouped into four types of lithics that are found in the diatreme fill. The stratigraphic ages of lithologies are used to group lithics that are visually distinct. The four lithic types are Jurassic, Oligocene, Miocene and Pliocene-age lithics. The country rocks contained in each group are discussed below in terms of characteristics that enable the four types to be distinguished in photographs and thin sections based on colour and texture.

3.1.1 LITHICS OF THE JURASSIC

The Jurassic lithic type includes the Puti Siltstone, Coleman Conglomerate and Waikorea Siltstone. The two siltstones are very similar in texture and mineralogy and is indistinguishable within the diatreme. The siltstones contain fine-grained quartz and rare feldspar crystals and are characterized by well-developed conchoidal fractures. In the diatreme the Jurassic lithics have smooth edges, a dark brown colour and apparent fractures in larger lithics. The Coleman Conglomerate is distinctive because of its coarse conglomeratic texture, undulating edges and vivid red iron stains. Jurassic-age lithics also contain fossils – typically belemnites and *Buchia* spp.

3.1.2 LITHICS OF THE OLIGOCENE

Two lithologies dominate the Oligocene lithic type. These are the Ahirau Sandstone and Carter Siltstone, the latter is highly calcareous and is found in the diatreme as a soft, baked siltstone. The edges of Carter Siltstone lithics are

often highly irregular and the clasts have been plastically deformed, or in some cases comminuted. These lithics have a distinctive pale cream colour.

The Ahirau Sandstone is a medium- to fine-grained, quartzofeldspathic sandstone with a pale yellow colour and dark-orange iron stains. In the diatreme this type of lithic is found as round to angular fragments, dark-brown in colour and with smooth edges. The Ahirau Sandstone lithics are distinguished from Miocene lithics, which have a similar appearance, having a yellow-brown colour rather than pale grey.

Two limestones are found in the Oligocene sequence. These limestones are relatively thin and have been obliterated within the diatreme to such extent that they can only be identified in thin section. The relative abundance of the limestone lithics is infinitesimal.

Figure 3.2 (p. 54) – Jurassic Lithics: a & b) Puti Siltstone thin section and hand specimen. c+d) Waikorea Siltstone thin section and hand specimen. e) Coleman Conglomerate. f) Jurassic lithics in diatreme deposit.

Figure 3.3 (p. 55)– Oligocene lithics: a & b) Ahirau Sandstone thin section and hand specimen. c & d) Carter siltstone thin section and hand specimen. e & f) Carter siltstone (baked) thin section and hand specimen.

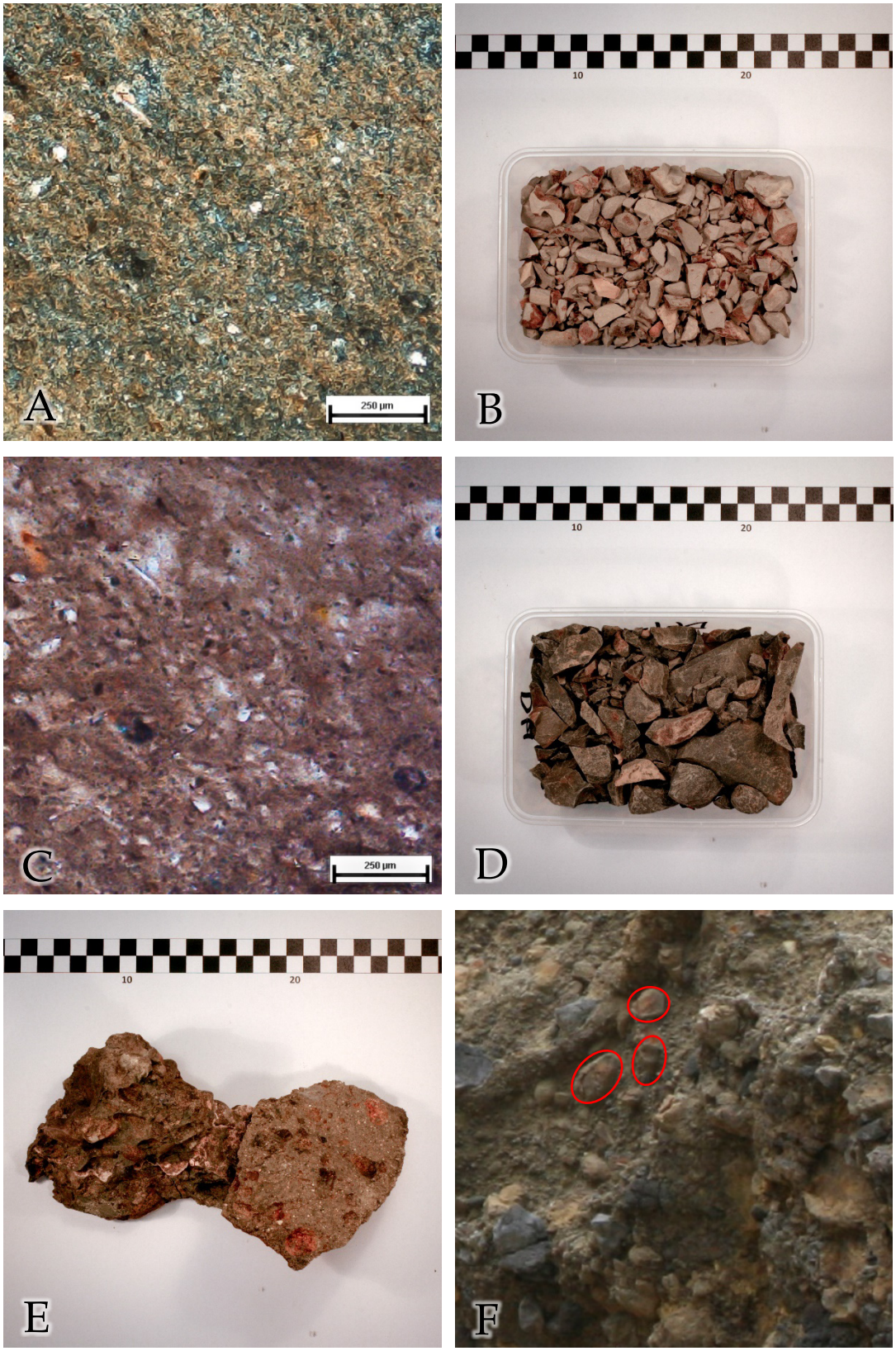

Figure 3.2

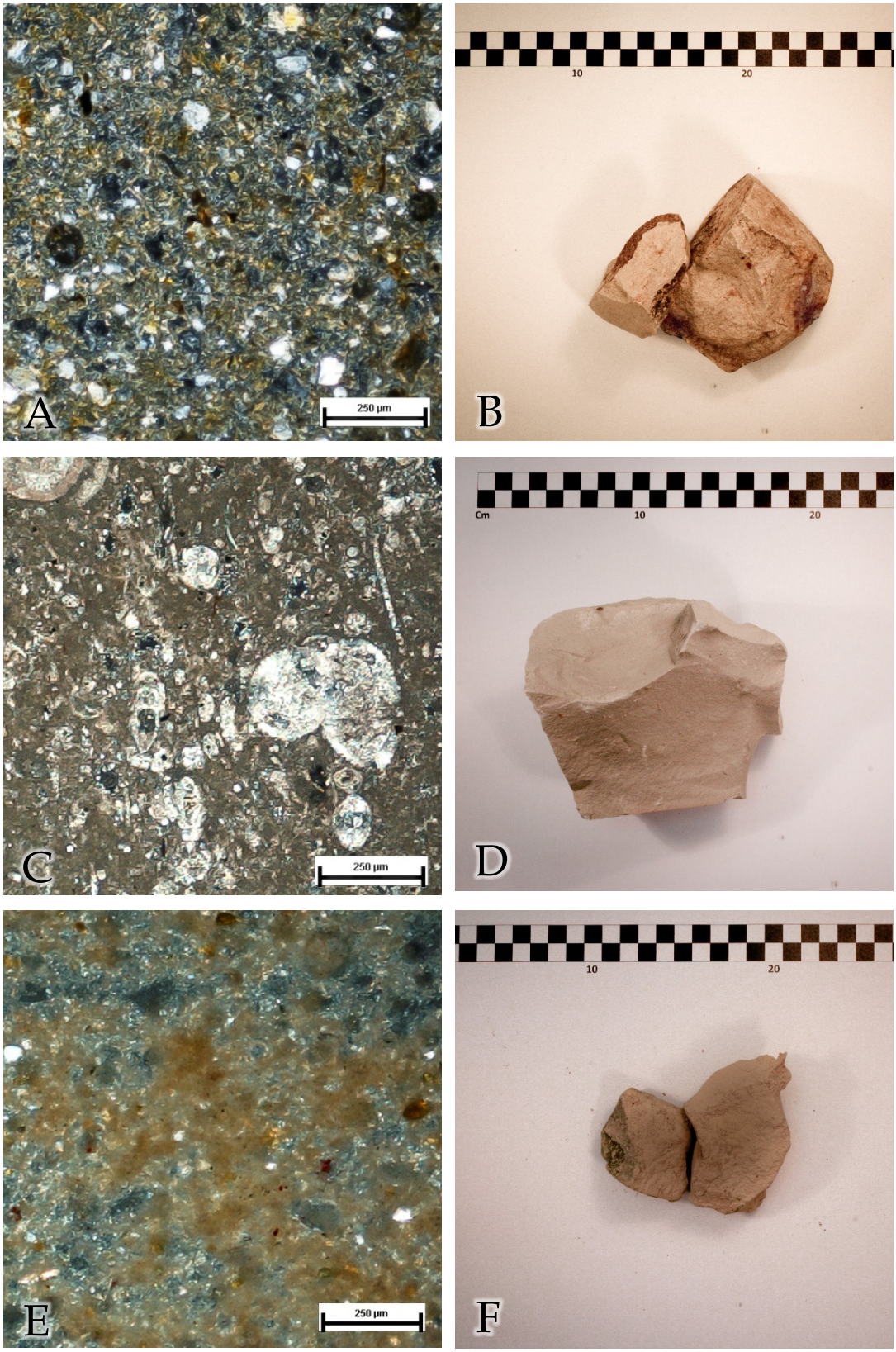

Figure 3.3

3.1.3 LITHICS OF THE MIOCENE

The Miocene lithic type comprise a single lithology: Waikawau Sandstone. The Waikawau Sandstone is a medium- to coarse-grained, quartzofeldspathic sandstone with abundant opaque magnetite grains. In outcrop the Waikawau Sandstone is interbedded with finer, silty beds. While these silty beds have a slightly finer texture to the sandstone, they are indurated to the same degree and show little difference visually as lithics in the diatreme. The Waikawau Sandstone is weakly indurated and is found as lithics in the diatreme with smooth edges and blocky to well-rounded form. The Miocene lithics have a pale-grey appearance, similar to their parent lithology.

Figure 3.4 – Lower diatreme deposit with Oligocene lithics (red - Carter Zst; blue – Ahirau Sst) and Miocene lithics (green – Waikawau Sst).

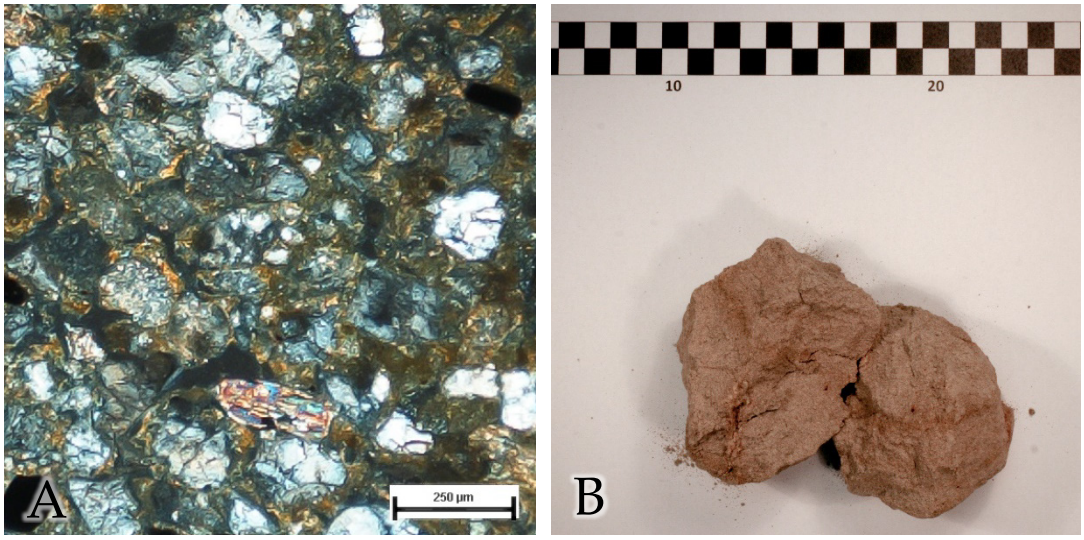

Figure 3.5 – Miocene lithics: Waikawau Sandstone. a) Thin section – quartz, feldspar and magnetite grains in a silty matrix. b) Waikawau Sst hand specimen.

3.1.4 LITHICS OF THE PLIOCENE

The Kaawa Formation is composed of a shell bed unit and a sandstone unit. These lithologies are the Pliocene lithic type that is found in the diatreme. In outcrop the shell bed has a pale yellow-grey colour and the overlying sandstone a rich yellow colour with some iron staining. In the diatreme these lithics are found as small blocks with smooth surfaces and edges. These lithologies are variably indurated ranging from friable to moderately indurated. The yellow colour of these lithics makes them distinctive from the other types.

3.4 THERMAL ANALYSIS

Thermal decomposition of calcium carbonate (equation 1) occurred at Ngatutura Bay where magma came into contact with calcareous country rock at dykes and within the diatreme. Samples were taken at regular intervals (20cm) at Dyke B where magma has intruded into the Carter Siltstone, from directly adjacent to the magma-country rock boundary to c. 1.6m from the contact where visual effects of baking are absent.

Figure 3.6 - Pliocene lithics in diatreme matrix. The area in the photograph measures 60cm x 80cm.

In addition, samples were obtained from Jurassic, Oligocene, and Miocene country rocks in order to quantify their carbonate content. Finally, Oligocene lithics were extracted from diatreme fill. These lithics were 5-15mm and 20-50mm in diameter. In order to determine the amount of calcium carbonate present, a known amount of HCl was introduced in excess to samples to react with any calcium carbonate present (equation 2). The acid solution was then back-titrated with sodium hydroxide to calculate how much HCl had been consumed in the reaction. Detailed methods are described below:

All samples were ground into a fine powder and subsequently washed in deionised water (boiled to remove CO_2), repeatedly, to dissolve and remove any CaO or $Ca(OH)_2$. These are alteration products of $CaCO_3$, soluble in water, and react readily with HCl, and would thus skew the results of the analysis.

The powders were then dried at room temperature and weighed. The powders, submersed in deionised water, were treated with 15mL aliquots of 1M HCl until no visible reaction occurred i.e. escape of CO_2 bubbles. After 24 hours the samples were agitated and tested with a pH indicator to ensure all samples contain excess HCl.

1. $CaCO^3 \xrightarrow{700-900℃} CaO + CO^2$

2. $CaCO^3 + HCl \longrightarrow CaCl^2 + H^2O + CO^2$

To calculate the amount of HCl consumed by any $CaCO_3$ in the samples, NaOH was titrated into each sample in the presence of phenolphthalein until the end-point of the reaction was reached and the solution was basic. The percentage of $CaCO_3$ in each sample was calculated stoichiometrically:

The NaOH dilution was standardised using potassium hydrogen phthalate. The HCl dilution was standardised with the NaOH dilution. Moles of HCl and NaOH added to samples were calculated against the standards.

Moles HCl – moles NaOH = moles HCl reacted to sample.

In addition, an unaltered sample of Carter Silstone, together with variably altered samples, was subjected to scanning electron microscopy at the Manawatu Microscopy Centre, Massey University, and backscattered electron images were produced to investigate structural and mineralogical differences in baked and unaltered samples.

3.5 ANALYSIS OF THERMALLY ALTERED SAMPLES

Samples from the Carter Siltstone at the baked zone at Dyke B were imaged under the Scanning Electron Microscope at the Manawatu Microscopy Centre. Pea-sized samples were cleaned in an ultrasonic bath and mounted onto a glass slide. The slide was powder coated with gold.

X-ray powder diffraction was also performed on powders from these samples (section 3.4). Analysis was performed on a GBC mini-materials analyser at Massey University, using an accelerating voltage of 15kV. Sample trays were set to rotate during analysis.

3.6 MICROPROBE ANALYSIS AND K-AR DATING

Basalt samples were analysed for major and trace elements in olivine, pyroxene and plagioclase, and glass using the JEOL JXA-5A electron microprobe at the Manawatu Microscopy Centre, Massey University, Palmerston North. Thin sections were polished and carbon coated. Accelerating voltage of kV15 was used for all analyses. For minerals a focused beam of ~2 μm was used and for glass a scattered beam of ~15 μm wide.

Samples of the lava pond, dykes, diatreme and Ngatutura Point lavas were sent for K-Ar dating. Samples were prepared by cutting rocks into thin slices. Unaltered pieces with few phenocrysts were then selected to be crushed and sieved. The 250μm-125μm fraction was then inspected under a binocular microscope and all remaining phenocrysts were removed along with ultramafic xenoliths. Samples were analysed at the Hungarian Academy of Sciences in the K-Ar Laboratory of the Institute for Nuclear Research. Analysis was performed by Prof Zoltan Pecskay..

CHAPTER 4 – RESULTS

4.1 INTRODUCTION

The volcanism at Ngatutura Bay comprises a network of intrusive features as well as features of explosive and effusive basaltic volcanism. Detailed field mapping revealed the stratigraphic relationships of the volcanic features and country rocks. The physical volcanology of the various features is described, followed by a more detailed analysis of some features including the componentry and grain size of the deposits of the diatreme, as well as the thermal alteration of country rock at one of the dykes and within the diatreme. Results of geochemical analyses and radiometric dating of the different basaltic features are also presented.

4.2 PHYSICAL VOLCANOLOGY

The volcanism at Ngatutura Bay had been emplaced in marine sediments spanning the Jurassic, Oligocene, Miocene and Pliocene. The country rock lithologies vary in texture as much as they do in hardness i.e. some (particularly younger) lithologies are friable and soft, while other, older lithologies are well-indurated and display complex jointing patterns. The stratigraphic relationship of the volcanic features with country rock is shown to be important. Intrusive volcanism occurs as different modes in well-indurated rock, compared to that in loose and friable sediment higher in the sequence. The structure of the country rock, particularly with regards to faulting, is also an important aspect for the migration of magma. The various volcanic features are described below in stratigraphic context.

4.2.1 DYKES AND THEIR RELATIONSHIP WITH FAULTS

Dykes are known to prefer faults or fractures as pathways in hard rock environments (Re et al., 2015; Rivalta et al., 2015). Two major dykes are found at Ngatutura Bay. The northern dyke, referred to as Dyke A, is located in the hanging wall of a normal fault, which offsets Miocene and Oligocene strata (figure 4.1). Pliocene strata (i.e. Kaawa Formation) are only slightly offset in lower parts.

Dyke B (the southern dyke) is found in an identical setting to Dyke A, in the hanging wall of a normal fault, but is emplaced in the Carter Siltstone. The southern fault dips in an opposite direction to that of the northern fault (Figure 4.1) and offsets Oligocene and Miocene strata. These faults appear to be ring faults encircling the diatreme structure in the centre of the bay, but they have not offset Kaawa Fm sediments and must therefore predate the volcanism, which occur as syn-sedimentary features in the Kaawa Fm..

In addition to the two dykes, a sill- and-dyke structure is preserved directly adjacent to the diatreme (Figure 4.3). The sill was fed by a thin dyke, only a few centimetres thick. The dyke becomes much thicker near the sill, but still only spans up to 25 cm in thickness, similar to that of the sill. The dyke has irregular walls and follows fracture patterns within the Carter Siltstone. The northern part of the sill becomes thicker (up to 50 cm) where it is ponded in the siltstone. The sill-and-dyke has baked the surrounding siltstone to a light brown colour. The sill is found at the contact between the Waikawau Sandstone and the Carter Siltstone.

Dyke A and B have similar structures. In both cases a margin of peperite encloses the solid core which displays complex cooling patterns and is variably fractured and mostly non-vesicular. The peperite varies in grain size and morphology and is described in section 4.2.3.

Figure 4.1 – The volcanic features of Ngatutura Bay, and the country rock stratigraphy. Field of view: 250 m.

4.2.2 EFFUSIVE VOLCANISM

A thick lava flow is exposed at Ngatutura Point (Figure 4.1). The main part of the flow overlies basal pillow lavas and is characterised by entablature-jointing, complex cooling patterns, and hackly fractures throughout, with irregular contacts to the surrounding colonnades and pillows. Some parts have rosette-shaped columnar jointing. The exposure is continued in Shag Rock, which is a small island adjacent to the main exposure. The basal pillows are 30-50 cm in diameter and are stacked up to 8-10 m high. The lava flow is emplaced upon Pliocene strata and is covered by Quaternary sand further inland. Near the base of the lava flow cliff is a small outcrop of volcaniclastic breccia appearing to be a submarine debris flow. The components include blocky basalt clasts, some sintered, and rafts of Kaawa Formation sandstone in a fine-grained matrix which is clayey in some places and containing palagonatized basalt clasts.

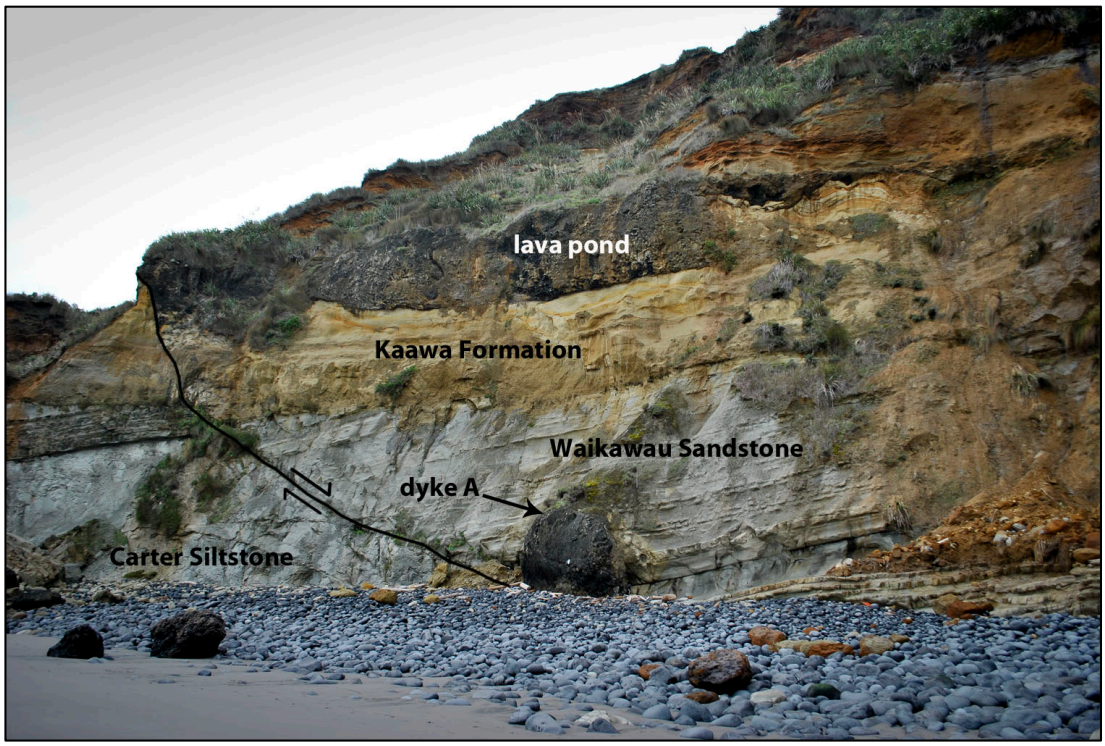

Figure 4.2 – Dyke A at the hanging wall of a fault, and overlying lava pond with hyaloclastite at its upper margins. The Kaawa Formation is only partially offset by the fault, indicating that the fault was still active during its deposition. Field of view: 45 m.

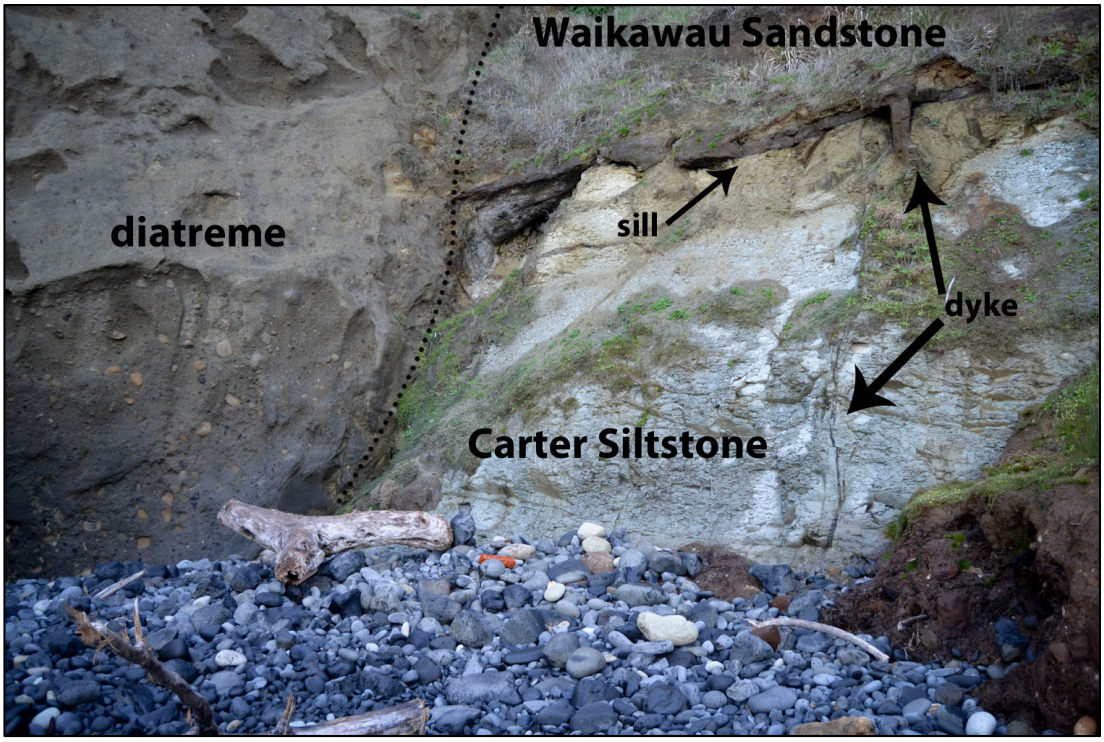

Figure 4.3 – A dyke and sill structure adjacent to the diatreme's southern wall. The sill is ponded on the left and appears to follow the contact between the Waikawau Sandstone and underlying Carter Siltstone. The sill was fed by a dyke, which, at depth, is only a few centimetres thick and follows fracture patterns in the siltstone. Field of view: 15 m.

At the northern end of the bay a lava pond is found in the Kaawa Formation (Figure 4.1 – 4.2). The lava pond is about 2 m thick and has partly intruded into the soft marine sediment of the Kaawa Formation. The main body of the pond is composed of non-vesicular basalt with hackly fractures throughout. The basal contact of the lava and sediment is slightly undulating and there is a very thin margin of globular peperite of a few centimetres. At the top of the flow there is a layer of hyaloclastite visible as a dark, fine-grained breccia, which contains very angular, non-vesicular basaltic glass. The hyaloclastite appears to have spilled from the main body onto surrounding sediment. Here, the hyaloclastite has intruded into, and plastically deformed, the soft, probably wet, sediment. At the margins, the hyaloclastite is mingled with sediment forming peperite.

4.2.3 VOLCANICLASTIC DEPOSITS

Peperite is found at the margins of Dyke A & B, as well as the basal margin of the lava pond. The peperite varies in form. In some places the peperite is fine-grained and the basalt clasts have globular to blocky shapes (cf. Martin & Németh, 2007). In other parts the peperite is poorly sorted and contain larger blocks of globular or blocky lava, as well as blocks of country rock. In places the peperite grades into fine-grained hyaloclastite near the dyke interface.

The country rock which is incorporated into the peperite at the dyke margins is the Waikawau Sandstone at Dyke A and the Carter Siltstone at Dyke B. The Waikawau Sandstone has been altered to have a bright yellow appearance and its structure is only preserved in larger inclusions which have not been baked to the same yellow colour. The sandstone forms a sandy matrix in fine-grained peperite deposits at Dyke A.

Figure 4.4 – Peperitic margin at Dyke A.

At Dyke B the Carter Siltstone has been baked to assume a dark yellow brown colour, and where it contacted the magma directly it is a very dark brown. When baked, the siltstone loses its structure upon destruction of its calcium carbonate cement. Here the peperite is a chaotic mix of deformed country rock clasts and globular to blocky to very angular basalt clasts.

Figure 4.5 – Peperite margin at Dyke B. Note the higher degree of baking in smaller clasts while the large central clast is much lighter in colour. The large clast is also intruded with fine-grained peperite where it is fractured.

4.2.4 THE NGATUTURA DIATREME

The deposits within the diatreme vary dramatically, both vertically and horizontally, in terms of bedding structure, componentry, grain size and juvenile content. Domains have been identified throughout the structure that display homogeneity in style. Each domain is described as a lithofacies. The focus of these observations is to assign emplacement processes to each domain and to gain a holistic perspective on the formation of the diatreme, all of which is discussed in chapter 5.

Adjacent to the diatreme, at the southern end of the exposure, a triangular remnant of Kaawa Formation is preserved between the diatreme and steeply dipping volcaniclastic deposits (Figure 4.6). These deposits are similar in form to diatreme deposits and comprise thin bedding that becomes more horizontally bedded near the top of the sequence.

Figure 4.6 – Steeply dipping volcaniclastic deposits adjacent to the diatreme (arrowed). These beds are truncated at the top where small, well-rounded basaltic boulders are found lying on the upper contact. The truncated beds and boulders are overlain by the Awhitu Sand. Field of view: 30 m

These beds contain vesicular and non-vesicular blocks of basalt and in the matrix abundant lithic components. Larger country rock lithic components are absent. The subvertical beds near the Kaawa Formation follow the contour of the country rock upon which it was emplaced. The beds are truncated at the top, at the same level at which the diatreme deposits terminate. The truncating contact is strewn with small basaltic boulders, which are well rounded and overlain by the Awhitu Sand, as is the diatreme.

4.3 THE DIATREME: FACIES ARCHITECTURE AND COMPONENTRY

This section describes the facies architecture of the diatreme. In the first part, each facies type is described in terms of structure, grain size, sedimentary features, distribution, and relationship with neighbouring sediment. In the second part of this section the componentry of the diatreme sediment is reported. Analyses reveal the distribution and abundance of different kinds of wall rock lithics and juvenile clasts. The grain size characteristics of the diatreme fill are reported in the third part of this section. Grain size populations from photographs and thin sections were combined to give an overall grain size distribution (figure 4.20).

4.3.1 FACIES DESCRIPTIONS

Type 1 – bedded, subsided deposits

This facies type is found at lower and intermediate levels within the diatreme. In the lower diatreme the sediment is indurated, while higher occurrences of this facies type are more friable. These deposits are classed as a lapilli tuff with a mean grain size of 19.5 mm and poor sorting. Beds of type 1 deposits are centimetres to decimetres in thickness, subparallel and sometimes truncated by overlying beds. In some areas decimetre beds with a fine sandy

matrix are interbedded with a coarse, better sorted sand of a few centimetres thick. These sandy beds contain very few larger lithics (>20mm) and have sharp, planar contacts with surrounding beds. Bomb sags are sparsely found in type 1 deposits and the deformation of beds surrounding impact sites are less well defined than occurrences in the upper diatreme. Bombs are mostly angular, blocky juvenile basalt.

Other sedimentary features are wavy bedforms and undulating contacts between beds, and some water escape structures (penecontemporaneous deformation). Type 1 deposits in the lower diatreme feature a margin of disrupted sediment adjacent to the diatreme wall. At the Papakura Limestone, intricate bedforms are preserved at the diatreme-wall rock interface. These bedforms protrude into crevices in the limestone and comprise laminated sand and very fine lapilli with tangential bedding.

These bedforms terminate in the disrupted margin of homogeneous sediment, which separates type 1 deposits from the wall rock. Type 1 deposits have a gradual contact with type 2 deposits in the lower diatreme, but in the upper diatreme type 1 deposits are found in distinct domains with clear, sharp boundaries to surrounding sediment.

Type 2 – deposits with convolute bedding

These deposits are found at a single location in the lower diatreme (figure 4.7). The deposits are typically well indurated and dark grey in colour. Type 2 deposits grade into type 1 deposits, which have more regular bedding, in the northern wall of the diatreme. Type 2 deposits have characteristic convolute and chaotic bedding patterns and water escape structures are common – in places, lower strata are extruded via small "dykes" into higher parts of the sequence, cutting through overlying strata (Figure 4.16).

Figure 4.7 – The northern face of the diatreme showing the facies architecture. Type 1 – bedded, subsided; Type 2 – convolute bedding; Type 3 – unbedded; Type 4 – unbedded, debris jet; Type 5 – bedded, country rock-poor; Type 6 – bedded, in situ. Field of view: 40 m.

These deposits are classed as a lapilli tuff with few larger interstitial lithic components and a mean grain size of 2.5 mm. Vertically, type 2 deposits have a gradual contact to underlying type 1 deposits and a sharper contact to overlying type 3 deposits. Laterally, type 3 deposits truncate type 2 deposits with a sharp contact. The contact of type 2 deposits to the wall rock is marked by a disrupted margin of a few centimetres which lacks any kind of bedding.

Type 3 – unbedded deposits

Unbedded diatreme deposits are found at lower and intermediate levels. These deposits are classed as a lapilli tuff/tuff breccia, are typically poorly sorted, and grain size varies laterally and vertically. In some places large blocks of country rock are concentrated and even arranged in a pipe-like structure (Figure 4.12). Some parts are enriched in juvenile components, while other parts take the form of a fine sandy gravel in which few larger lithics are present.

Unbedded facies generally have sharp boundaries to neighbouring deposits and often truncate adjacent deposits. This type of deposit comprises a large part of the southern wall, but there are internal differences in grain size and componentry. A ubiquitous feature is a fine sandy matrix that contains a mixture of comminute country rock clasts and juvenile fragments, including silt-sized particles which have their origin in their parent country rock siltstone.

Type 4 – unbedded deposits of the debris jet

A debris jet is found in the northern wall of the diatreme. The debris jet outcrop probably represents an oblique transect through a pipe-like feature that is a debris jet. The abundance of lapilli and block sized lithics, along with the sandy matrix results in very poor sorting of the grain size population of

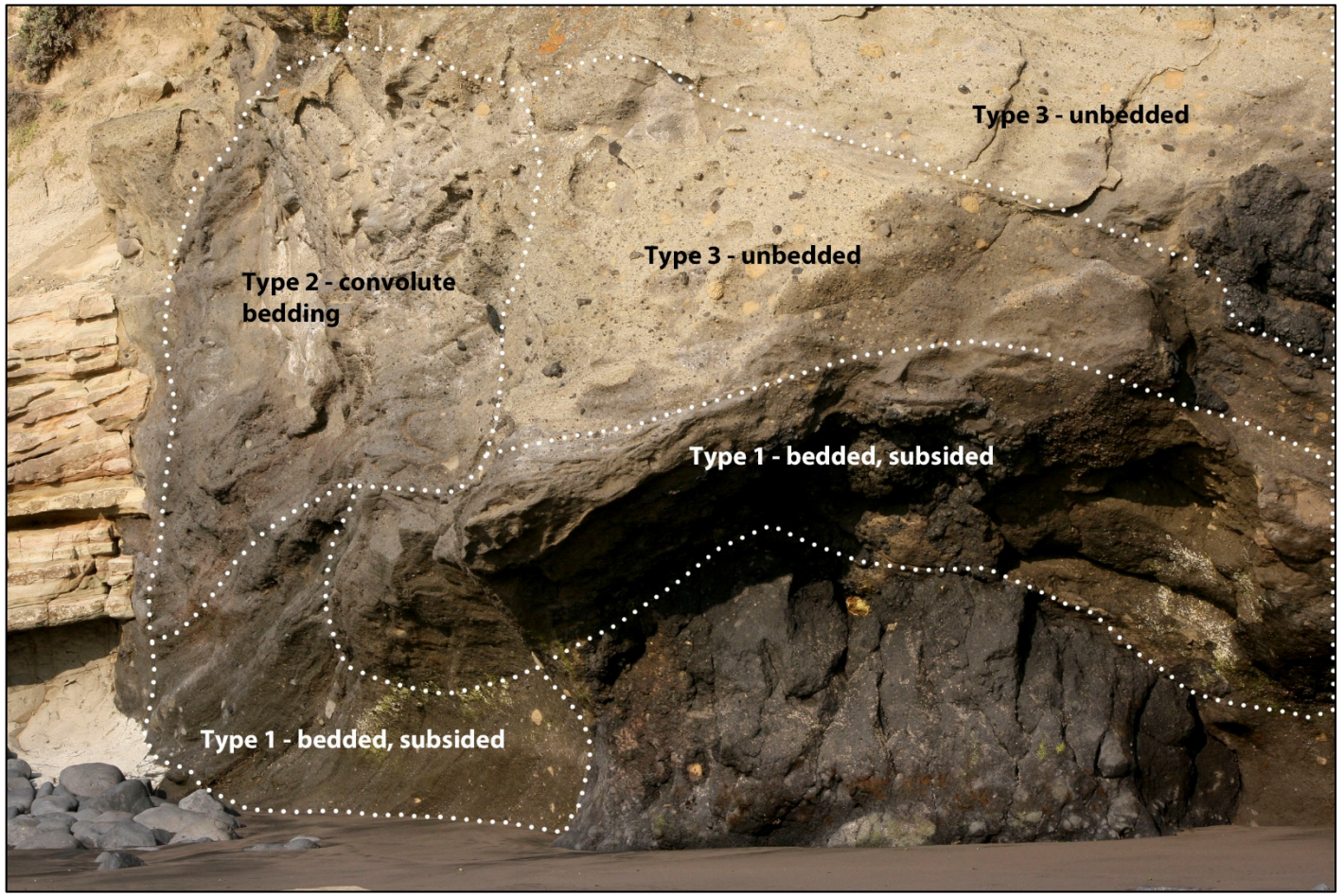

Figure 4.8 – Central view of the diatreme and its facies architecture. The northern face is to the left and the southern face to the right. Type 1 – bedded, subsided; Type 2 – convolute bedding; Type 3 – unbedded; Type 4 – unbedded, debris jet; Type 5 – bedded, country rock-poor; Type 6 – bedded, in situ. Field of view:12 m.

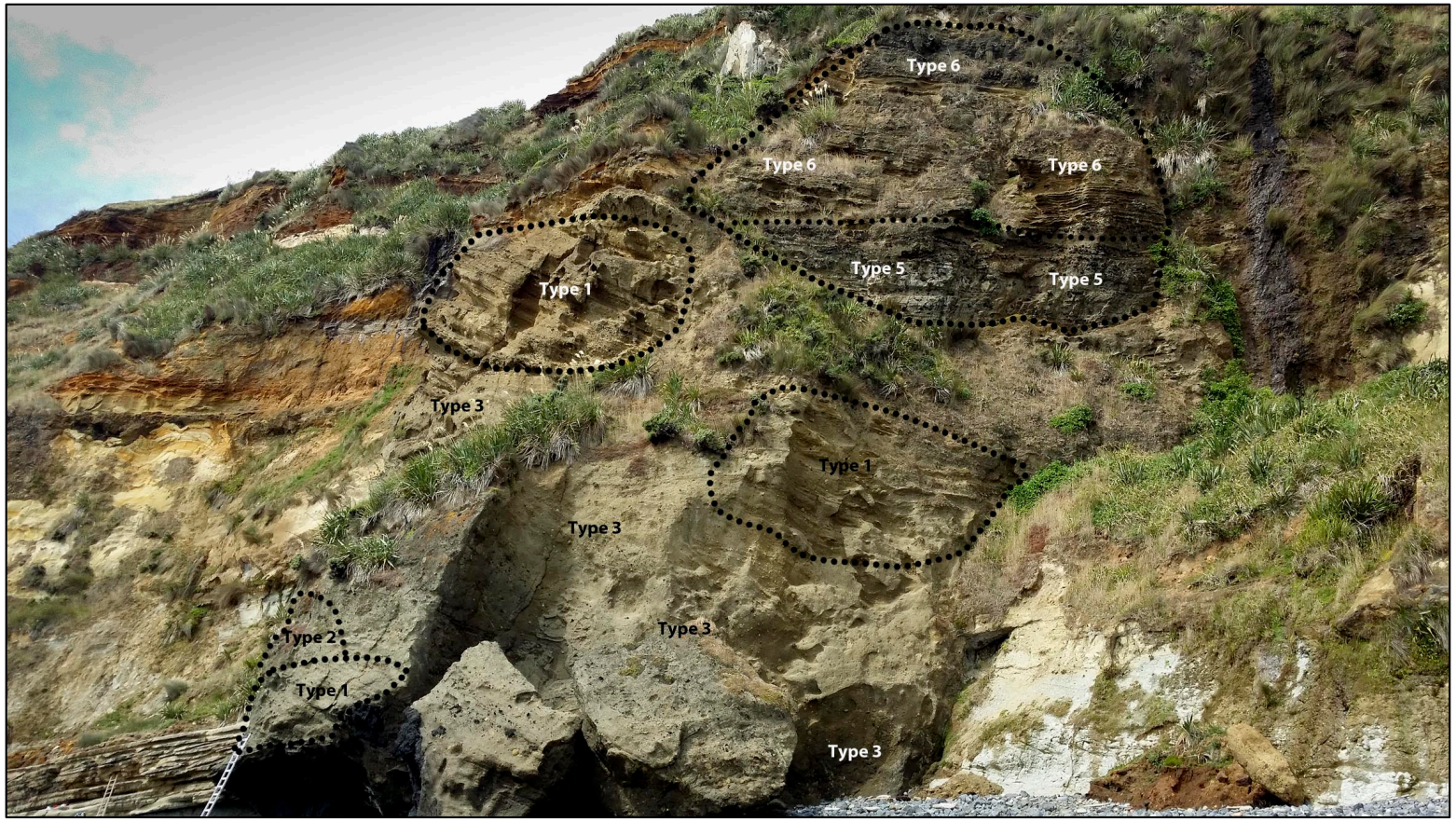

Figure 4.9 – The facies architecture of the diatreme's southern wall. Type 1 – bedded, subsided; Type 2 – convolute bedding; Type 3 – unbedded; Type 4 – unbedded, debris jet; Type 5 – bedded, country rock-poor; Type 6 – bedded, in situ. Field of view: 50 m.

these deposits, and they are classed as a lapilli tuff. The debris jet deposits are the most heterogeneous, in terms of componentry, of the diatreme deposits. These deposits lack any form of bedding or sedimentary structure and the matrix component is less pronounced. The matrix in the debris jet is much sandier than in other types of diatreme deposits. This deposit is mostly matrix-supported but grain-grain contacts are found in clusters.

The boundaries of the debris jet are poorly defined at a small scale, but becomes more pronounced at a distance. An oblong shape can clearly be traced within the surrounding type 3 deposits, and while some parts of the boundary is irregular the debris jet forms a distinct feature on the northern wall of the diatreme structure. The concentration of a wide variety of lapilli-block sized lithics and overall coarser grain size adds to its distinction.

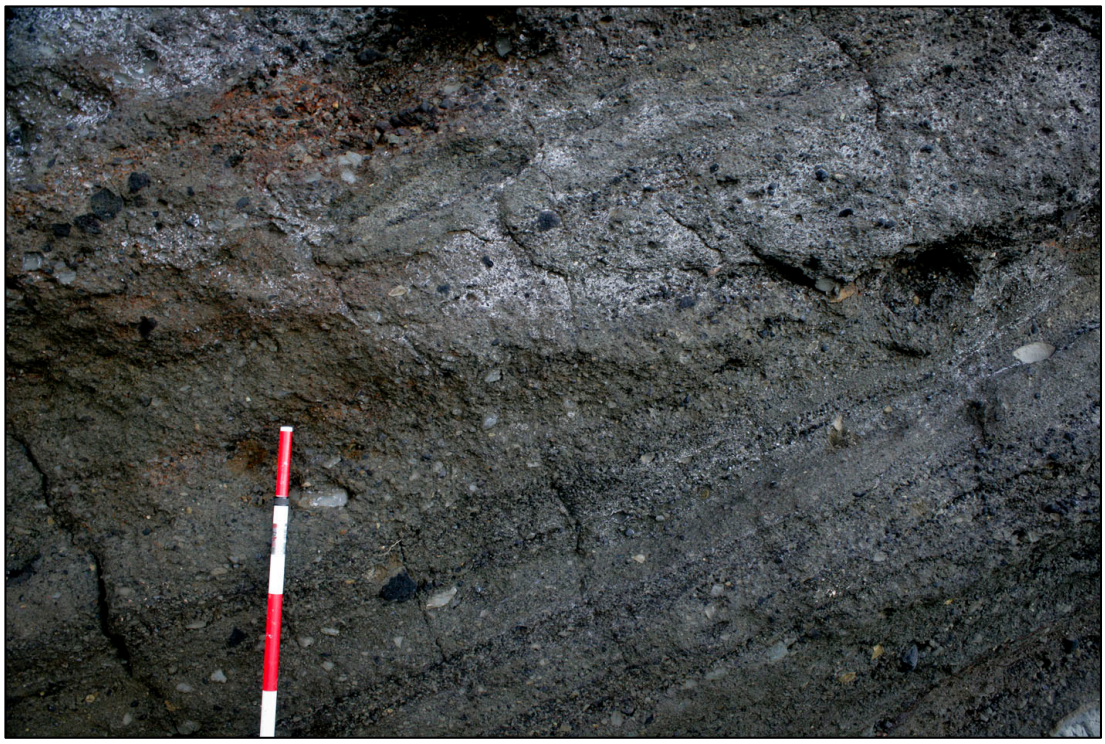

Figure 4.10 – Type 1 deposit: bedded, subsided lapilli tuff. Graduates on survey pole: 20 cm.

Type 5 – bedded, country rock-poor deposits

Type 5 deposits are tuff/tuff breccia deposits, which comprise planar, horizontal to sub-horizontal beds centimetres to decimetres in thickness, and are well sorted or bimodal where larger lithic clasts are present. These beds can vary sharply in grain size profiles and sedimentary textures. A defining feature of this facies type is the presence of variably thick, ash-rich layers, which often have a strongly erosive surface at their base, truncating thicker, coarser beds below. Sedimentary features of type 5 deposits exclude any form of syn- or diagenetic influence of water i.e. bomb sags or water escape structures. Matrix content comprise up to 91% of the total deposits and is generally pale brown in colour. Ash-rich layers have a matrix that is yellower in colour and have very few, if any, lapilli or block-sized lithics.

Figure 4.11 – Type 2 deposit: lapilli tuff with convolute bedding. Field of view: 2 m.

The lithics contained in type 5 deposits are almost exclusively basalt. The basalt lithics are usually non-vesiculated blocks, which are blocky and angular in shape. Some cauliflower-shaped blocks that are vesicular are found in a lesser quantity throughout this facies. In some places block-sized lithics are concentrated in bands, which form irregular beds, but the blocks are always supported by matrix and clast-clast contacts are rare.

On the surface of the outcrop a white precipitate covers extensive parts of the matrix. This effect is less apparent in the finer-grained ash-rich beds, compared to the sandier matrix which is found with abundant basalt lithics.

Figure 4.12 – Type 3 deposit: unbedded tuff breccia/lapilli tuff. Graduates on survey pole: 20 cm.

Figure 4.13 – Type 4 deposit: unbedded lapilli tuff of the debris jet. Field of view: 5 m.

Type 6 – bedded, in situ deposits

Type 6 deposits form the uppermost part of the diatreme structure. These deposits have the most well defined bedding structures, which are curved around the wider part of the cone-shaped diatreme wall. These tuff deposits are intricately bedded; beds vary from millimetres to several centimetres in thickness. Beds are laterally continuous, but in some places subhorizontal beds had been eroded and replaced by more horizontal beds (upper right, figure 4.15).

With less than 13% block- and lapilli-sized lithics these upper diatreme deposits are classed as a tuff; although, lithics are concentrated in bands several centimetres thick in places, while being absent from other areas. The grain size population therefore varies in grain size and degree of sorting throughout the facies. The matrix, which comprises up to 87% of these

deposits, is light brown in colour and the upper part is slightly ferruginised due to leaching from the overlying Awhitu Sand which is rich in iron.

The presence of country rock lithics is much less pronounced than in type 1 deposits, while clearly identified by their lighter, yellow colour being dominantly Pliocene in age (refer section 4.3.2). Basalt lithics are found as sporadic blocks of dense rock and smaller lapilli-sized basalt which are often concentrated in clusters.

Figure 4.14 – Type 5 deposit: bedded, country rock-poor tuff breccia/tuff. Field of view: 10 m.

Figure 4.15 – Type 6 deposit: in situ, bedded tuff of the upper diatreme. Field of view: 7 m.

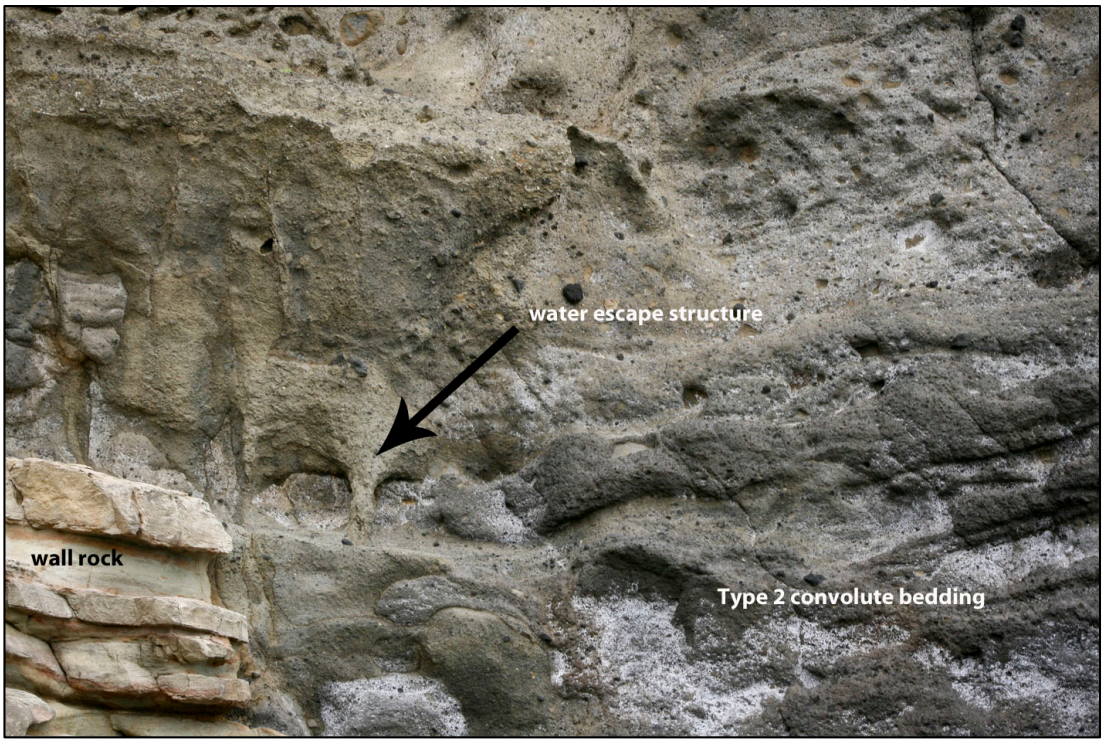

Figure 4.16 – Water escape structures in the Type 2 "convolute bedding" facies in the northern face of the diatreme. Field of view: 2 m.

Figure 4.17 – A raft of rotated and fallen beds of diatreme fill preserved in tact in the southern diatreme wall. Field of view: 15 m.

4.3.2 COMPONENTRY

The aim of the following two sections is to provide data that will shed light on the explosion dynamics within the diatreme during its formation. The abundance of components in a vertical profile can be used to determine the degree of wall rock erosion, as well as the proximity of explosion locales and the successive history of explosions and sedimentation during the formation of the diatreme.

Five types of lithic components were identified in the diatreme. Defining characteristics of each type are described in section 3.3. Analysis of photo and thin section data provided relative abundances of each lithic type in terms of area. Results of this analysis are summarized in table 4.1. Abundance of components are shown as area% and results have been normalized to exclude the matrix, therefore showing relative abundance.

Table 4.1 – Relative abundances of lithic types in the diatreme. Values have been normalised to exclude matrix.

Location	Height (m)	Jurassic %	Oligocene %	Miocene %	Pliocene %	Basalt %	Matrix %
L1	**2**	2.9	66.0	1.3	0.0	29.8	24.1
L2	**5**	7.1	57.1	0.0	0.0	35.7	86.0
L3	**10**	5.0	50.0	5.0	0.0	40.0	81.0
L4	**14**	2.5	45.0	15.0	0.0	37.5	59.0
L5	**23**	22.0	34.0	2.0	4.0	38.0	50.0
L6	**32**	0.0	1.1	8.2	24.7	66.0	87.9
R1	**2**	0.8	79.3	5.0	0.0	14.9	58.7
R2	**7**	2.6	53.4	16.8	0.0	27.2	57.6
R3	**14**	3.4	58.7	1.2	0.0	36.7	85.4
R4	**19**	0.0	19.0	4.8	0.0	76.2	79.0
R5	**25**	0.0	0.0	1.6	0.5	97.9	78.6
R6	**33**	0.0	0.0	10.0	10.0	80.0	91.0
R7	**38**	0.0	0.0	0.0	2.3	97.7	83.6

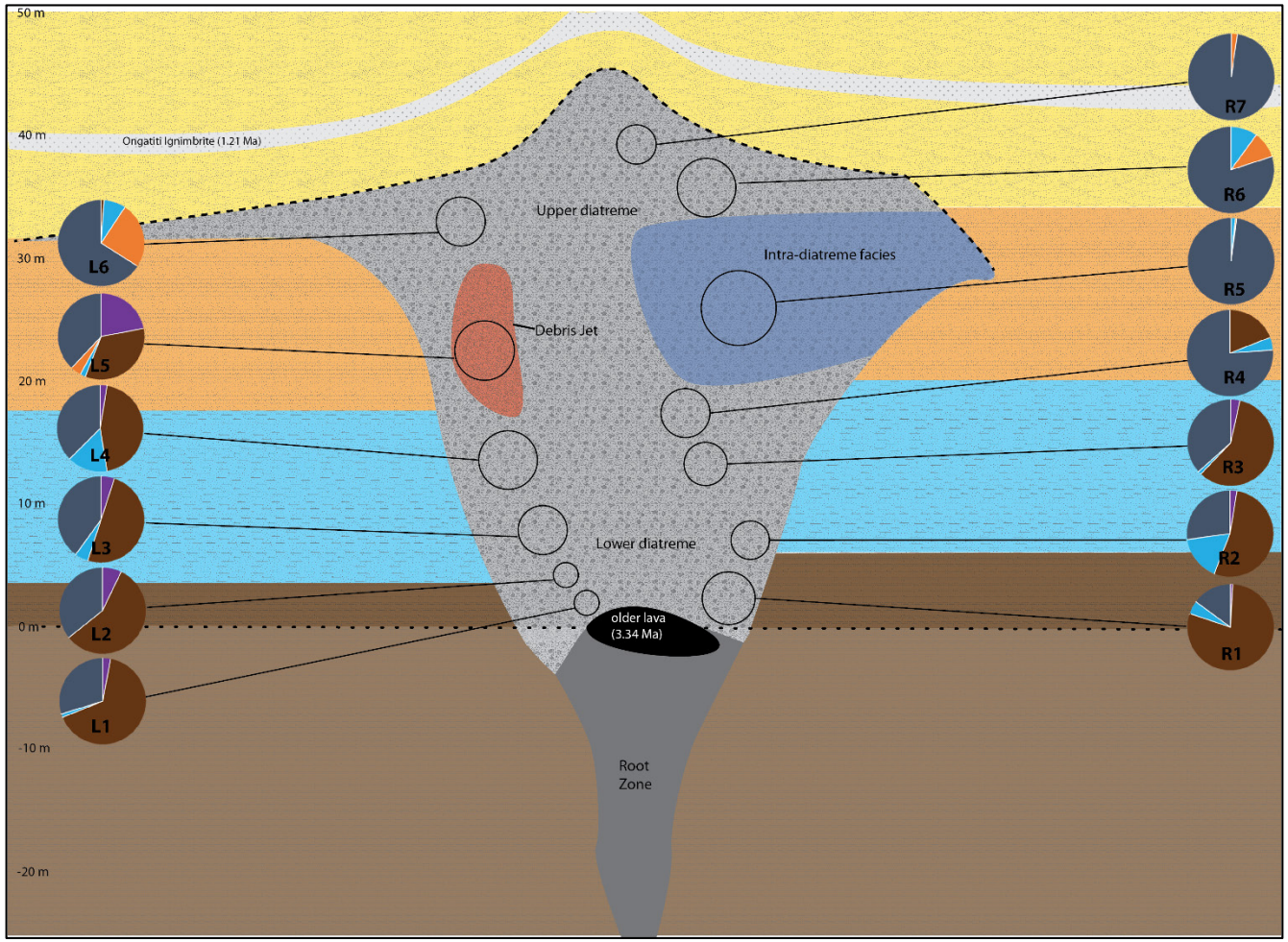

Figure 4.18 – Componentry of the diatreme. Circle graphs show percentages (excluding matrix) of each type of lithic found in corresponding sampling areas within the diatreme. Jurassic-age lithics are shown in purple.

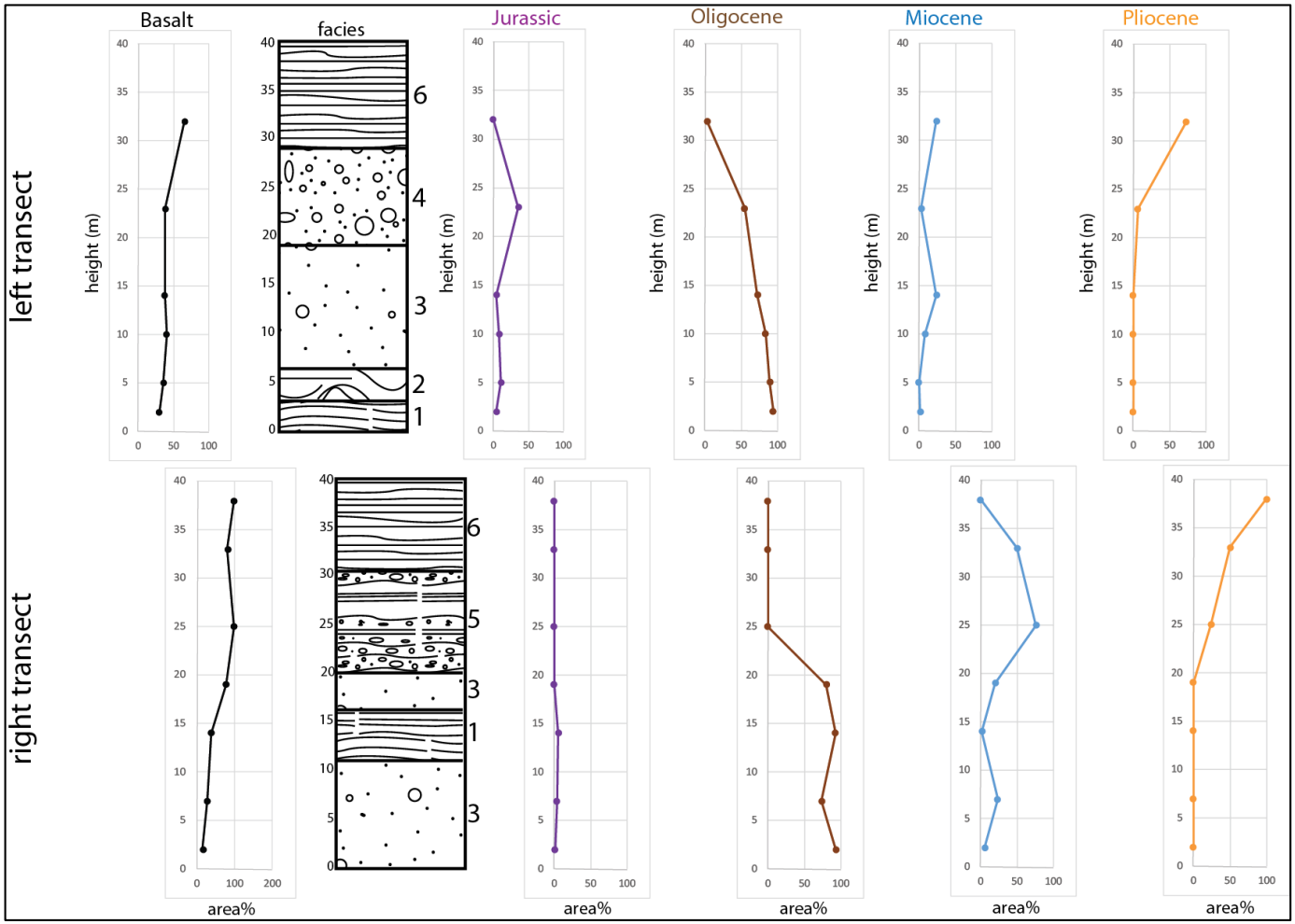
left transect
right transect
Basalt
facies
Jurassic
Oligocene
Miocene
Pliocene
height (m)
area%
6
5
4
3
2
1

Figure 4.19 (p. 84) – Abundance of lithic components (area%) in two vertical transects of the diatreme structure. Data have been normalized to exclude basalt and matrix components for country rock lithics, and to exclude matrix for basalt lithics.

The distribution of each type of lithic (Jurassic-, Oligocene-, Miocene- and Pliocene-age lithics) is discussed below:

Lithics of Jurassic age are the oldest in the country rock stratigraphy. These siltstone (and some conglomerate) lithics are most commonly found as medium to large lapilli, often well rounded with fracture patterns of the parent lithology preserved within. The abundance of this type of lithic is shown in figures 4.18 - 4.19 and table 4.1. The Jurassic-age lithics are common in lower parts of the diatreme, but only in low concentrations comprising up to 7% of the total lithic components. However, concentrations of up to 22% are found in the debris jet (L5, figure 4.18). Jurassic-age lithics are absent from the upper diatreme above the debris jet.

Lithics of the Oligocene comprise the Ahirau Sandstone, Carter Siltstone and some minor limestones. This is the most common lithic type and is almost ubiquitous in the diatreme. While absent from the intra-diatreme facies type 5 (R5, figure 4.18) it is found in high concentrations (<79%) in the lowermost part of the diatreme exposure and comprises 20-50% of lithics at intermediate levels. The concentrations of Oligocene-age lithics decrease with height (figure 4.19).

Miocene-age lithics are clearly distinguishable from lithics of the Oligocene by having a much coarser sand component and being much more friable than the well indurated Oligocene sediments. Miocene-age lithics of the Waikawau Sandstone are found ubiquitously in the diatreme, albeit in very low concentrations in most parts. Miocene-lithics are most common around the central lower diatreme, which is adjacent to their parent rock (4-18 m, figure 4.18). However, when the prevalence of this lithic type is compared with

others, excluding basalt, the Miocene-age lithics are more common in the upper diatreme, especially in the country rock-poor facies (R5, figure 4.18).

Lithics of the Pliocene (Kaawa Fm. sandstone) are found exclusively in the upper diatreme in which concentrations never exceed 25%. The lowermost occurrence of Pliocene lithics is in the debris jet at 4%. The deposits in which Pliocene lithics are found are dominated by basaltic lithics. The Pliocene sandstone lithics are typically obliterated and concealed in the fine matrix.

A few key observations are made:

- Jurassic lithics have their origin at ~ 90-220 metres below the surface and are present in relatively strong concentrations in the debris jet, yet is completely absent from the upper diatreme.
- Oligocene lithics are very abundant in the lowermost part of the exposure, close to their source lithologies, and maintain a strong presence throughout most of the diatreme, but is absent from the upper diatreme.
- The concentration of Miocene lithics is highest adjacent to its source, but is also the most abundant country rock lithic in the upper diatreme (figure 4.19).
- Pliocene-age lithics are found exclusively in the upper diatreme and debris jet, and are found only in relatively low concentrations. Pliocene lithics are not found at levels below their source lithology.
- Overall, Jurassic lithics comprise 3.56% of the total componentry, Oligocene lithics 35.66%, Miocene lithics, 5.46%, Pliocene lithics 3.19%, and basaltic lithics 52.13%.

4.3.3 GRAIN SIZE ANALYSIS

Grain size distributions were calculated for each of the sample areas shown in figure 4.18. The results are combined data from photos and thin sections (coarse and fine fractions, respectively) with the -2φ fraction interpolated using the Cubic Spline method (section 3.3). Results are summarized in table 4.2 and figures 4.20 – 4.23.

The diatreme fill deposits are characterised by bimodal grain size distributions consisting of block to lapilli sized lithics suspended in a fine, sandy matrix. This is true not only of the deposits in their entirety, but also of the grain size distributions of individual components e.g. basalt or Oligocene-age lithics. Almost all of the samples show bimodal distributions in the basalt and Oligocene-lithics populations (figure 4.20). The distributions of these populations are strikingly similar to that of the overall population.

The proportion of block, lapilli, and ash-sized clasts for each sample was plotted on the ternary volcaniclastic rock classification diagram (figure 4.22) of Fisher & Schminke (1984). Some of the block-rich basal samples plot in the tuff breccia field (R1, R2), however, most samples with modes in the lapilli and ash fractions are classed as lapilli tuff. Samples of the uppermost diatreme lack significant block or lapilli populations and so plot in the tuff field (L6, R6, R7).

Variations in the ratios between finer and coarser components for both the overall grain size and basalt populations were quantified by plotting ratios of fine (3 - 4φ) & coarse ash (-1 - 0φ), and lapilli (-5 - -3φ) & blocks (-7 - -6φ) vs. height. The ratio between fine and coarse ash increases with height in the right transect while remaining low in the left transect. For the basalt population the ratio between fine and coarse ash decreases slightly with height in both transects.

Table 4.2 – Grain size analysis of diatreme deposits (phi-classes shown as area%)

	-7Φ	-6Φ	-5Φ	-4Φ	-3Φ	-2Φ	-1Φ	0Φ	1Φ	2Φ	3Φ	4Φ	$Mean_{\Phi}$	$Sorting_{\Phi}$	$Skewness_{\Phi}$	$Kurtosis_{\Phi}$
L1	10	11	25	24	6	4	9	5	3	2	1	0	-4.3	1.8	1.0	0.5
L2	1	3	8	2	0	12	24	27	13	5	3	1	-1.1	2.0	-0.2	1.6
L3	0	3	12	4	1	14	24	18	12	8	4	2	-1.7	2.6	-0.2	1.2
L4	4	14	15	5	2	12	20	15	6	5	1	0	-2.9	2.7	-0.2	0.7
L5	14	7	16	9	4	11	16	12	8	2	1	0	-3.4	2.1	0.6	0.3
L6	1	2	4	3	1	-	-	-	-	-	-	-	-5.5	0.6	-4.1	-0.1
R1	16	12	10	2	1	14	22	14	7	2	1	0	-3.2	2.0	0.4	0.2
R2	12	14	11	4	2	-	-	-	-	-	-	-	-5.1	-0.8	-2.8	-2.1
R3	2	2	6	3	1	19	31	20	11	2	1	0	-1.5	1.8	-0.2	1.4
R4	4	6	8	3	1	9	19	25	14	8	4	1	-1.8	2.8	-0.4	1.4
R5	5	9	5	2	0	10	22	21	8	7	8	2	-1.8	3.2	-0.3	1.5
R6	2	3	3	1	0	-	-	-	-	-	-	-	-5.4	-0.4	-32.4	-0.7
R7	3	6	5	3	0	-	-	-	-	-	-	-	-5.9	0.1	-1.1	-0.6

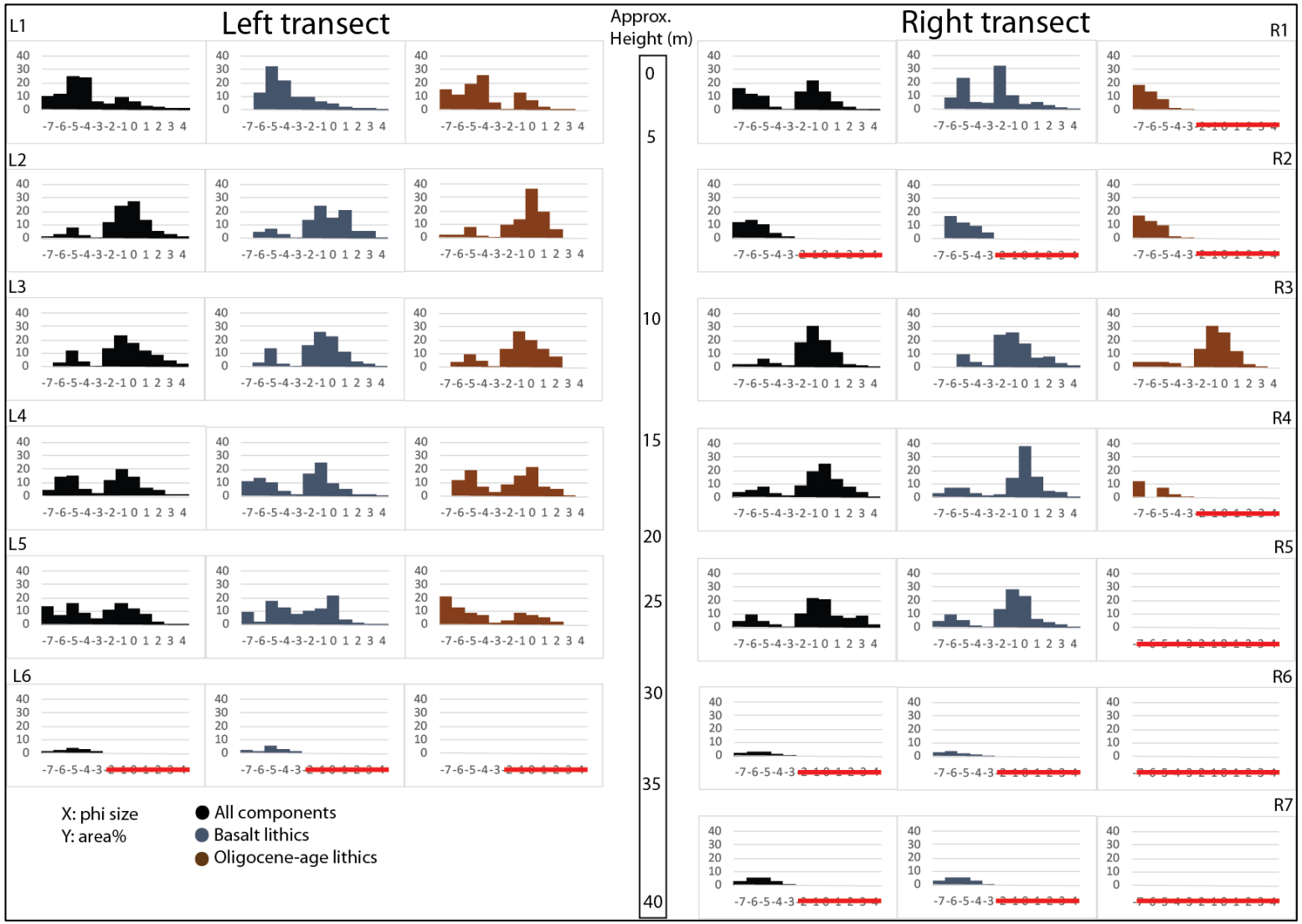
Left transect
Right transect
Approx. Height (m)
L1
L2
L3
L4
L5
L6
R1
R2
R3
R4
R5
R6
R7
0
5
10
15
20
25
30
35
40
X: phi size
Y: area%
All components
Basalt lithics
Oligocene-age lithics

Figure 4.20 (p. 89) – Grain size distributions of diatreme deposits in two vertical transects. Overall grain size is shown in black, basalt lithic population in grey, and Oligocene-age lithics in brown. Red zones are indicated where data were not obtained

For the overall distribution, the ratio between blocks and lapilli remains low throughout the left transect, while fluctuating more in the right transect following a slightly decreasing trend with height. The basalt population shows very similar variations in the block to lapilli ratio, but instead shows a slightly increasing trend in the right transect.

The statistical parameters of each grain size distribution was calculated with the Gradistat.xls program (Blott & Pye, 2001) using the Folk & Ward (1957) method. However, these parameters might not represent bimodal distributions accurately. Sorting values are typically quite low, partially due to the bimodality of samples. The kurtosis of individual peaks of modes are quite similar overall, but some variation does occur, especially in some of the samples from the upper diatreme, which have platykurtic modal distributions The mean grain size of the samples is highly variable and reflects the generally poorly sorted nature of the diatreme deposits.

Cumulative grain size distributions (figure 4.21) show variability in overall grain size of the diatreme deposits. In the left transect, the lowermost sample (L1) is enriched in lapilli-sized grains, while L2 (located c. 2 m above L1) is much more depleted in the coarser fraction with 50% of the grains being finer than -1φ. The distributions in the right transect are less variable than those in the left transect, and the variability is slightly more systematic. Lower samples are slightly enriched in the coarse fraction, while stratigraphically higher samples are typically depleted in coarse grains.

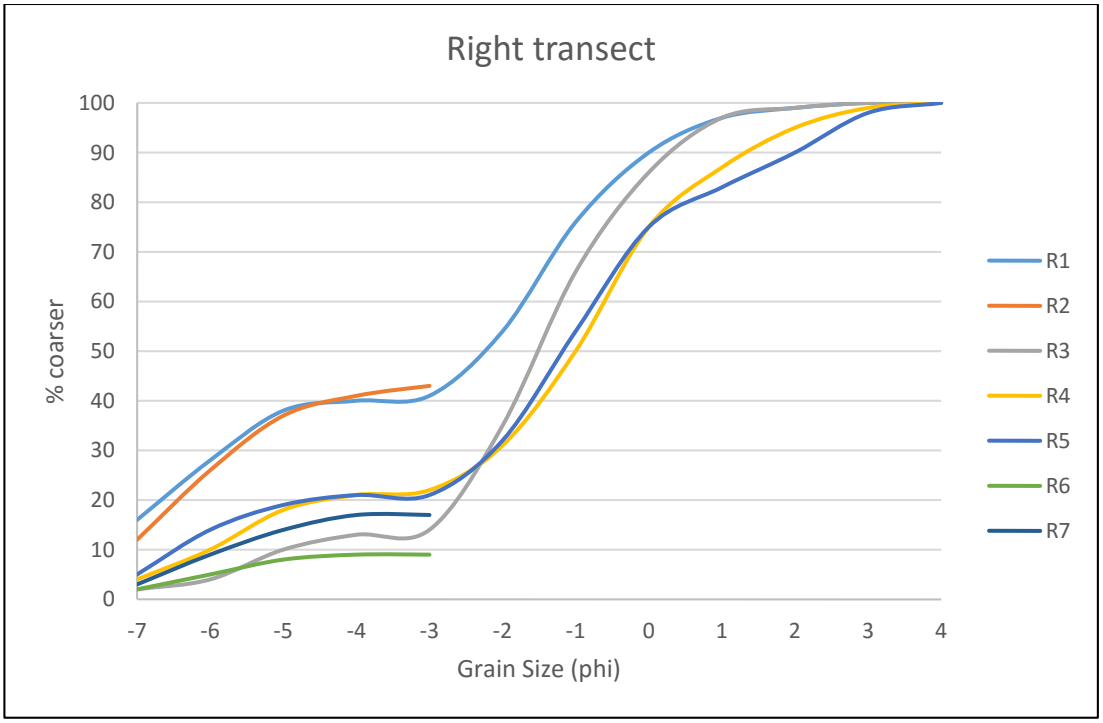

Figure 4.21 – Cumulative grain size distributions of the left and right vertical transects of the diatreme. L6, R2, R6 & R7 are truncated distributions showing only the coarse fraction (-7 - -3φ)

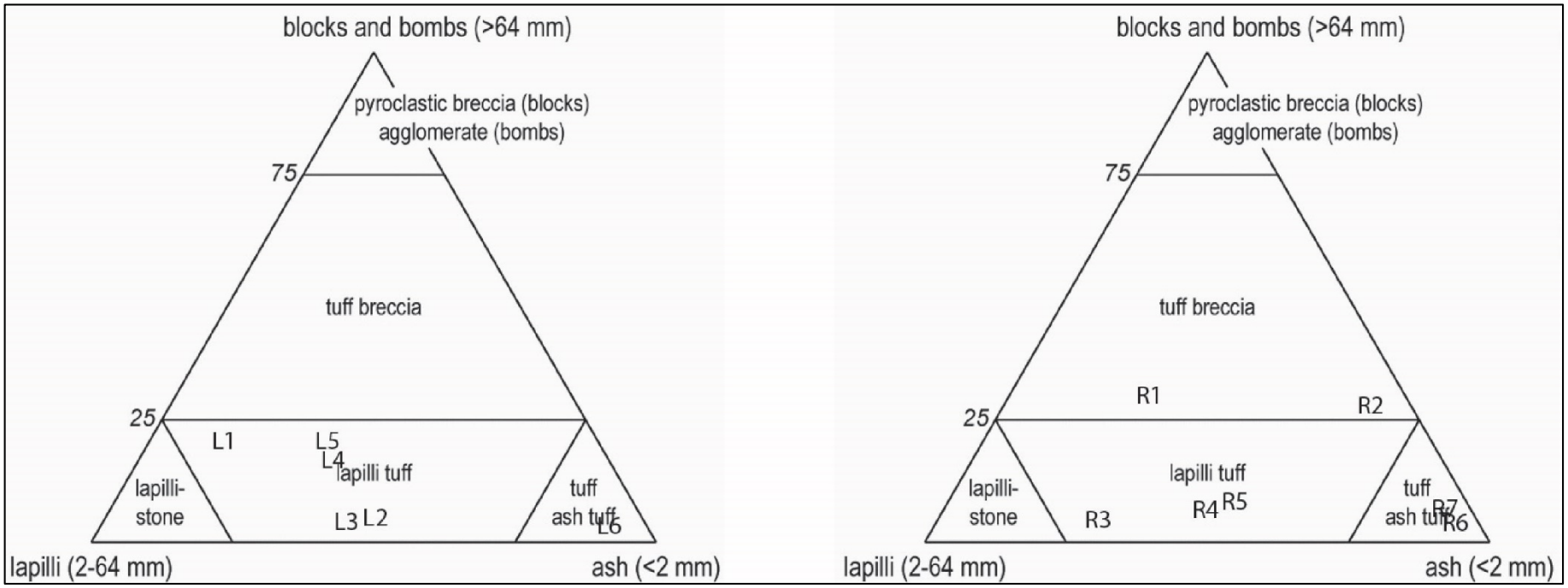

Figure 4.22 – Volcaniclastic rock classification (after Fisher & Schminke, 1984) of vertical transect intervals (left and right transects) of the diatreme. Sample locations are shown in figure 4.18.

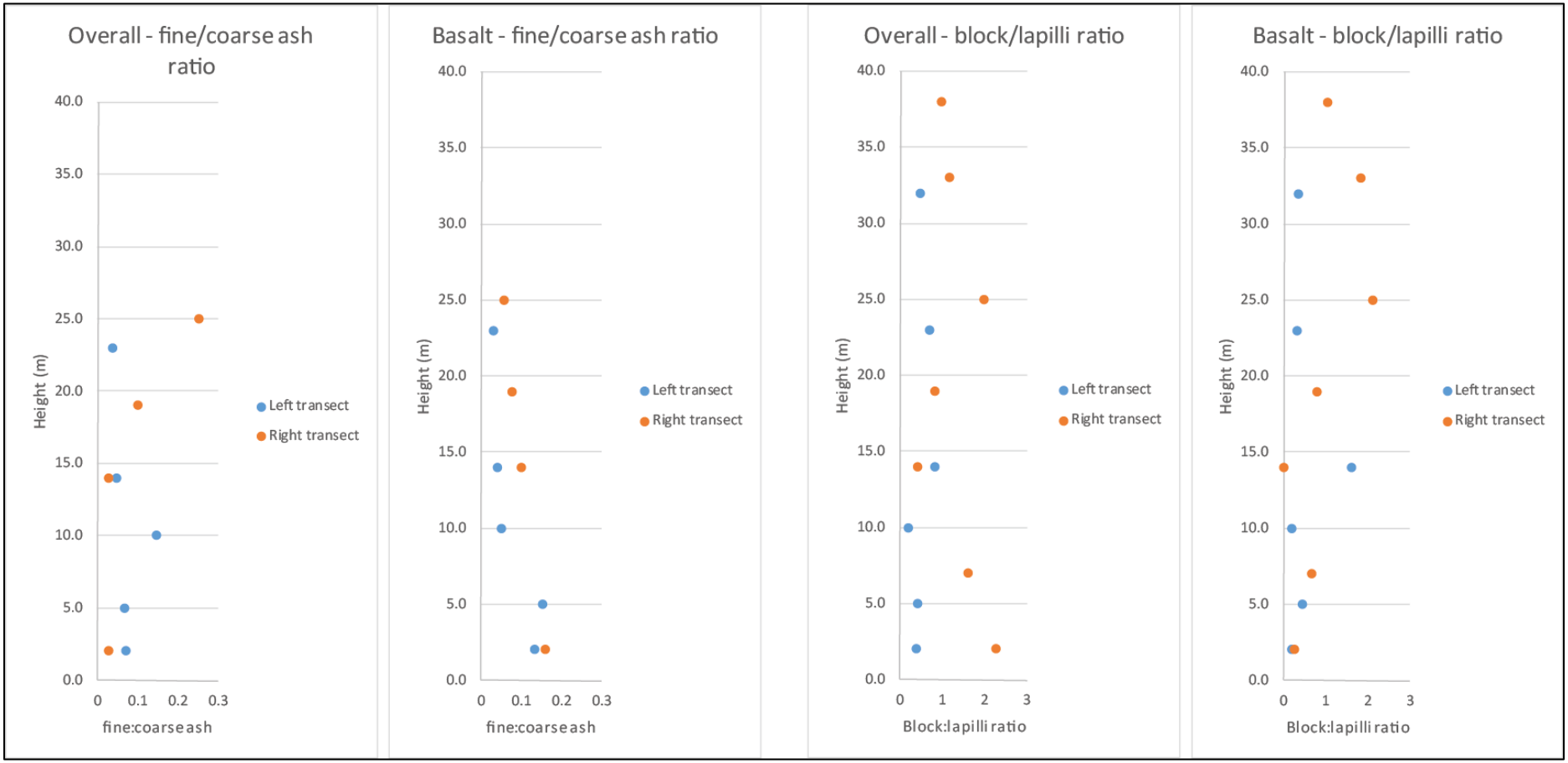

Figure 4.23 – Ratio of fine to coarse ash and block to lapilli size clasts for all components, and basalt, for the two vertical transects of the diatreme. Fine ash (3 ~ 4φ); coarse ash (-1 ~ 0φ); lapilli (-5 ~ -3φ); blocks (-7 ~ -6φ).

4.4 THERMAL ALTERATION OF COUNTRY ROCKS

The emplacement of Dyke B in the Carter Siltstone has resulted in thermal alteration of the highly calcareous siltstone. A baked zone of more than 1.5 m wide is found surrounding the dyke. The following sections report on the degree of decarbonisation of the siltstone, as well as the mineralogical changes that accompany the loss of calcium carbonate as a result of thermal alteration.

4.4.1 CALCIUM CARBONATE CONTENT

At Dyke B, the calcium content of the Carter Siltstone was measured in a horizontal transect with 20 cm intervals from the dyke-contact through a baked margin of more than 1.5 m. Based on the amount of HCL consumed in titrations (section 3.4) the calcium carbonate content of the baked margin at Dyke B is 2.4-3.0% (table 4.3). XRD-results reveal, however, that there is no calcite present in these samples at all. These findings are discussed in section 4.4.2.

The apparently unbaked sample at 160 cm from the dyke shows the effects of some thermal alteration, with its carbonate content being 27% lower than a reference sample taken from unaltered Carter Siltstone ~300 m from the dyke. The effects of baking decline rapidly after 140 cm from the dyke, but it is now apparent that ambient heat affected a larger portion of the siltstone than is visible in outcrop.

Carter Siltstone lithics were extracted from samples of the diatreme deposits of the left and right vertical transects. Samples 20-50 mm in diameter are shown in bold in table 4.3. Samples from smaller lithics (5-10 mm) contain infinitesimal amounts of carbonate. The larger lithics, however, contain significant amounts of carbonate, up to 29%.

Table 4.3 – Percentage of calcium carbonate consumed by HCL in titrations.

Sample	$CaCO_3$ (wt.%)
Carter Siltstone	77
Dyke 20cm	2.62*
Dyke 40cm	2.59*
Dyke 60cm	2.40*
Dyke 80cm	2.62*
Dyke 100cm	2.62*
Dyke 120cm	2.78*
Dyke 140cm	3.00*
Dyke 160cm	50.26
Diatreme L1_A	0.05
Diatreme L1_B	**28.9**
Diatreme L2_A	0.05
Diatreme L2_B	0.2
Diatreme L3_A	0.1
Diatreme L3_B	0.01
Diatreme L4_A	0.03
Diatreme L4_B	0.05
Diatreme L5	0.04
Diatreme R1	**4.49**
Diatreme R3_A	0.05
Diatreme R3_B	0.2
Diatreme R4	0.05
Diatreme R5_A	**7.5**
Diatreme R5_B	0.07

Samples in bold indicate lithics 20-50 mm in diameter. All other diatreme samples contain lithics 5-10 mm in diameter.

*These values should be around zero. The higher values are attributed to mineralogical changes due to hydrothermal alteration of the siltstone, discussed in section 4.4.2.

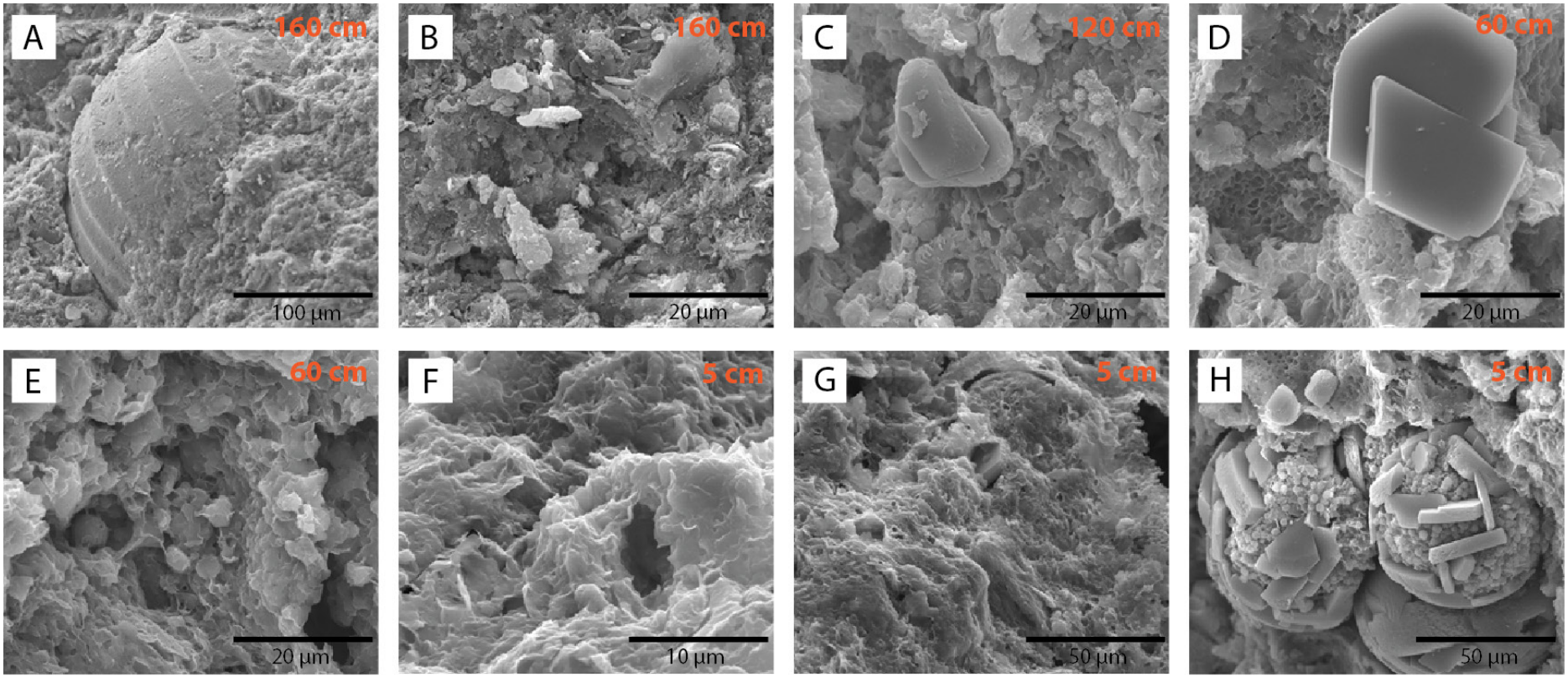

Figure 4.24 – BSE-images of unaltered and baked samples of the Carter Siltstone at Dyke B. Distance from dyke is shown in upper right corners. (A) Unaltered siltstone with shell fragment and calcite cement. (B) Unaltered siltstone with calcite platelets. (C) Partially baked siltstone with remnants of a coccolith plate, portlandite crystal (centre) and MgO crystal clusters (upper right). (D) Portlandite crystal in baked siltstone. (E) Early stages of sepiolite growth in baked siltstone. (F) Baked siltstone with sepiolite, close to the dyke. (G) Small portlandite crystals in sepiolite. (H) Microfossil spheres: calcite shells replaced with portlandite (larger crystals) and MgO micro-crystal clusters.

4.4.2 MINERALOGICAL CHANGES

When heat (700-900°C) is applied to calcium carbonate, its molecular structure breaks down to release carbon dioxide. The resultant solid is calcium oxide, which readily hydrates to form calcium hydroxide, when exposed to the atmosphere or pore water. In a heated environment calcium hydroxide can precipitate from oversaturated fluids to form portlandite crystals. These crystals were identified based on their hexagonal structures in BSE images (figure 4.24) and XRD traces match that of portlandite with peaks at 35.01(2.98), 17.89(8.09) and 47.11(4.53).

Magnesium oxide microcrystal structures are found in baked samples, often closely associated with larger, portlandite crystals and in one case have formed within ichnofossil spheres (H, figure 4.24). Magnesium oxide microcrystal structures are widely reported in the literature, especially in the field of nanostructures (e.g. He, 2006.)

In well-baked samples abundant clay structures were found (figure 4.24). Based on XRD peaks at 12.3(9.01), 2.39(0.9) and 3.9(1.2) these clays were identified as sepiolite in the minerals database (c.f. Yalcin & Bozkaya, 1995). Sepiolite forms in hydrothermal environments as a product of serpentinite alteration (Korbel & Novak, 2001). Its sister mineral, palygorskite, is reported in similar environments in the Waikato region (Kirkman & Wallace, 1994).

Sepiolite is a magnesium-rich clay with a complex inverted tetrahedral structure (Franco et al., 2014). When reacted with hydrochloric acid, the structure is partially digested by the acid to release Mg^{2+} ions in an aqueous solution. This reaction therefore consumes acid. When samples from the baked zone at Dyke B were tested for calcium carbonate content, sepiolite was present in all but the least baked samples. The indicated presence of calcium carbonate is thus attributed to the presence of clay, which reacted with the acid, and BSE images (figure 4,24) confirmed that no calcite is present in baked samples.

However, the mineralogical changes described above are not seen in the baked lithics of the diatreme. No sepiolite or portlandite was detected in these samples. Where acid reacted to the sample to indicate the presence of calcite, the reaction was visible in the form of gas bubbles escaping. The baked lithics from the diatreme also lacked the dark-brown colouring of the samples at Dyke B.

4.5 GEOCHEMISTRY OF THE NGATUTURA BASALTS

4.5.1 MINERALOGY

Olivine, clinopyroxene and plagioclase phenocrysts from basalt of the Ngatutura Bay Volcanics were analysed. Results are shown in figures 4.25-2.27. The clinopyroxene phenocrysts plotted at the compositional boundary between diopside and augite. Older (e.g. Ngatutura Point lavas) and younger features (e.g dykes A & B) have similar compositions and in light of the mafic composition of the lava the clinopyroxe phenocrysts are diopside-rich augite.

Plagioclase phenocrysts of the Ngatutura Bay Volcanics plot near the andesine-labradorite boundary. The older volcanic features, Ngatutura Point lava and lava at the base of the diatreme, plot deeper in the andesine field, while the younger Dykes A & B plot in the labradorite field, indicating a slight compositional shift during the history of the volcanism.

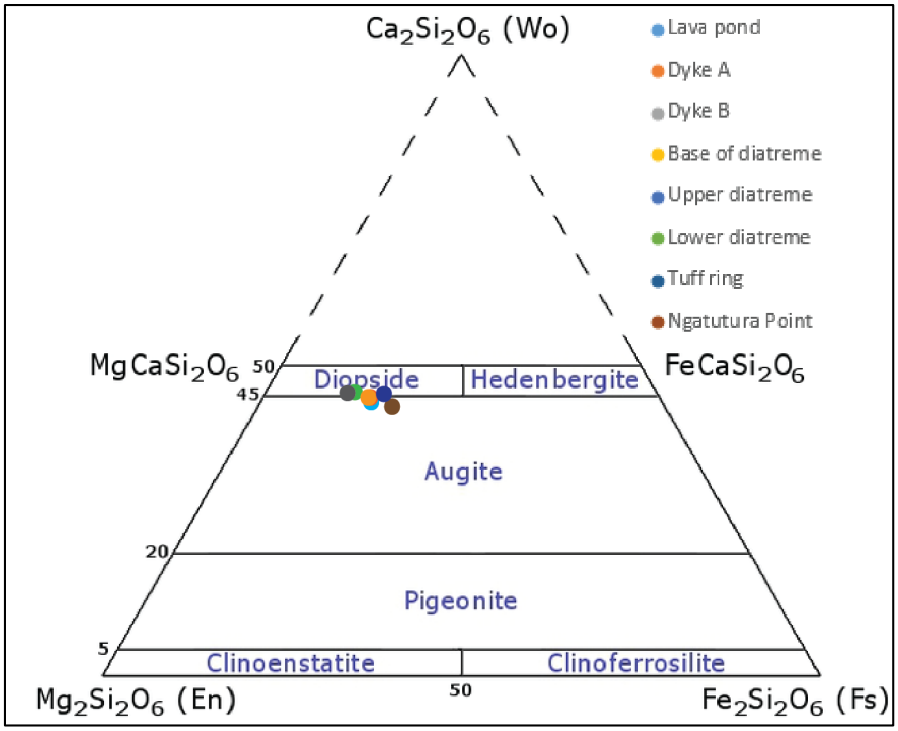

Figure 4.25 – Quadrilateral clinopyroxene classification of the Ngatutura Basalts (after Morimoto, 1988).

Table 4.4 – Representative compositions of olivine crystals from the Ngatutura Bay Volcanics.

	Lava Pond	Dyke A	Dyke B	Lava at base of diatreme	Upper Diatreme	Lower Diatreme	Tuff Ring	Ngatutura Point Lava
SiO_2	39.48	39.49	39.53	39.34	39.80	39.28	39.87	37.76
MgO	40.70	40.55	40.96	40.43	40.88	39.15	40.28	33.18
FeO^{tot}	18.99	19.67	18.99	18.96	19.67	20.47	20.85	28.63
CaO	0.29	0.24	0.30	0.25	0.28	0.29	0.30	0.43
NiO	0.14	0.12	0.15	0.19	0.14	0.13	0.09	0.01
MnO	0.40	0.38	0.32	0.33	0.33	0.33	0.40	0.78
Total	100.21	100.59	100.62	99.95	101.40	100.26	102.24	100.93
Fo (mol%)	78.39	78.01	78.75	78.59	78.16	76.53	76.78	76.78

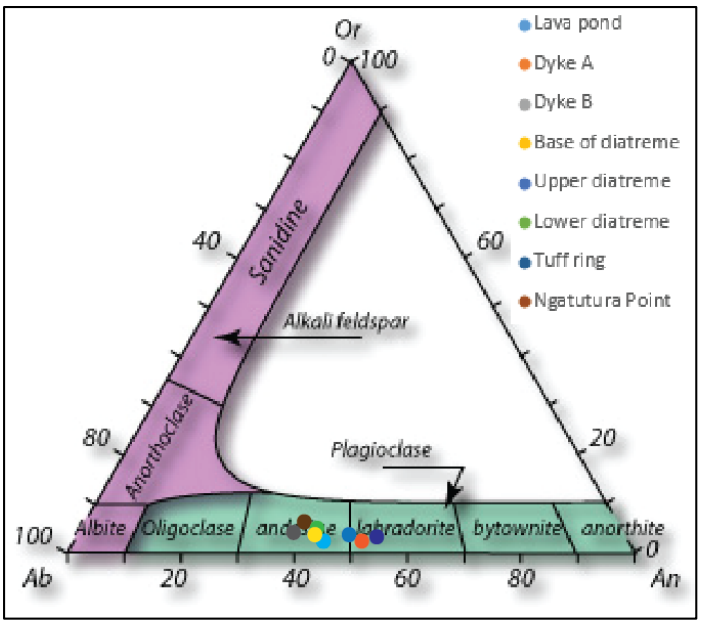

Figure 4.26 – Ternary classification diagram for plagioclase – Ngatutura Basalts.

4.5.2 OLIVINE GEOCHEMISTRY

Olivine phenocrysts are up to 3 mm in diameter and are euhedral to subhedral in shape, in some cases with an altered margin of iddingsite or bowlingite. Forsterite content is variable (figure 4.27) and fall in the range $Fo_{(81-65)}$. Utting (1986) reports values of $Fo_{(90-49)}$ for the Ngatutura Volcanic Field, while Rafferty & Heming (1979) report values of $Fo_{(85-55)}$ for the South Auckland Volcanic Field, and Briggs & Goles (1985) report values of $Fo_{(90-55)}$ for the Okete Volcanics.

The compositional variation of olivine phenocrysts in the Ngatutura Bay basalts is shown in figure 4.27. The most distinctive group is from the Ngatutura Point lavas, which is low in forsterite, but contain higher amounts of CaO. Lava at the base of the diatreme (which is similar in age to the Ngatutura Point lavas) also plot in a distinctive group, however with contrasting high forsterite and low CaO contents. Lithics from the diatreme show more diverse compositions – $Fo_{(80-70)}$. The olivines of dykes A & B have very similar compositions and are relatively tightly grouped.

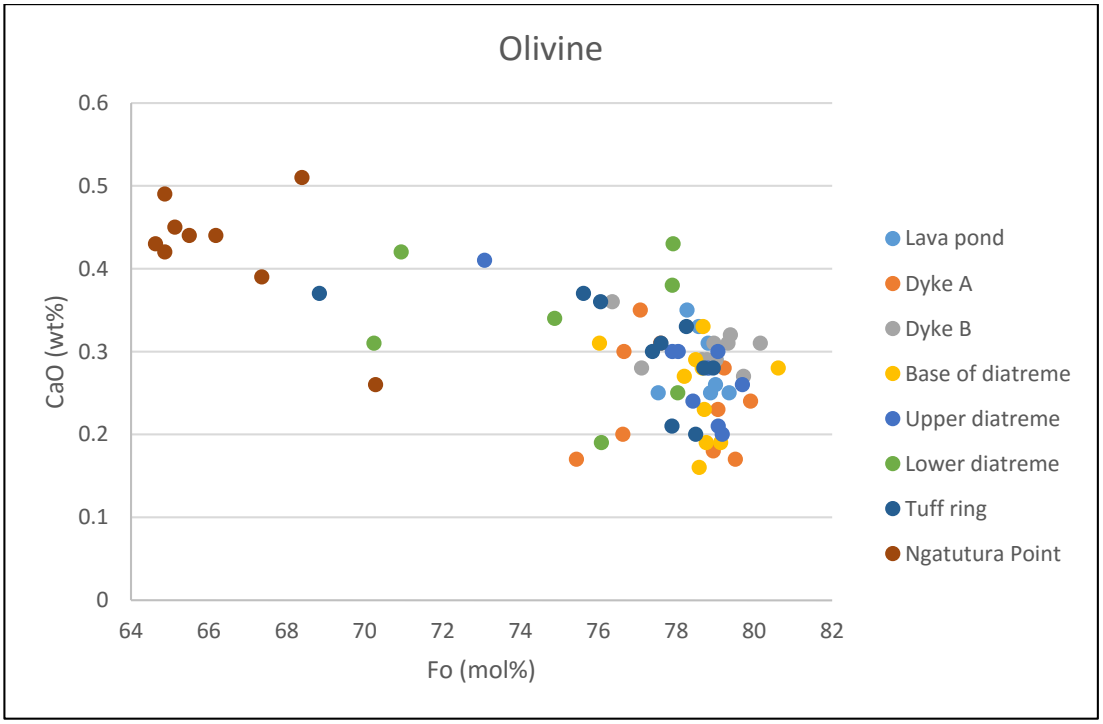

Figure 4.27 – Olivine geochemistry of the Ngatutura Bay Volcanics: Fo (mol%) vs. CaO (wt.%).

4.6 K-Ar Dating

K-Ar dates were obtained for five samples of the Ngatutura Bay Volcanics. None of the samples contained ultramafic xenocrysts or excessively large phenocrysts. The groundmass of the samples is microcrystalline with some interstitial glass. Microlites include plagioclase, clinorpyroxene, magnetite, olivine, and rare nepheline.

The ages of younger features fall within the range of 1.83-1.54 Ma reported by Briggs et al. (1989), while the older features returned ages considerably older than any of the Pliocene-Pleistocene volcanic fields of the upper North Island, at 3.22-3.34 Ma. The oldest ages reported by Briggs et al. (1989) are for the Alexandra Volcanic Field at 2.74 Ma.

Table 4.5 – K-Ar age determinations for Ngatutura Bay Volcanics

No. of K/Ar	Sample	Formation	K (%)	$^{40}Ar_{rad}$ (ccSTP/g)	$^{40}Ar_{rad}$ (%)	K/Ar age (Ma)
8482	Dyke B	g.m.	1.042	6.9799 x10^{-8}	16.4	1.72±0.14
8483	Dyke A	g.m.	1.010	7.1317 x10^{-8}	17	1.81±0.14
8619.	Ngatutura Point	g.m.	1.045	1.2511 x10^{-7} 1.3649 x10^{-7}	6.6 14.3	3.08 3.36
8620.	Lava at diatreme base	g.m.	1.299	1.6891 x10^{-7}	6.9	3.34±0.06
8621.	Tuff ring	g.m.	0.864	5.9057 x10^{-8} 1.4723 x10^{-8}	2.5 2.4	1.76 0.438 ??

Figure 4.28 – K-Ar dates determined for the volcanic features of Ngatutura Bay. While the accuracy of the tuff ring age is questioned, the date fits well within the timeframe of the emplacement of dykes A & B.

CHAPTER 5 – DISCUSSION

5.1 PALEOENVIRONMENTAL RECONSTRUCTION

The influence of environmental factors on volcano development has been demonstrated to be profound, particularly at basaltic volcanic fields (e.g. Kereszturi & Németh, 2013; Kereszturi et al., 2011; Kienle et al., 1980; White, 1991). Environmental factors to volcanism include the presence and supply of water at the surface and in the substrate, the nature of sediments near or at the surface, and the tectonic regime (both affecting the local stress field and fracture patterns in the substrate). The development of certain volcanic features, e.g. the diatreme at Ngatutura Bay, depends on specific environmental conditions i.e. groundwater availability. In time, the evolution of the paleoenvironment also controls the erosion of volcanic features and the landscape in which they formed.

The Ngatutura Bay Volcanics are deeply incised, but features are extremely well preserved, often in three dimensions. The various volcanic features represent long-lived basaltic volcanism with two major eruption episodes inferred from K-Ar dates (section 5.1.1). The volcanic features of Ngatutura Bay have an intricate connection with the substrate. Through detailed mapping of features a volcanic stratigraphy was established, which aided interpretation of the paleoenvironment.

5.1.1 K-AR DATES: AN APPRAISAL

K-Ar dates obtained for the Ngatutura Bay Volcanics are shown in table 4.5 and figure 4.28. The Ngatutura Point lava flow returned an average age of 3.22 ± 0.02 Ma., while lava at the base of the diatreme returned an age of 3.34 ± 0.06 Ma. These ages are much older than any of the dates obtained previously in the Ngatutura Volcanic Field (NVF). Briggs et al. (1989) provides a summary

of K-Ar dates from all of the Late Cenozoic basaltic volcanic fields of the upper North Island.

In the summary of Briggs et al. (1989), the date range for the NVF is listed as 1.83 – 1.54 Ma. However, the oldest ages obtained in the region were from the Alexandra Volcanic Field, which has an age range of 2.74 – 1.60 Ma. The Alexandra Volcanic Field is located directly south of the NVF and its volcanic centres vary in age by up to 1.14 million years within the volcanic field. Briggs et al. (1989) note that there is no systematic younging of ages in any direction within the volcanic field – this is true of the NVF as well. Previously, Robertson (1976) obtained K-Ar ages as old as 3.79 Ma for some centres in the Alexandra Volcanic Field, however, these dates were deemed anomalous, and likely erroneous, by Briggs et al. (1989) and were ignored in their publication.

The ages of centres in the NVF are much less variable than those of the Alexandra Volcanics, with centres varying in age rarely by more than 200 000 years. Dates obtained for the Ngatutura Bay Volcanics, as listed by Briggs et al. (1989), are much more variable than other centres of the NVF, with ages between 1.8 – 1.4 Ma as determined by Stipp (1968). However, Stipp (1968) reports alteration in all of his samples, making them unsuitable for dating. The age range of 1.8 – 1.4 Ma was preferred, although this spans the entire range of the NVF (Briggs et al., 1989). The sample locations of Stipp (1968) are obscure. The spatial density of the age data for the NVF is low, and the existence of older vents within the field cannot be excluded.

Table 5.1 – K-Ar age data: Ngatutura Volcanic Field

Lab nr. (Author)	Sample name	Volcanic Centre	Grid Reference	K (%)	$^{40}Ar_{rad}$ (ccSTP/g)	$^{40}Ar_{rad}$ (%)	K/Ar age (Ma)
8482	Dyke B	Ngatutura		1.042	6.9799×10^{-8}	16.4	1.72±0.14
8483	Dyke A	Ngatutura		1.010	7.1317×10^{-8}	17.0	1.81±0.14
8619	Ngatutura Point	Ngatutura		1.045	1.308×10^{-7}	14.3	3.22±0.03
8620	Lava at diatreme base	Ngatutura		1.299	1.6891×10^{-7}	6.9	3.34±0.06
8621	Tuff ring	Ngatutura		0.864	5.9057×10^{-8}	2.5	1.76
(RMB)	Naike Stream (tributary)	Ahuroa	R13/771070	1.10	7.82×10^{-8}	48.0	1.83±0.04
(RMB)		Foxs	R13/743070	1.14	7.99×10^{-8}	25.1	1.81±0.07
(RMB)		Bothwell	R13/767118	1.36	9.03×10^{-8}	48.2	1.71±0.04
(RMB)		Pukekawa	R13/703021	1.53	9.91×10^{-8}	50.6	1.67±0.04
(RMB)	Matira Stream	Matira	R14/700998	1.15	7.35×10^{-8}	44.6	1.65±0.04
(RMB)		Waikaretu	R13/670048	1.56	9.85×10^{-8}	48.4	1.63±0.05
(RMB)		Awaroa	R13/740050	1.52	9.26×10^{-8}	41.5	1.57±0.04
(RMB)		Pungatiki	R13/743108	1.29	7.69×10^{-8}	52.3	1.54±0.05
(RMB)	Waiaruhe Stm. (tributary)	Waiaruhe	R13/707073	1.53	10.76×10^{-8}	28.3	1.81±0.06
(JJS)	Ohuka Quarry	Pukerepo	R13/687085	1.7		40	1.58±0.01
(JJS)	Waikaretu Stream	Kokonga	R14/688042	1.264		58	1.68±0.04

RMB = Briggs et al. (1986). JJS = Stipp (1968)
Grid reference for the national 1000m grid of the 1 : 50 000 topographical map series (NZMS 260).

In contrast to Stipp's (1968) methods, the samples selected for our analysis were free from any alteration products and care was taken to exclude any large phenocrysts or mantle xenoliths. Repeated analysis on some samples returned consistent results and analytic errors were low for all samples. The older ages of 3.22 Ma for the Ngatutura Point lava flow and 3.34 Ma for the adjacent vent are therefore deemed reliable. Samples of the various features show some variations in geochemistry. Olivines from the Ngatutura Point lava flow have much lower Fo-values than all the other features (figure 4.27), but mineral assemblages are similar in all samples. Whole-rock geochemical analysis should be undertaken to determine important geochemical variations between features.

The younger volcanic features of Ngatutura Bay returned ages which fall within the age range of 1.83 – 1.54 Ma, as reported by Briggs et al. (1989). While these ages fit well with the geochronology of the Ngatutura Volcanic Field, the ages within the volcanic centre are variable by up to 100 000 years. This continues a trend of longevity at the Ngatutura Bay Complex, with the older succession around 3.3 Ma also spanning more than 100 000 years. Longevity of volcanism is reported at a number of centres of the Alexandra Volcanics, however, all other centres in the NVF have single ages assigned (probably due to poor spatial density of samples; Briggs et al., 1989). The high sampling density at Ngatutura Bay enabled a much more detailed picture to be sketched of the life of this volcanic centre.

5.1.2 VOLCANIC STRATIGRAPHY OF NGATUTURA BAY

The K-Ar ages obtained for the various volcanic features of Ngatutura Bay suggest two major episodes of volcanism. The first episode (3.34 – 3.22 Ma) consists mainly of massive lava flows emplaced in a subaerial setting. During this episode the lava flows of Ngatutura Point were emplaced. The Ngatutura Point lava flows are described in section 4.2 and are characterised by strongly developed cooling fractures with entablature joints near the top of the flow,

and some pillows in the lowermost parts of Shag Rock, indicating that at least the lower part of the flow was emplaced in water. This synsedimentary volcanism coincides with the deposition of the Kaawa Formation. The Kaawa Formation was deposited between 4.8 – 2.6 Ma (Edbrooke, 2001) in a shallow marine – estuarine environment.

This phase of volcanism was also accompanied by intrusion of basalt along fault planes. One such exposure is found at the base of the Ngatutura diatreme (figure 4.1, 4.8). Here, the dyke has a thin veneer of agglutinate at its head and is overlain by volcaniclastic sediment of the diatreme. This feature was first thought to represent the root zone of the diatreme (e.g. Heming, 1980), but has now been demonstrated to be part of a much older succession and its location at the base of the diatreme is merely a coincidence. In outcrop, the lava at the base of the diatreme is well below (>30m) the Kaawa Fm., while the Ngatutura Point lava is at levels much higher than the Kaawa sediments in its upper parts, but extends down to sea level (>30m below Kaawa Fm).

The paleotopography of the Kaawa Formation is highly variable (Edbrooke, 2001) and the Ngatutura Point lava likely filled a valley in the soft sediment and underlying strata, and eventually reached shallow sea water, possibly in an estuary. These features probably formed part of a larger volcanic edifice, which has since been eroded.

The initial phase of volcanism at Ngatutura Bay was followed by a period of quiescence of up to 1.4 million years. The second phase of volcanism is marked by widespread basaltic intrusions along faults and major fractures in the Late Mesozoic – Cenozoic marine strata, forming a complex plumbing system underneath the Ngatutura Bay Volcanic Centre. The earliest feature of the second phase of volcanism is Dyke A with a K-Ar age of 1.81 ± 0.14 Ma. Along with the abundant intrusive features, explosive subaerial volcanism is represented by a diatreme which formed on the Ngatutura Fault.

A basaltic block found as juvenile lithic in the tuff ring of the diatreme was dated and returned a K-Ar age of 1.76 Ma. This places the diatreme in the middle of the second phase of volcanism, and was followed by the intrusion of a second major dyke, Dyke B, at 1.72 Ma.

While the diatreme is preserved in excellent detail, the tuff ring has largely been eroded and only a small remnant remains in a small valley in the Kaawa Formation. The lava pond above Dyke A (figure 4.28) is found at a stratigraphic level just below the eroded tuff ring. The lava pond was emplaced when the Kaawa Fm was still soft and wet, with intrusions of hyaloclastite fingers found at the margins of the lava pond. The deformation of the Kaawa sediments and the protruding hyaloclastite intrusions indicate that the lava pond did not originate from the diatreme as late-stage effusion, but rather was fed from further north (towards the left in figure 4.28).

5.2 SUBSURFACE PROCESSES & VOLCANO DEVELOPMENT

In section 1.2 the following research question was posed: "How did the subsurface influence the development of the volcanic features at Ngatutura Bay?" By ascertaining the sequence of events that took place during the formation of this volcanic centre, it becomes apparent that the substrate, as well as the subsurface conditions i.e. water supply and tectonic structure, are closely related to the mode, style and geography of the various volcanic features at Ngatutura Bay. This section describes the relationship of the volcanism with the substrate and takes a closer look at the plumbing systems of the volcanic centre, as well as the effects of the substrate on volcano morphology.

Structural control on the volcanism at Ngatutura Bay is immediately apparent, with most of the volcanic features situated on faults. Both Dyke A & B are intruded along the strikes of Late Cenozoic normal faults, which trend approximately north to north-east. Moreover, a diatreme has developed on

the Ngatutura Fault, a prominent regional fault, which also has a north-easterly trend. The diatreme overlies an older intrusion which has followed a similar path along the fault plane. On a regional scale, all of the centres in the Ngatutura Volcanic Field (with the exception of only a few) lie directly on a regional fault (figure 1.1). This tectonic relationship is significant, because the geography of the volcanic field had been determined by the structure of the subsurface.

The Cenozoic marine strata at Ngatutura Bay varies from porous sandstone (Ahirau Sandstone, Waikawau Sandstone) to indurated and impermeable siltstone (Carter Siltstone). While the weakly indurated sandstones have good hydraulic conductivity, the Carter Siltstone and minor limestones found in the stratigraphy have very weak water transport capabilities, being well indurated and essentially non-porous. In spite of this, water involvement is implicated in the emplacement of both Dyke A and B, the latter of which was emplaced within the Carter Siltstone, as evident from their peperitic margins.

Dyke B, at its margins, is characterised by well-developed globular peperite, as well as a ~1.5 m margin of thermally altered siltstone. Development of crystalline clays in the siltstone during thermal alteration required hydrothermal fluids to be present, again implicating water involvement.

Since the Carter Siltstone has poor qualities as an aquifer, water must have flowed through small joints in the siltstone, or more importantly, along the fault plane on which the dyke has intruded. Dyke A is also surrounded by a peperite margin, however the Waikawau Sandstone is the host rock here and the sandstone is porous and has good hydraulic conductivity and transmissivity.

The shape and form of diatremes have been shown in a number of studies to be highly dependent on the nature of the substrate in which it forms. Lorenz (2003) explains that different kinds of substrate causes variations in the groundwater regime. For example, in hard-rock settings with impermeable

lithologies, water is introduced to the substrate via "joint aquifers" which can supply considerable amounts of water to the substrate via cracks and joints in the hard rock (Lorenz, 2003). In contrast, soft-rock environments may rely on porosity alone to provide adequate water in the substrate for phreatomagmatic activity to occur.

Auer et al. (2007), in their study of the Fekete-hegy maar volcano in Hungary, demonstrate the differences in diatreme geometry in soft- and hard-rock settings. Auer et al. (2007) explain that in soft-rock settings diatremes typically have a wider, champagne glass-shaped structure, in response to large-scale failure of soft strata, block sliding and slumping at the crater walls, and the ability of shock waves to liquefy groundwater-bearing sediment.

In contrast, hard-rock settings typically house diatremes with steep walls and narrow craters. Excavation of diatreme structures in these environments rely mostly on fracturing of wall rock through shock waves during explosions, and minor collapse and block tilting/sliding of wall rock (Auer et al., 2007).

Cases of mixed substrates have also been reported. Ross et al. (2011), at the Pali Aike volcanic field in Argentina, reports the formation of a maar and diatreme in a mixed soft- and hard-rock substrate. In this case the soft and hard lithologies are interbedded and the resultant diatreme structure resembles that of a typical soft-rock environment (Auer et al., 2007), despite the presence of hard lithologies, including lava flows, in the local stratigraphy.

At Ngatutura Bay, the Cenozoic stratigraphy is composed of indurated sandstone and well-indurated siltstone in lower parts, and poorly indurated to friable and wet sandstones in the upper part. The diatreme structure has steep, sub-vertical walls in its lower parts where the substrate is harder and more competent. However, in the upper parts the gradient of the wall rock decreases rapidly when it encounters the soft and wet (at the time of diatreme formation) Kaawa Formation sandstones.

Intrusive features at Ngatutura Bay are highly varied in shape and form. Dykes can be large with peperitic margins and situated on fault planes, but much smaller dykes are also encountered (some only a few centimetres thick). These smaller dykes have propagated along fractures in the country rock. Analysis of thermal alteration of the country rock further illustrates the variability in subsurface processes. No baking is observed at the margins of the very thin dykes (e.g. figure 4.3), while extensive portions of country rock are baked at the margins of the larger dykes (e.g. Dyke B, figure 4.5). Moreover, in the analysis of baked samples at Dyke B (section 4.4) it was revealed that crystalline clays have formed in the most thoroughly baked samples, along with portlandite crystals. Whether Dyke A & B stalled and cooled or continued to feed other structures, the period of heating was sufficient to induce hydrothermal alteration of the carbonate-rich country rock, which led to the mineralogical changes observed.

In comparison, baked samples from the diatreme deposits showed complete loss of calcium carbonate (smaller lithics, table 4.3), but no development of clay structures or portlandite crystals. This indicates that the smaller lithics in the diatreme were subjected to temperatures high enough to cause loss of carbonate (in the order of 700°C), but temperatures were not sustained and no further (hydro)thermal alteration occurred.

5.3 FORMATION OF THE DIATREME

The diatreme at Ngatutura Bay is exposed in three dimensions in a cliff face and the exposure is vertically near-complete. This excellent exposure enabled detailed analysis of the diatreme's structure and morphology, as well as the sedimentary characteristics of the diatreme fill. This section includes a discussion about the sequential formation of the diatreme through a series of phreatomagmatic explosions, as inferred from componentry and grain size data, as well as the role of intradiatreme explosions as a fragmentation process. Finally, the results of this study are compared to existing models and theories of diatreme formation.

5.3.1 THE GROWTH OF A DIATREME

The sequence of events that had led to the excavation of the diatreme and subsequent infilling of the structure with volcaniclastic sediment is inferred from the distribution of lithic components within the diatreme, as well as grain size characteristics of the volcaniclastic fill. The assemblage of lithic components is such that stratigraphically younger lithic types are found only in upper parts of the diatreme, and that older lithic types tend to be more common in lower parts and absent from the upper diatreme.

Oligocene-age lithics are the most abundant, but concentrations decrease consistently with height and are absent from the upper diatreme. Jurassic-age lithics, which have a much deeper origin, are found only in low concentrations in the lower diatreme, but increase in abundance in the debris jet. Miocene-age lithics have a more irregular distribution, being most abundant closest to the parent rocks. Pliocene lithics are found exclusively in the upper diatreme and abundance of these lithics increase rapidly with height, from levels above the debris jet.

Figure 5.1 shows the stages of diatreme development, as inferred from componentry and grain size data. The protodiatreme likely formed by an

initial blast at depth along the fault plane where magma intruded and encountered water which entered the ground via the fault plane and through joints in impermeable lithologies. This blast created a crater with steep walls and formed the initial diatreme structure. Subsequent subaerial explosions (MFCI) led to further excavation of the diatreme structure, along with progressive infilling with volcaniclastic sediment generated through fragmentation of wall rock and influx of juvenile basalt.

Sedimentation of the lower diatreme was in a "wet" eruptive environment, as indicated by impact structures or bomb sags in type 1 deposits, and water escape structures and plastically deformed, convolute beds in type 2 deposits (cf. section 4.3). Deposits in the lower diatreme also show signs of small-scale subsidence, having been tilted and having disrupted margins. These deposits represent early-stage sedimentation during the formation of the diatreme.

The deposits here typically lack a significant ash population and the grain size profile is dominated by lapilli-sized particles. Fine ash was likely elutriated in sustained phreatomagmatic explosions and ejected along with juvenile bombs and lapilli to contribute towards the tuff ring. The deposits of the lower diatreme are rich in Oligocene-age lithics, with their parent rock units being located directly below this level of the diatreme and likely corresponding to the level of the root zone in the subsurface

Sedimentation was continued in the diatreme, with explosions occurring at different levels - wherever suitable conditions were encountered i.e. sufficiently low geostatic pressure and adequate water supply. Continued excavation of the diatreme structure at depth led to small-scale subsidence of bedded deposits in the lower diatreme. At higher levels, excavation resulted in continued sedimentation. Explosions below the free surface (stage 3, figure 5.1) caused disruption of bedded deposits, forming unbedded and chaotic deposits (type 3 deposits), and in some cases initiated debris jets that propagated through bedded or unbedded deposits, forming type 4 debris jet deposits.

Explosions occurring in central parts, distal to the wall rock, led to the deposition of country rock-poor sediment (type 5 deposits). These bedded deposits are composed of decimetre-thick tuff breccia, interbedded with finer, ash rich lapilli tuff, suggesting repeated explosions inside the diatreme, but varying in intensity and leading to different degrees of fragmentation of the juvenile basalt. Large bomb sags are found in some of the finer beds, as well as wavy bedforms, which are typical of pyroclastic surge deposits (Fisher & Schminke, 1984). These deposits were eventually overlain by bedded, upper diatreme deposits (type 6 deposits), which further eroded the soft, surrounding Kaawa Formation upon which a tuff ring accumulated.

While initial explosions are thought to have been sustained and violent, leading to both the excavation of the crater, as well as deposits in which fine ash had been elutriated, later explosion were likely smaller and less sustained. This is indicated by the succession of surge deposits in the intradiatreme facies, representing a series of repeated explosions, and a more prominent ash population in deposits that are at mid- and upper levels in the diatreme, in which the ash had not been elutriated.

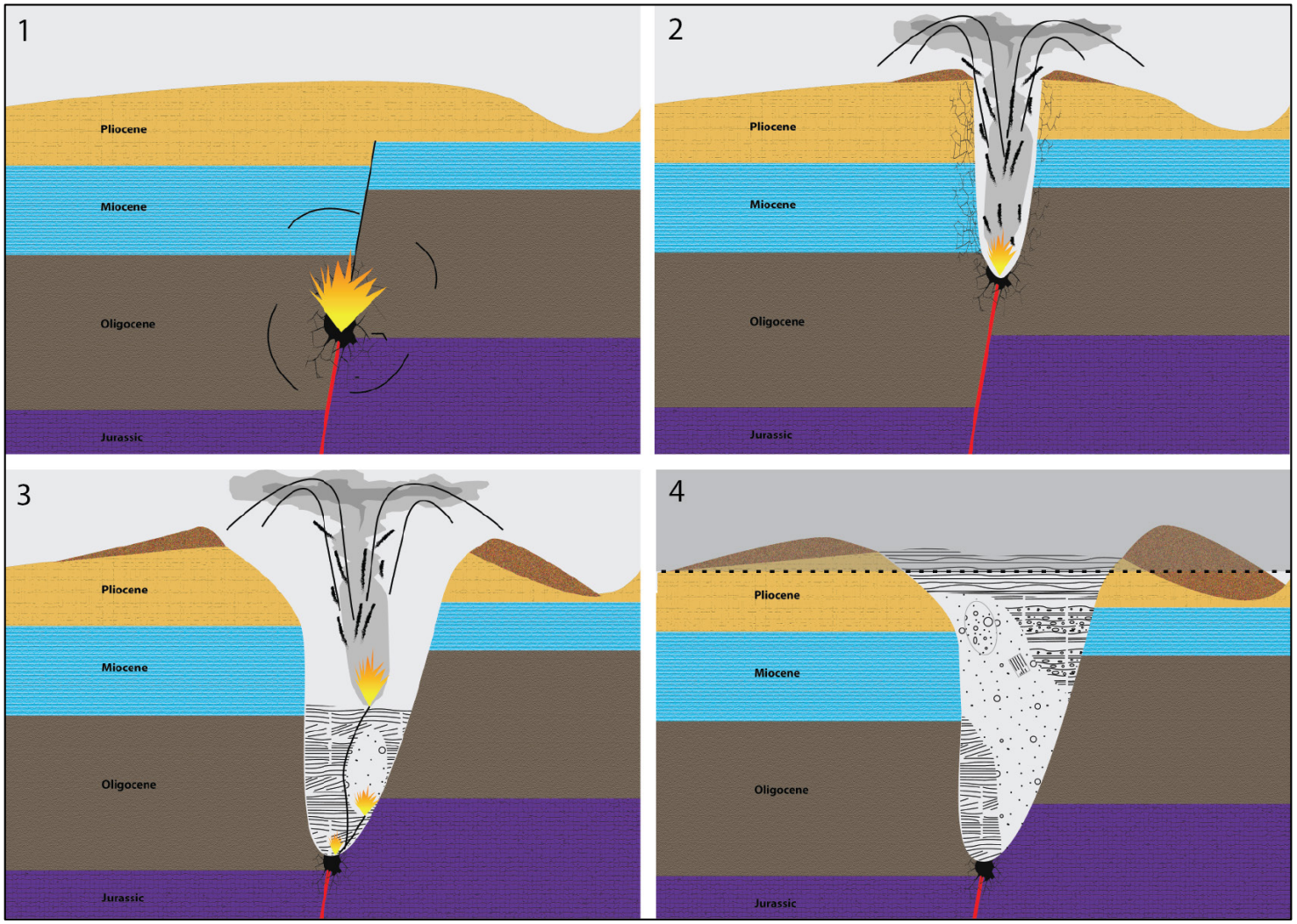
1
Pliocene
Miocene
Oligocene
Jurassic
2
Pliocene
Miocene
Oligocene
Jurassic
3
Pliocene
Miocene
Oligocene
Jurassic
4
Pliocene
Miocene
Oligocene
Jurassic

Figure 5.1 (p. 117) – The formation of the Ngatutura Diatreme. (1) Magma intrudes along the Ngatutura Fault and encounters water. A MFCI explosion is generated. (2) The initial explosion excavates the protodiatreme. (3) A series of explosions lead to further excavation of the structure and sequential sedimentation. (4) The completed diatreme structure with a tuff ring at the pre-eruptive surface. Bedded deposits in the lower diatreme are slightly subsided. Explosions at depth disrupted sediment to form unbedded deposits. Shaded area shows level of erosion of the structure.

To support this concept for the formation of the diatreme (as outlined in figure 5.1) the following arguments are presented:

- In order to explain the distribution of older and younger lithic components in the diatreme, it is necessary for an initial crater or protodiatreme to have formed first (cf. Andrews et al., 2015), followed by quasisystematic sedimentation of the structure, such that older lithic types are absent from the upper diatreme, and younger lithic types (which had been eroded during further excavation of the protodiatreme) are only found in the upper diatreme. An exception is the deposits of the debris jet, which have an increased abundance of Jurassic-age lithics, and originate from several tens to hundreds of metres below the diatreme.

  With the structure being filled from the bottom up, older lithic types would be more common in the lower diatreme and would decrease upwards. This can be seen in the abundance of Oligocene-age lithics (figure 4.19). During late stage sedimentation the lower diatreme would remain undisturbed, apart from subsurface explosions forming unbedded deposits, and only younger lithic types would be implicated at this time, forming the upper diatreme deposits. The latter is shown in the abundance of Pliocene-age lithics, which increases rapidly from the debris jet upwards (figures 4.18, 4.19).

- The presence of bedded deposits throughout the diatreme, which have not subsided much after deposition, indicate that the protodiatreme structure was excavated during early stages of its formation: subaerial eruption conditions were maintained to an extent that allowed for the formation of bedded deposits. Bedded diatreme sediments are emplaced subaerially during explosions that excavate wall-rock or underlying diatreme fill (White & Ross, 2011). Bedded diatreme deposits within diatremes are often subsided in response to continued excavation of the diatreme during explosions, in which case the subsided deposits can be found at levels considerably lower than their origin, and often tilted or overturned (White & Ross, 2011; Lorenz, 1986).

  In the Ngatutura diatreme, bedded deposits that are subsided must be relatively close to their original height at deposition, since lithic components show discrete distributions in the lower and upper diatreme. Following initial excavation, the structure would be filled sequentially with debris generated from continued excavation of wall rock through a series of explosions.

  In this way the structure would be developed to its final form, assuming the classic conical shape of many diatremes. The slightly subsided beds also indicate that the protodiatreme was expanded downwards, implying that explosions at the base of the diatreme occurred at successively lower levels.

- Cumulative grain size distributions show that the lowermost sample area in the left transect is highly enriched in lapilli-sized particles, while lacking a finer matrix component, which has a strong presence in samples from higher stratigraphic levels. This indicates that ash had been elutriated during the crater-forming blast during which open air contact was maintained in a sustained explosion.

- Comparing the grain size distributions of the entire deposit with that of the basalt and Oligocene-lithics populations (figure 4.21) the three populations have very similar distributions. In areas where the reworking of sediment is suspected (i.e. debris jet and unbedded deposits), grain size distributions between populations are markedly different and do not display the striking consistency in profiles observed in unperturbed, bedded sediments.

  However, the grain size profiles of basalt populations remain most similar to overall grain size distributions. Quenched juvenile components are much stronger than any of the country rock lithic types, and further fragmentation of these clasts would occur only close to a blast locus. This illustrates that bedded deposits are preserved in situ (with the exception of some subsidence in places), with grain size profiles reflecting primary fragmentation processes.

- The facies architecture of the diatreme indicates that explosions occurred at sporadic locations at any level within the diatreme. The protodiatreme developed to become wider and slightly deeper, with explosions occurring at varying levels within the diatreme, wherever conditions were favourable i.e. magma meeting sufficient amounts of water at sufficiently low geostatic pressures. The presence of a debris jet, and unbedded deposits in the lower diatreme indicates that not all explosions erupted subaerially (cf. Lefebvre et al., 2013; Sweeney & Valentine, 2015). With explosions occurring at any location, the protodiatreme could be excavated at higher levels without disturbance to lower diatreme deposits, and without requiring the subsidence of wall rock.

- There is little evidence for recycling of sediment, which would have led to a more chaotic distribution of components i.e. younger lithic types being present at lower levels or older lithics found higher in the diatreme. The lack of large-scale recycling is also seen in the presence of undisturbed, bedded deposits at all levels. Without the recycling of sediment as a major diatreme-forming process, the structure had to have been filled from the bottom up, given that lithic components retain a stratigraphically oriented distribution.

5.3.3 COMPARING CURRENT MODELS & THEORIES

The first comprehensive model for the formation of a diatreme, as part of a maar-diatreme volcanic system, was provided by Lorenz (1986). In this model an initial phreatomagmatic explosion occurs close to the surface, creating a small crater. The process is continued by a series of explosions, each occurring at a deeper level due to the exhaustion of groundwater around the explosion sites. The explosions cause the wall rock to fragment, and pyroclastic sediments form at the free surface within the crater. The Lorenz (1986) model relies on continued subsidence of these beds to lower levels in step with the successively deeper explosion sites, thus forming a pipe-like structure up to several kilometres deep. The Lorenz model accounts for lower diatreme deposits to be unbedded, particularly in the vicinity of explosion locals, while bedded deposits are found mostly in the upper diatreme where explosions penetrate through overlying strata to erupt at the surface and form bedded deposits in a subaerial environment.

Challenging this concept, Valentine & White (2012) provided an alternative model for diatreme formation. In their model, Valentine & White (2012) argue that MFCI can occur at any level within the developing diatreme, wherever conditions are favourable. With continued explosions excavating wall rock, the diatreme structure becomes wider at the top where explosions are more effective and where there is less support for the wall rock from volcaniclastic

fill in the diatreme. In this way, bedded deposits form in the upper diatreme where explosions erupt subaerially, and unbedded deposits form in the lower diatreme where explosions remain in the subsurface.

Diatremes, with a conical shape, bedded upper deposits, and unbedded lower deposits are a well-documented feature in many volcanic settings and are typically associated with maars at the surface (White & Ross, 2011; Valentine & Van Wyk De Vries, 2014; Valentine & White, 2012; Ross et al., 2011; Németh et al., 2007; Lefebrve et al., 2013; Kienle et al., 1977; etc.). Diatremes vary in size and can be up to several kilometres deep (Lorenz, 1986) and several hundred metres wide (White & Ross, 2011). The Ngatutura Diatreme is small in comparison with most documented diatremes, being only c. 40 m in height and width (excluding the root zone).

Attempts have been made to reproduce the complex facies architecture of diatremes through experiments of various scales (e.g. Andrews et al., 2014, 2015; Graettinger et al., 2015; Valentine et al., 2015; Ross et al., 2008, 2013; etc.). While researchers typically view concepts of diatreme formation as mutually exclusive sets of processes, it has also been demonstrated that diatremes can form as a mixture of concepts (e.g. Andrews et al., 2015).

Andrews et al. (2015) conducted bench-scale experiments which investigated the differences in facies architecture in diatremes produced by single blasts vs. those produced in ascending or descending blast series. Fundamentally, Andrews et al. (2015) determined that subsurface blasts partition energy roughly equally between crater excavation and the mass movement of juvenile material. In their experiments the inception of debris jets is demonstrated to be an important sedimentation process with respect to blasts in the subsurface. Andrews et al. (2015) also highlight the importance of deepening vs. shallowing blast series in the sedimentation of a diatreme, with the different scenarios producing distinct characteristics. Andrews et al. (2015) demonstrated that it is possible for diatremes to form as a result of a single blast, as well as through a series of ascending or descending blasts.

The Ngatutura Diatreme shows several characteristics of classic diatreme morphology (White & Ross, 2011), having both bedded and unbedded facies, rotated and subsided beds, debris jet deposits, floating rafts of bedded sediment, a conical shape and lithic components composed of country rock and juvenile basalt. It has been demonstrated that this diatreme formed through a series of phreatomagmatic explosions or MFCI, at various depths, to excavate and fill the crater with volcaniclastic sediment.

Componentry and grain size studies indicated that the diatreme was formed by an initial crater-forming blast, which was further excavated and the structure filled with sediment from the bottom up. The efficacy of MFCI as a country rock fragmentation mechanism has been demonstrated by a number of researchers (Lorenz et al., 1999, 2002; Lorenz & Zimanowski, 2000; Kurszlaukis et al., 1998). Explosions at the base of the structure are shown to have occurred at progressively deeper levels, while explosions also occurred at higher levels within the diatreme. Some explosions erupted at the surface to form bedded pyroclastic deposits, and other explosions remained in the subsurface to initiate debris jets and mix bedded deposits to become unbedded.

The subsided beds in the lower diatreme can be related to the Lorenz (1986) model, as can the successively lower explosion locals at the base of the diatreme. However, explosions occurring at varying levels within the diatreme relate to the Valentine & White (2012) model. Similarly, the occurrence of unbedded deposits at intermediate levels and debris jet activity are also related to the Valentine & White (2012) model. With features relatable to both these fundamental models, the Ngatutura Diatreme demonstrates that models of diatreme formation are not mutually exclusive, and that a mixture of diatreme-forming processes from different concepts can lead to the formation of a diatreme that is distinguished with all the classifying characteristics of a classic diatreme, as described for example, by White & Ross (2011).

CONCLUSIONS

In light of the uncertainty that surrounds the knowledge of current research on the roles of subsurface processes in volcano development at small basaltic volcanoes, as well as the lack of consensus on the processes of diatreme formation, this research aimed to answer three research questions:

1. How did the subsurface influence the development of the volcanic features at Ngatutura Bay?

   Various volcanic features at Ngatutura Bay were studied in terms of their physical and chemical characteristics, as well as the ages of these features, to reveal to roles of subsurface processes in the development of a small basaltic volcano. The strong relationship between faults and volcanism was illustrated not only at the Ngatutura Bay Volcanic Centre, but also in the wider Ngatutura Volcanic Field, with dykes and entire volcanic centres being situated on faults. Smaller dykes were also shown to intrude along cracks in the country rock. Thermal data indicated that some intrusive features supplied long-lived heat to the substrate, while country rock was less affected by heat in explosive features i.e. the diatreme.

   The availability of groundwater was shown to be an important aspect not only in the emplacement of dykes with peperitic margins, but also in the development of a diatreme. In this case water was delivered to the subsurface via pores or joints in country rock, but more importantly through the fault plane on which the diatreme formed. The supply of water was intrinsic to the phreatomagmatic explosions by which the diatreme was shown to have formed.

2. What was the paleoenvironment at the time the eruption took place?

   Detailed mapping revealed a complex history of the Ngatutura Volcanic Centre, with K-Ar ages varying from 3.34 – 1.72 Ma and indicating two main phases of volcanism, each lasting for c. 100 000 years. Both phases of syn-sedimentary volcanism were emplaced in a shallow marine/estuarine environment during the deposition of the Pliocene Kaawa Shellbed and Sandstone, with some subaerial features also being present. The first phase (around 3.34 Ma) is marked by extensive lava flows and some intrusive features, while the second phase consisted of widespread intrusion of basalt, along with the formation of a diatreme.

3. Are the processes interpreted for the evolution of the diatreme consistent with current theories and models?

   The diatreme deposits were analysed in two near-complete vertical transects. The well-defined country rock stratigraphy enabled detailed analysis of the lithic componentry of the diatreme deposits, as well as grain size characteristics. These analyses enabled a comprehensive interpretation of the events during which the diatreme had formed. Results show that the diatreme formed via multiple phreatomagmatic explosions, occurring at variable depths, that excavated an initial crater and the structure was sequentially filled with continued excavation driving the sedimentation. Early bedded deposits became buried and continued explosions disrupted these sediments to form unbedded deposits. Late-stage explosions formed bedded deposits in the upper diatreme. The formation of the Ngatutura Diatreme is described as a new concept and is shown to relate to more than one of the current models on diatreme formation.

REFERENCES

Agustin-Flores, J., Németh, K., Cronin, S.J., Lindsay, J.M., Kereszturi, G., Brand, B.D., Smith, I.E.M. 2014. Phreatomagmatic eruptions through unconsolidated coastal plain sequences, Maungataketake, Auckland Volcanic Field (New Zealand). Journal of Volcanology and Geothermal Research 276, 46-63.

Akbulut, A., Kadir, S. The geology and origin of sepiolite, palygorskite and saponite in Neogene lacustrine sediments of the Serinhisar-Acipayam Basin, Deizli, SW Turkey. Clays and Clay Minerals 51(3), 279-292.

Andrews, R.G., White, J.D.L., Durig, T., Zimanowski, B. 2014. Discrete blasts in granular material yield two-stage process of cavitation and granular fountaining. Geophysical Research Letters 41, 1-6.

Andrews, R.G., White, J.D.L., Durig, T., Zimanowski, B. 2015. Simulating maar-diatreme volcanic systems in bench-scale experiments. Journal of the Geological Society 73.

Ar, I., Dogu, G. 2001. Calcination kinetics of high purity limestones. Chemical Engineering Journal 83, 131-137.

Araña, V., Aparicio, A., Martin Escorza, C., Garcia, C.L., Ortiz, R., Vaquer Navarro, R., Barberi, F., Ferrara, G., Alberti Beltran, J.F., Gassiot, X. 1983. El volcanismo neógeno-cuaternario de Catalunya: caracteres estructurales, petrológicos y geodinámicos. Acta Geológica Hispánica 18(1), 1-17.

Auer, A., Martin, U., Németh, K. 2007. The Fekete-hegy (Balaton Highland Hungary) "soft-substrate" and "hard-substrate" maar volcanoes in an aligned volcanic complex – Implications for vent geometry, subsurface stratigraphy and the palaeoenvironmental setting. Journal of Volcanology and Geothermal Research 159, 225-245.

Balance, P.F. 1976. Stratigraphy and bibliography of the Waitemata Group of Auckland. New Zealand Journal of Geology and Geophysics 19(6), 897-932.

Balance, P.F., Nelson, C.S. 1969. Differential cementation in the Waikawau Limestone (Waitemata Group), West Auckland. New Zealand Journal of Geology and Geophysics 12(1), 67-86.

Batiza, R., Fornari, D.J., Vanko, D.A., Lonsdale, P. 1984. Craters, calderas, and hyaloclastites on young Pacific seamounts. Journal of Geophysical Research 89(B10), 8371-8390.

Berghuijs, J.F., Mattsson, H.B. 2013. Magma ascent, fragmentation and depositional characteristics of "dry" maar volcanoes: Similarities with vent-facies kimberlite deposits. Journal of Volcanology and Geothermal Research 252, 53-72.

Blackburn, E.A., Wilson, L., Sparks, R.S.J. 1976. Mechanisms and dynamics of strombolian activity. Journal of the Geological Society of London 132, 429-440.

Blaike, T.N., Ailleres, L., Betts, P.G., Cas, R.A.F. 2014. A geophysical comparison of the diatremes of simple and complex maar volcanoes, Newer Volcanics Province, south-eastern Australia. Journal of Volcanology and Geothermal Research 276, 64-81.

Blott, S.J., Pye, K. 2001. GRADISTAT: a grain size distribution and statistics package for the analysis of unconsolidated sediments. Earth Surface Processes and Landforms 26(11), 1237-1248.

Brenna, M., Cronin, S.J., Smith, I.E.M., Sohn, Y.K., Németh, K. 2010. Mechanisms driving polymagmatic activity at a monogenetic volcano, Udo, Jeju Island, South Korea. Contributions to Mineralogy and Petrology 160, 931-950.

Briggs, R.M. 1983. Distribution, form, and structural control of the Alexandra Volcanic Group, North Island, New Zealand. New Zealand Journal of Geology and Geophysics 26(1), 47-55.

Briggs, R.M., Goles, G.G. 1984. Petrological and trace element geochemical features of the Okete Volcanics, western North Island, New Zealand. Contributions to Mineralogy and Petrology 86, 77-88.

Briggs, R.M., Itaya, T., Lowe, D.J., Keane, A.J. 1989. Ages of the Pliocene-Pleistocene Alexandra and Ngatutura Volcanics, western North Island, New Zealand, and some geological implications. New Zealand Journal of Geology and Geophysics 32.

Briggs, R.M., Utting, A.J., Gibson, I.L. 1990. The origin of alkaline magmas in an intraplate setting near a subduction zone: The Ngatutura Basalts, North Island, New Zealand. Journal of Volcanology and Geothermal Research 40, 55-70.

Brown, D.J., Bell, B.R. 2007. How do you grade peperites? Journal of Volcanology and Geothermal Research 159, 409-420.

Buchanan, D.J. 1974. A model for fuel-coolant interactions. Journal of Physics D: Applied Physics 7(10), 1441-1457.

Buettner, R., Zimanowski, B. 2003. Phreatomagmatic explosions in subaqueous volcanism. In: White, J.D.L., et al. (Eds). Explosive subaqueous volcanism. American Geophysical Union Geophysical Monograph 140, 51-60.

Busby-Spera, C.J., White, J.D.L. 1987. Variation in peperite textures associated with differing host-sediment properties. Bulletin of Volcanology 49, 765-775.

Carlisle, D. 1963. Pillow breccias and their aquagene tuffs in Quadra Island, British Columbia. Journal of Geology 71, 48-71.

Cas, R., Porritt, L., Pittari, A., Hayman, P. 2008. A new approach to kimberlite facies terminology using a revised general approach to the nomenclature of all volcanic rocks and deposits: descriptive to genetic. Journal of Volcanology and Geothermal Research 174, 226-240.

Cashman, K.V., Sturtevant, B., Papale, P., Navon, O. 2000. Magmatic fragmentation. In: Sigurdsson, H. (Ed.). Encyclopaedia of Volcanoes. New York: Elsevier. pp. 331-343.

Cassidy, J., Locke, C.A. 2010. The Auckland volcanic field, New Zealand: Geophysical evidence for structural and spatio-temporal relationships. Journal of Volcanology and Geothermal Research 195, 127-137.

Challinor, A.B. 2001. Stratigraphy of Tithonian (Ohauan-Puaroan) marine beds near Port Waikato, New Zealand, and a redescription of *Belemnopsis aucklandica* (Hochstetter). New Zealand Journal of Geology and Geophysics 44, 219-242.

Clement, C.R., Skinner, E.M.W. 1985. A textural-genetic classification of kimberlites. South African Journal of Geology 88, 403-409.

Connor, C.B. 1987. Structure of the Michoacán-Guanajuato Volcanic Field, Mexico. Journal of Volcanology and Geothermal Research 33, 191-200.

Connor, C.B., Conway, F.M. 2000. Basaltic Volcanic Fields. In: Sigurdsson, H. (Ed.). Encyclopaedia of Volcanoes. New York: Elsevier. pp. 331-343.

Cortés, J.A., Smith, E.I., Valentine, G.A., Johnsen, R., Rasoazanamparany, C., Widom, E., Sas, M., Ruth, D. 2015. Intrinsic conditions of magma genesis at the Lunar Crater Volcanic Field (Nevada), and implications for internal plumbing and magma ascent. American Mineralogist 100, 396-413.

Dadd, K.A., Van Wagoner, N.A. 2002. Magma composition and viscosity as controls on peperite texture: an example from Passamaquoddy Bay, southeastern Canada. In: Skilling, I.P., White, J.D.L., McPhie, J. (Eds.). Peperite: Processes and products of magma-sediment mingling. Journal of Volcanology and Geothermal Research 114, 63-80. Special Issue.

Delaney, P.T. 1982. Rapid intrusion of magma into wet rock: groundwater flow due to pore pressure increases. Journal of Geophysical Research 87, 7739-7756.

Dingwell, D.D. 1996. Volcanic dilemma: Flow or blow? Science 273, 1054.

Doyle, M.G. 2000. Clast shape and textural associations in peperite as a guide to hydromagmatic interactions: upper Permian basaltic and basaltic andesite examples from Kiama, Australia. Australian Journal of Earth Sciences 47, 167-177.

Edbrooke, S.W. (compiler). 2001. Geology of the Auckland area. Institute of Geological & Nuclear Sciences 1:250 000 geological map 3. Lower Hutt: Institute of Geological & Nuclear Sciences.

Edbrooke, S.W. (compiler). 2005. Geology of the Waikato area. Institute of Geological & Nuclear Sciences 1:250 000 geological map 4. Lower Hutt: Institute of Geological & Nuclear Sciences.

Fisher, R.V., Schmincke, H-U. 1984. Pyroclastic rocks. Berlin: Springer-Verlag

Fleming, C.A., Kear, D. 1960. The Jurassic Sequence at Kawhia Harbour – Kawhia Sheet, N73. New Zealand Geological Survey Bulletin 67.

Folk, R.L., Ward, W.C. 1957. Brazos River bar: a study in the significance of grain size parameters. Journal of Sedimentary Petrology 27, 3-26.

Forbes, A.E.S., Blake, S., Tuffen, H. 2014. Entablature: fracture types and mechanisms. Bulletin of Volcanology 76, 820.

Fornaciai, A., Favalli, M., Karatson, D., Tarquini, S., Boschi, E. 2012. Morphometry of scoria cones, and their relation to geodynamic setting: A DEM-based analysis. Journal of Volcanology and Geothermal Research 217-218, 56-72.

Franco, F., Pozo, M., Cecilia, J.A., Benitez-Guerrero, M., Pozo, E., Martin-Rubi, J.A. 2014. Microwave assisted acid treatment of sepiolite: The role of composition and "crystallinity". Applied Clay Science 10, 15-27.

Galindo, I., Gudmundsson, A. 2012. Basaltic feeder dykes in rift zones: geometry, emplacement, and effusion rates. Natural Hazards and Earth System Sciences 12, 3683-3700.

Geshi, N., Kusumoto, S., Gudmundsson, A. 2010. Geometric difference between non-feeder and feeder dikes. Geology 38, 195-198.

Gonnermann, H.M. 2015. Magma fragmentation. Annual Review of Earth and Planetary Sciences 43, 431-458.

Gonzalez-Jimenez, J.M., Villaseca, C., Griffin, W.L., O'Reilly, S.Y., Belousova, E., Ancochea, E., Pearson, N.J. 2014. Significance of ancient sulphide PGE and Re-Os signatures in the mantle beneath Calatrava, Central Spain. Contributions to Mineralogy and Petrology 168, 1047.

Graettinger, A.H., Valentine, G.A., Sonder, I. 2015. Circum-crater variability of deposits from discrete, laterally and vertically migrating volcanic explosions: Experimental evidence and field implications. Journal of Volcanology and Geothermal Research 308, 61-69.

Hanson, R.E., Hargrove, U.S. 1999. Processes of magma/wet sediment interaction in a large-scale Jurassic andesitic peperite complex, northern Sierra Nevada, California. Bulletin of Volcanology 60, 610-626.

Hasenaka, T., Carmichael, I.S.E. 1985. The cinder cones of Michoacán-Guanajuato, central Mexico: their age, volume and distribution, and magma discharge rate. Journal of Volcanology and Geothermal Research 25, 105-124.

Hayward, B.W., Brook, F.J. 1984. Lithostratigraphy of the basal Waitemata Group, Kawau Supergroup (new), Auckland, New Zealand. New Zealand Journal of Geology and Geophysics 27(2), 101-123.

He, Y. 2006. MgO nanostructured microspheres synthesized by an interfacial reaction in a solid-stabilized emulsion. Materials Letters 60(29-30), 3511-3513.

Heiken, G. 1971. Tuff Rings: Examples from the Fort Rock-Christmas Lake Valley Basin, South-Central Oregon. Journal of Geophysical Research 76(23), 5615-5626.

Heiken, G. 1972. Morphology and petrography of volcanic ashes. Geological Society of America Bulletin 83, 1961-1988.

Heiken, G., Wohletz, K. 1985. Volcanic Ash. Berkeley: California University Press.

Heming, R.F. 1980. The Ngatutura diatreme. New Zealand Journal of Geology and Geophysics 23(5-6), 569-573.

Henderson, J., Grange, L.I. 1926. The geology of the Huntly-Kawhia Subdivisions, Pirongia and Hauraki Divisions. Bulletin of the New Zealand Geological Survey 28.

Hillaire-Marcel, C., Carro, O., Casanova, J. 1986. ^{14}C and U/Th Dating of Pleistocene and Holocene stromatolites from East African Paleolakes. Quaternary Research 25, 312-329.

Hochstetter, F. von. 1864. Geologie von Neu Zeeland. Beitrage zur Geologie der Provinzen Auckland und Nelson. Novara-Expedition. Geologischer Theil 1(1).

Hood, S.D., Tripathi, A., Nelson, C.S., Kamp., P.J.J. 2005. Petrology of transgressive cool-water limestone sequences in northern Te Kuiti Group, Waikato Basin, New Zealand. P. 38-39 In: Pettinga, J.R., Wandres, A.M. (Eds.) *Geological Society of New Zealand 50th annual conference, 28 November – 1 December 2005.* Geological Society of New Zealand miscellaneous publication 119A.

Hornibrook, N.B., Schofield, J.C. 1963. Stratigraphic relations in the Waitemata Group of the lower Waikato District. New Zealand Journal of Geology and Geophysics 6(1), 38-51.

Houghton, B.F., Gonnermann, H.M. 2008. Basaltic explosive volcanism: Constraints from deposits and models. Chemie der Erde 68, 117-140.

Houghton, B.F., Nairn, I.A. 1991. The 1976-1982 Strombolian and phreatomagmatic eruptions of Whit Island, New Zealand: eruptive and depositional mechanisms at a "wet" volcano. Bulletin of Volcanology 54, 25-49.

Houghton, B.F., Schminke, H-U. 1989. Rothenberg scoria cone, East Eifel: a complex Strombolian and phreatomagmatic volcano. Bulletin of Volcanology 52, 28-48.

Hu, N., Scaroni, A.W. 1996. Calcination of pulverized limestone particles under furnace injection conditions. Fuel 75(2), 177-186.

Huang, Y., Hawkesworth, C., van Calsteren, P., Smith, I., Black, P. 1997. Melt generation models for the Auckland Volcanic Field, New Zealand: constraints from U-Th isotopes. Earth and Planetary Science Letters 149, 67-84.

Hutton, F.W. 1871. On the relative ages of the Waitemata Series and the Brown Coal Series of Drury and Waikato. Transactions and proceedings of the New Zealand Institute 3, 244-249.

Jaeger, J.C., Cook, N.G.W. 1979. Fundamentals of rock mechanics. London: Chapman and Hall.

Jafri, S.H., Sarma, D.S., Sheikh, J.M. 2010. Hyaloclastite in pillow basalts, South Andaman Island, Bay of Bengal, India. Current Science 99(12), 1825-1829.

Kamp, P.J.J., Tripathi, A.R.P., Nelson, C.S. 2014. Paleogeography of Late Eocene to earliest Miocene Te Kuiti Group, central-western North Island, New Zealand. New Zealand Journal of Geology and Geophysics 57(2), 128-148.

Kamp., P.J.J., Tripathi, A.R.P., Nelson, C.S. 2008. Stratigraphic columns and correlations for the Late Eocene-Oligocene Te Kuiti Group, central-western North Island, New Zealand. Ministry of Economic Development Petroleum Report Series PR3901. Hamilton: University of Waikato.

Kear, D. 1966. Sheet N55 – Te Akau, Geological Map of New Zealand 1:63 360. Lower Hutt: Department of Scientific and Industrial Research.

Kear, D. 1987. Te Akau: Notes on the geological map of New Zealand 1:63 360 Sheet N55. New Zealand Geological Survey Record 17.

Kear, D., Schofield, J.C. 1959. Te Kuiti group. New Zealand Journal of Geology and Geophysics 2(4), 685-717.

Kear, D., Schofield, J.C. 1978. *Geology of the Ngaruawahia Subdivision. Wellington: New Zealand Geological Survey.* New Zealand Geological Survey Bulletin 88.

Keating, G.N., Valentine, G.A., Krier, D.J., Perry, F.V. 2008. Shallow plumbing systems for small-volume basaltic volcanoes. Bulletin of Volcanology 70, 563-582.

Kereszturi, G., Németh, K. 2012. Monogenetic basaltic volcanoes: Genetic classification, growth, geomorphology and degradation (chapter 1). Updates in Volcanology – New Advances in Understanding Volcanic Systems, Karoly Németh (Ed.). Available from http://www.intechopen.com/books/updates-in-volcanology-new-advances-in-understanding-volcanic-systems/monogenetic-basaltic-volcanoes-genetic-classification-growth-geomorphology-and-degradation

Kereszturi, G., Németh, K., Csillag, G., Balogh, K., Kovacs, J. 2011. The role of external environmental factors in changing eruption styles of monogenetic volcanoes in a Mio/Pleistocene continental volcanic field in western Hungary. Journal of Volcanology and Geothermal Research 201, 227-240.

Kermode, K. 1992. Geology of the Auckland urban area, geological map 1:50 000. Institute of Geological and Nuclear Sciences Ltd, Lower Hutt, New Zealand. 63p.

Khinast, J., Krammer, G.F., Brunner, C., Staudinger, G. 1996. Decomposition of limestone: the influence of CO_2 and particle size on the reaction rate. Chemical Engineering Science 51(4), 623-634.

Kienle, J., Kyle, P.R., Self, S. Motyka, R.J., Lorenz, V. 1980. Ukinrek maars, Alaska, I. April 1977 eruption sequence, petrology and tectonic setting. Journal of Volcanology and Geothermal Research 7, 11-37.

Kirkman, J.H., Wallace, R.C. 1994. Palygorskite in the regolith from the Mokau District, North Island, New Zealand. Clay Minerals 29, 265-272.

Kokelaar, B.P. 1982. Fluidization of wet sediments during the emplacement and cooling of various igneous bodies. Journal of the Geological Society of London 139, 21-33.

Kokelaar, B.P. 1983. The mechanism of Surtseyan volcanism. Journal of the Geological Society of London 140, 939-944.

Kokelaar, B.P. 1986. Magma-water interactions in subaqueous and emergent basaltic volcanism. Bulletin of Volcanology 48, 275-289.

Korbel, P., Novak, M. 2001. The Complete Encyclopaedia of Minerals. Rochester: Grange Books PLC.

Kurszlaukis, S., Franz, L., Lorenz, V. 1998. On the volcanology of the Gibeon Kimberlite Volcanic Field, Namibia, Journal of Volcanology and Geothermal Research 84, 257-272.

Kurszlaukis, S., Fulop, A. 2013. Factors controlling the internal facies architecture of maar-diatreme volcanoes. Bulletin of Volcanology 75, 761.

Kurszlaukis, S., Lorenz, V. 2008. Formation of "Tuffisitic Kimberlites" by phreatomagmatic processes. Journal of Volcanology and Geothermal Research 174, 68-80.

Leat, P.T. 1985. Interaction of a rheomorphic peralkaline ash-flow tuff and underlying deposits, Menengai Volcano, Kenya. Geothermal Research 26, 131-145.

Lefebrve, N.S., White, J.D.L, Kjarsgaard, B.A. 2013. Unbedded diatreme deposits reveal maar-diatreme-forming eruptive processes: Standing Rocks West, Hopi Buttes, Navajo Nation, USA. Bulletin of Volcanology 75, 739.

Long, P., Wood, B. 1986. Structures, textures, and cooling histories of Columbia River basalt flows. Geological Society of America Bulletin 97(9), 1144-1155.

Lorenz, V. 1973. On the formation of maars. Bulletin Volcanologique 37, 183-204.

Lorenz, V. 1975. Formation of phreatomagmatic maar-diatreme volcanoes and its relevance to the formation of kimberlite diatremes. Physics and Chemistry of the Earth 9, 17-27.

Lorenz, V. 1979. Phreatomagmatic origin of the olivine melenite diatremes of the Swabian Alb, Germany. In: Boyd, F.R., Meyer, H.O.A. (Eds.), Kimberlites, Diatremes, and Diamonds: their Geology, Petrology, and Geochemistry. American Geophysical Union, Washington, pp. 354-363.

Lorenz, V. 1985. Maars and diatremes of phreatomagmatic origin, a review. Transactions of the Geological Society of South Africa 88, 459-470.

Lorenz, V. 1986. On the growth of maars and diatremes and its relevance to the formation of tuff rings. Bulletin of Volcanology 48, 265-274.

Lorenz, V. 1987. Phreatomagmatism and its relevance. Chemical Geology 62, 149-156.

Lorenz, V. 2003. Maar-diatreme volcanoes, their formation, and their setting in hard-rock or soft-rock environments. Geolines 15, 72-83.

Lorenz, V. 2007. Syn- and posteruptive hazards of maar-diatreme volcanoes. Journal of Volcanology and Geothermal Research 159-285-312.

Lorenz, V., Haneke, J. 2004. Relationship between diatremes, dykes, sills, laccoliths, intrusive-extrusive domes, lava flows, and tephra deposits with unconsolidated water-saturated sediments in the Late Variscan intermontane Saar-Nahe Basin, SW Germany. In: Breitkreuz, C., Petford, N. (Eds.), Physical geology of high level magmatic systems. Geological Society, London, Special Publication, vol. 234, pp. 75-124.

Lorenz, V., Kurszlaukis, S. 1997. On the last explosions of carbonatite pipe G3b, Gross Brukkaros, Namibia. Buleltin of Volcanology 59, 1-9.

Lorenz, V., Kurszlaukis, S. 2007. Root zone processes in the phreatomagmatic pipe emplacement model and consequences for the evolution of maar-diatreme volcanoes. Journal of Volcanology and Geothermal Research 159, 4-32.

Lorenz, V., Zimanowski, B., Buettner, R. 1999. Discussion on the formation of kimberlite pipes: the phreatomagmatic model. IAVCEI-CEV Newsletter: 11-17 September 1999. Flagstaff, Arizona.

Lorenz, V., Zimanowski, B., Buettner, R. 2002. On the formation of deep-seated subterranean peperite-like magma-sediment mixtures. Journal of Volcanology and Geothermal Research 114, 107-118.

Marquez, A., De Ignacio, C. 2002. Mineralogical and geochemical constraints for the origin and evolution of magmas in Sierra Chichinautzin, Central Mexican Volcanic Belt. Lithos 62, 35-62.

Marquez, A., Verma, S.P., Anguita, F., Oyarzun, R., Brandle, J.L. 1999. Tectonics and volcanism of Sierra Chichinautzin: extension at the front of the Central Trans-Mexican Volcanic belt. Journal of Volcanology and Geothermal Research 93, 125-150.

Marshall, A., Connor, C., Kruse, S., Malservisi, R., Richardson, J., Courtland, L., Connor, L., Wilson, J., Karegar, M.A. 2015. Subsurface structure of a maar-diatreme and associated tuff ring from a high-resolution geophysical survey, Rattlesnake Crater, Arizona. Journal of Volcanology and Geothermal Research 304, 253-264.

Marti, J., Mitjavila, J., Roca, E., Aparicio, A. 1992. Cenozoic magmatism of the Valencia through (western Mediterranean): relationship between structural evolution and volcanism. Tectonophysics 203, 145-165.

Martin, U., Németh, K. 2002a. Magma-wet sediment interaction in a crater lake of a tuff ring, developed in a pyroclastic mound dammed valley: Kissomlyo Volcano (Western Hungary). In: White, J.D.L. (Ed.). American Geophysical Union Chapman Conference on Explosive Subaqueous Volcanism, 21-25 January 2002. University of Otago, p. 37.

Martin, U., Németh, K. 2002b. Interaction between lava lakes and pyroclastic sequences in phreatomagmatic volcanoes: Halap and Badacsony, Western Hungary. Geologica Carpathica 53.

Martin, U., Németh, K. 2004. Mio/Pliocene phreatomagmatic volcanism in the Western Pannonian Basin. Geologica Hungarica 26.

Martin, U., Németh, K. 2005. Eruptive and depositional history of a Pliocene tuff ring that developed in a fluvio-lacustrine basin: Kissomlyo Volcano (Western Hungary). Journal of Volcanology and Geothermal Research 147, 342-356.

Martin, U., Németh, K. 2007. Blocky versus fluidal peperite textures developed in volcanic conduits, vents and crater lakes of phreatomagmatic volcanoes in Mio/Pliocene volcanic fields of Western Hungary. Journal of Volcanology and Geothermal Research 159, 164-178.

Mastin, L.G. 2007. Generation of fine hydromagmatic ash by growth and disintegration of glassy rinds. Journal of Geophysical Research 112, B02203.

Mastin, L.G., Spieler, O., Downey, W.S. 2009. An experimental study of hydromagmatic fragmentation through energetic, non-explosive magma-water mixing. Journal of Volcanology and Geothermal Research 180, 161-170.

Mattsson, H.B., Tripoli, B.A. 2011. Depositional characteristics and volcanic landforms in the Lake Natron-Engaruka monogenetic volcanic field, northern Tanzania. Journal of Volcanology and Geothermal Research 203(1-2), 23-34.

McBirney, A.R. 1963. Factors governing the nature of submarine volcanism. Bulletin of Volcanology 26, 455-469.

McClintock, M.K., White, J.D.L. 2002. Granulation of weak rock as a precursor to peperite formation: coal peperite, Coombs Hills, Antarctica. Journal of Volcanology and Geothermal Research 114, 205-217.

Mertes, H., Schminke, H-U. 1983. Age distribution of volcanoes in the West-Eifel. Neues Jarhbuch für Geologie und Paläontologie – Abhandlungen 166, 260-283.

Morrissey, M., Zimanowski, B., Wohletz, K., Buettner, R. 2000. Phreatomagmatic fragmentation. In: Sigurdsson, H. (Ed.). Encyclopaedia of Volcanoes. New York: Elsevier. pp. 331-343.

Mortimer, N., Rattenbury, M.S., King, P.R., Bland, K.J., Barrell, D.J.A., Bache, F., Begg, J.G., Campbell, H.J., Cox, S.C., Crampton, J.S., Edbrooke, S.W., Forsyth, P.J., Johnston, M.R., Jongens, R., Lee, J.M., Leonard, G.S., Raine, J.I., Skinner, D.N.B., Timm, C., Townsend, D.B., Tulloch, A.J., Turnbull, I.M., Turnbull, R.E. 2014. High-level stratigraphic scheme for New Zealand rocks. New Zealand Journal of Geology and Geophysics 57(4), 402-419.

Mundula, F., Cioni, R., Funedda, A., Leone, F. 2013. Lithofacies characteristics of diatreme deposits: Examples from a basaltic volcanic field of SW Sardinia (Italy). Journal of Volcanology and Geothermal Research 255, 1-14.

Murcia, H., Németh, K., El-Masry, N.N., Lindsay, J.M., Moufti, M.R.H., Wameyo, P., Cronin, S.J., Smith, I.E.M., Kereszturi, G. 2015. The Al-Du'aythah volcanic cones, Al-Madinah City: implications for volcanic hazards in northern Harrat Rahat, Kingdom of Saudi Arabia. Bulletin of Volcanology 77, 54.

Nalin, R., Nelson, C.S., Basso, D., Massari, F. 2008. Rhodolith-bearing limestones as transgressive marker beds: fossil and modern examples from North Island, New Zealand. Sedimentology 55(2), 249-274.

Namiki, A., Manga, M. 2008. Transition between fragmentation and permeable outgassing of low viscosity magmas. Journal of Volcanology and Geothermal Research 169, 48-60.

Németh, K. 2010. Mongenetic volcanic fields: Origin, sedimentary record, and relationship with polygenetic volcanism. The Geological Society of America Special Paper, 470, 43-66.

Németh, K., Cronin, S.J., Smith, I.E.M., Agustin-Flores, J. 2012. Amplified hazard of small-volume monogenetic eruptions due to environmental controls, Orakei Basin, Auckland Volcanic Field, New Zealand. Bulletin of Volcanology 74, 2121-2137.

Németh, K., Goth, K., Martin, U., Csillag, G., Suhr, P. 2008. Reconstructing paleoenvironment, eruption mechanism and paleomorphology of the Pliocene Pula maar, (Hungary). Journal of Volcanology and Geothermal Research 177, 441-456.

Németh, K., Kereszturi, G. 2015. Monogenetic volcanism: personal views and discussion. International Journal of Earth Sciences 104, 2131-2146.

Németh, K., Martin, U. 2007. Shallow sill and dyke complex in western Hungary as a possible feeding system of phreatomagmatic volcanoes in "soft-rock" environment. Journal of Volcanology and Geothermal Research 159, 138-152.

Németh, K., Martin, U., Csillag, C. 2007. Pitfalls in erosion level calculation based on remnants of maar and diatreme volcanoes. Geomorphologie: relief, processus, environnement 2007(3).

Németh, K., Martin, U., Harangi, Sz. 2001. Miocene phreatomagmatic volcanism at Tihany (Pannonian Basin, Hungary). Journal of Volcanology and Geothermal Research 111, 111-135.

Németh, K., White, C.M. 2009. Intra-vent peperites related to the phreatomagmatic 71 Gulch Volcano, western Snake River Plain volcanic field, Idaho (USA). Journal of Volcanology and Geothermal Research 183, 30-41.

Parker, A.J., Rickwood, P.C., Tucker, D.H. (Eds). 1990. Mafic dykes and emplacement mechanisms. International Geological Correlation Program Project 257, Publication Number 23.

Peckover, R.S., Buchanan, D.J., Ashby, D.E.T.F. 1973. Fuel-coolant interactions in submarine volcanism. Nature 245, 307-308.

Purser, B.H. 1961. Geology of the Port Waikato Region – Onewhero Sheet N51. New Zealand Geological Survey Bulletin 69.

Qiu, T., Wu, X.L., Jin, F.Y., Huang, A.P., Chu, P.K. 2007. Self-assembled growth of MgO nanosheet arrays via a micro-arc oxidation technique. Applied Surface Science 253(8), 3987-3990.

Rafferty, W.J., Heming, R.F. 1979. Quaternary Alkalic and Sub-Alkalic Volcanism in South Auckland, New Zealand. Contributions to Mineralogy and Petrology 71, 139-150.

Re, G., White, J.D.L., Ort, M.H. 2015. Dikes, sills, and stress-regime evolution during emplacement of the Jagged Rocks Complex, Hopi Buttes Volcanic Field, Navajo Nation, USA. Journal of Volcanology and Geothermal Research 295, 65-79.

Rittman, A. 1960. Vulkane und ihre Tatigkeit. Stuttgart: Enke.

Rivalta, E., Taisne, B., Bunger, A.P., Katz, R.F. 2015. A review of mechanical models of dike propagation: Schools of thought, results and future directions. Tectonophysics 638, 1-42.

Ross, P-S., White, J.D.L. 2006. Debris jets in continental phreatomagmatic volcanoes: A field study of their subterranean deposits in the Coombs Hills vent complex, Antarctica. Journal of Volcanology and Geothermal Research 149, 62-84.

Ross, P-S., White, J.D.L. 2012. Quantification of vesicle characteristics in some diatreme-filling deposits, and the explosivity levels of magma-water interactions within diatremes. Journal of Volcanology and Geothermal Research 245-246, 55-67.

Ross, P-S., White, J.D.L., Valentine, G.A., Taddeucci, J., Sonder, I., Andrews, R.G. 2013. Experimental birth of a maar-diatreme volcano. Journal of volcanology and Geothermal Research 260, 1-12.

Ross, P-S., White, J.D.L., Zimanowski, B., Buttner, R. 2008. Multiphase flow above explosion sites in debris-filled volcanic vents: Insights from analogue experiments. Journal of Volcanology and Geothermal Research 178, 104-112.

Ross., P-S., Delpit, S., Haller, M.J., Németh, K., Corbella, H. 2011. Influence of the substrate on maar-diatreme volcanoes – An example of a mixed setting from the Pali Aike volcanic field, Argentina. Journal of Volcanology and Geothermal Research 201, 253-271.

Rubin, A. 1993. Dikes vs. diapirs in viscoelastic rocks. Earth and Planetary Science Letters 19, 641-659.

Runge, M.G., Bebbington, M.S., Cronin, S.J., Lindsay, J.M., Kenedi, C.L., Moufti, M.R.H. 2014. Vents to events: determining an eruption event record from volcanic vent structures for the Harrat Rahat, Saudi Arabia. Bulletin of Volcanology 76, 1-16.

Sanchez, M.C., Sarrionandia, F., Juteau, T., Ibarguchi, J.I.G. 2012. Structure and organization of submarine basaltic flows: sheet flow transformation into pillow lavas in shallow submarine environments. International Journal of Earth Sciences (Geologische Rundschau) 101, 2201-2214.

Schipper, C.I., Sonder, I, Schmid, A., White, J.D.L., Durig, T., Zimanowski, B., Buettner, R. 2013. Vapour dynamics during magma-water interaction experiments: hydromagmatic origins of submarine volcaniclastic particles (limu o Pele). Geophysical Journal International 192, 1109-1115.

Schipper, C.I., White, J.D.L., Zimanowski, B., Buettner, R., Sonder, I., Schmid, A. 2011. Experimental interaction of magma and "dirty" coolants. Earth and Planetary Science Letters 303, 323-336.

Schminke, H-U. 2004. Volcanism. Berlin: Springer-Verlag.

Schminke, H-U. 2007. The Quaternary volcanic fields of the East and West Eifel (Germany). In: Ritter, J.R., Christensen, U.R. (Eds.). Mantle Plumes 24. Springer, Berlin Heidelberg (241-322 pp.).

Schminke, H-U., Lorenz, V., Seck, H.A. 1983. The Quaternary Eifel volcanic fields. In: Fuchs, et al. (Ed.). Plateau Uplift. The Rhenish Shield – A Case History. Berlin: Springer. pp. 139-151.

Schminke, H-U., Robinson, P.T., Ohmacht, W., Flower, M.F.J. 1978. Basaltic hyaloclastites from hole 396B, DSDP Leg 46. Initial Report: Deep Sea Drilling Project 46, 341-355.

Seghedi, I., Maicher, D., Kurszlaukis, S. 2009. Volcanology of Tuzo pipe (Gacho Kue cluster) – Root-diatreme processes re-interpreted. Lithos 1125, 553-565.

Self, S., Kienle, J., Huot, J-P. 1980. Ukinrek maars, Alaska, II. Deposits and formation of the 1977 craters. Journal of Volcanology and Geothermal Research 7, 39-65.

Shane, P. 2012. The evolution of basaltic volcanism in Northland in space and time. EQC research paper number 4612. Available from http://www.eqc.govt.nz/research/research-papers/evolutiion-basaltic-volcanism-northland-space-time

Shane, P., Gehrels, M., Zawalna-Geer, A., Augustinus, P., Lindsay, J., Chaillou, I. 2013. Longevity of a small shield volcano revealed by crypto-tephra studies (Rangitoto volcano, New Zealand): Change in eruptive behaviour of a basaltic field. Journal of Volcanology and Geothermal Research 257, 174-183.

Shane, P., Sandiford, A. 2003. Paleovegetation of Marine Isotope Stage 4 and 3 in Northern New Zealand and the age of the widespread Rotoehu tephra. Quaternary Research 59, 420-429.

Sheridan, M.F., Wohletz, K.H. 1983. Hydrovolcanism: Basic considerations and review. Journal of Volcanology and Geothermal Research 17, 1-29.

Skilling, I.P., White, J.D.L., McPhie, J. 2002. Peperite: a review of magma-sediment mingling. Journal of Volcanology and Geothermal Research 114, 1-17.

Smith, D. 2010. Antigorite peridotite, metaserpentinite, and other inclusions within diatremes on the Colorado Plateau, SW USA: Implications for the mantle wedge during low-angle subduction. Journal of Petrology 51(6), 1355-1379.

Smith, I.A.E., Okada, T., Itaya, T., Black, P.M. 1993. Age relationships and tectonic implications of late Cenozoic basaltic volcanism in Northland, New Zealand. New Zealand Journal of Geology and Geophysics 36, 385-393.

Smith, T.L., Batiza, R. 1989. New field and laboratory evidence for the origin of hyaloclastite flows on seamount summits. Bulletin of Volcanology 51, 96-114.

Son, M., Kim, J.S., Jung, S, Ki, J.S., Kim, M-C., Sohn, Y.K. 2012. Tectonically controlled vent migration during maar-diatreme formation: An example from a Miocene half-graben basin in SE Korea. Journal of Volcanology and Geothermal Research 223-224, 29-46

Sparks, R.S.J. 1978. The dynamics of bubble formation and growth in magmas: a review and analysis. Journal of Volcanology and Geothermal Research 3, 1-37.

Sparks, R.S.J., Brown, R.J., Field, M., Gilbertson, M. 2007. Kimberlite ascent and eruption. Nature 450, E21.

Sparks, R.S.J., Pinkerton, H., Macdonald, R. 1977. The transport of xenoliths in magma. Earth and Planetary Science Letters 35, 234-238.

Spratt, P.R. 1975. The Ngatutura Colcanics, Southwest Auckland. Journal of the Royal Society of New Zealand 5(2), 163-178.

Staudigel, H., Schminke, H-U. 1984. The Pliocene seamount series of La Palma/Canary Islands. Journal of Geophysical Research 89, 11 195-11 215.

Stipp, J.J. 1968. The Geochronology and petrogenesis of the Cenozoic volcanics of North Island, New Zealand. Unpublished PhD Thesis, Australian National University, Canberra.

Stoppa, F. 1996. The San Venanzo maar and tuff ring, Umbria, Italy: eruptive behaviour of a carbonatite-melilitite volcano. Bulletin of Volcanology 57, 563-577.

Suiting, I., Schminke, H-U. 2009. Internal vs. external forcing in shallow marine diatreme formation: A case study from the Iblean Mountains (SE-Sicily, Central Mediterranean). Journal of Volcanology and Geothermal Research 186, 361-378.

Sweeney, M., R., Valentine, G.A. 2015. Transport and mixing dynamics from explosions in debris-filled volcanic conduits: Numerical results and implications for maar-diatreme volcanoes. Earth and Planetary Science Letters 425, 64-76.

Tchamabe, B.C., Ohba, T., Kereszturi, G., Németh, K., Aka, F.T., Youmen, D., Issa, Miyabuchi, Y., Ooki, S., Tanyileke, G., Hell, J.V. 2015. Towards the reconstruction of the shallow plumbing system of the Barombi Mbo Maar (Cameroon) Implications for diatreme growth processes of a polygenetic maar volcano. Journal of Volcanology and Geothermal Research 301, 293-313.

Thordarson, T., Self, S. 1993. The Laki (Skaftar-Fires) and Grimsvotn eruptions in 1783-1785. Bulletin of Volcanology 55(4), 233-263.

Trigila, R., Battaglia, M., Manga, M. 2007. An experimental facility for investigating hydromagmatic eruptions at high-pressure and high-temperature with application to the importance of magma porosity for magma-water interaction. Bulletin of Volcanology 69, 365-372.

Utting, A.J. 1986. The petrology and geochemistry of the Ngatutura Basalts. Unpublished M.Sc. thesis, lodged in the Library, University of Waikato, Hamilton.

Valentine, G.A. 2012. Shallow plumbing systems for small-volume basaltic volcanoes, 2: Evidence from crustal xenoliths at scoria cones and maars. Journal of Volcanology and Geothermal Research 223-224, 47-63.

Valentine, G.A., Cortés, J.A. 2013. Time and space variations in magmatic and phreatomagmatic eruptive processes at Easy Chair (Lunar Crater Volcanic Field, Nevada, USA). Bulletin of Volcanology 75, 752.

Valentine, G.A., Graettinger, A, H., Macorps, E., Ross, P-S., White, J.D.L., Dohring, E., Sonder, I. 2015. Experiments with vertically and laterally migrating subsurface explosions with applications to the geology of phreatomagmatic and hydrothermal explosion craters and diatremes. Bulletin of Volcanology 77, 15.

Valentine, G.A., Gregg, T.K.P. 2008. Continental basaltic volcanoes – Processes and problems. Journal of Volcanology and Geothermal Research 177, 857-873

Valentine, G.A., Groves, K.R. 1996. Entrainment of country rock during basaltic eruptions of the Lucero Volcanic Field, New Mexico. Journal of Geology 104, 71-90.

Valentine, G.A., Sottili, G., Palladino, D.M., Taddeucci, J. 2015. Tephra ring interpretation in light of evolving maar-diatreme concepts: Stracciacappa maar (central Italy). Journal of Volcanology and Geothermal Research 308, 19-29.

Valentine, G.A., van Wyk de Vries, B. 2014. Unconventional maar-diatreme and associated intrusions in the soft sediment-hosted Mardoux structure (Gergovie, France). Bulletin of Volcanology 76, 807.

Valentine, G.A., White J.D.L. 2012. Revised conceptual model for maar-diatremes: Subsurface processes, energetics, and eruptive products. Geology 2012.

Valentine, G.A., White, J.D.L., Ross, P-S., Amin, J., Taddeucci, J., Sonder, I., Johnson, P.J. 2012. Experimental craters formed by a single and multiple buried explosions and implications for volcanic craters with emphasis on maars. Geophysical Research Letters 39.

Van Otterloo, J., Cas, R.A.F., Scutter, C.R. 2015. The fracture behaviour of volcanic glass and relevance to quench fragmentation during formation of hyaloclastite and phreatomagmatism. Earth Science Reviews 151, 79-116.

Waichel, B.L., de Lima, E.F., Sommer, C.A., Lubachesky, R. 2007. Peperite formed by lava flows over sediments: An example from the central Parana Continental Flood Basalts, Brazil. Journal of Volcanology and Geothermal Research 159, 343-354.

Walker, G.P.L. 1973. Explosive volcanic eruptions – a new classification scheme. Geologische Rundschau 62(2), 431-446.

Walker, G.P.L. 1993. Basaltic-volcano systems. Geological Society of London Special Publication 76, 3-38.

Walker, G.P.L. 2000. Basaltic volcanoes and volcanic systems. In: Sigurdsson, H., Houghton, B.F., McNutt, S.R., Rymer, H, Stix, J. (Eds.). Encyclopaedia of Volcanoes. San Diego: Academic Press, 283-290.

Walker, G.P.L., Croasdale, R. 1972. Characteristics of some basaltic pyroclasts. Bulletin of Volcanology 35, 303-312.

White, J.D.L. 1991. Maar-diatreme phreatomagmatism at Hopi Buttes, Navajo Nation (Arizona), USA. Bulletin of Volcanology 53, 239-258.

White, J.D.L. 1996. Impure coolants and interaction dynamics of phreatomagmatic eruptions. Journal of Volcanology and Geothermal Research 74, 155-170.

White, J.D.L., Busby-Spera, C.J. 1987. Deep marine arc deposits and syndepositional magmatism in the Alisitos group at Punta Cono, Baja California, Mexico. Sedimentology 34, 911-927.

White, J.D.L., McPhie, J., Skilling, I. 2000. Peperite: a useful genetic term. Bulletin of Volcanology 62, 65-66.

White, J.D.L., Ross, P-S. 2011. Maar-diatreme volcanoes: A review. Journal of Volcanology and Geothermal Research 201, 1-29.

White, P.J., Waterhouse, B.C. 1993. Lithostratigraphy of the Te Kuiti Group: A revision. New Zealand Journal of Geology and Geophysics 36(2), 255-266.

Wohletz, K.H. 1983. Mechanisms of hydrovolcanic pyroclast formation: Grain-size, scanning electron microscopy, and experimental studies. Journal of Volcanology and Geothermal Research 17, 31-63.

Yalcin, H., Bozkaya, O. 1995. Sepiolite-palygorskite from the Hekimhan Region (Turkey). Clays and Clay Minerals 43(6), 705-717.

Zimanowski, B., Buettner, R. 2002. Dynamic mingling of magma and liquefied sediments. In: Skilling, I.P., White, J.D.L., McPhie, J. (Eds). Peperite: Processes and products of magma-sediment mingling. Journal of Volcanology and Geothermal Research 114, 37-44.

Zimanowski, B., Buettner, R., Lorenz, V. 1997. Premixing of magma and water in MFCI experiments. Bulletin of Volcanology 58, 491-495.

Zimanowski, B., Buettner, R., Lorenz, V., Hafele, H-G. 1997. Fragmentation of basaltic melt in the course of explosive volcanism. Journal of Geophysical Research 102(B1), 803-814.

Zimanwoski, B., Froehlich, G., Lorenz, V. 1991. Quantitative experiments on phreatomagmatic eruptions. Journal of Volcanology and Geothermal Research 48, 341-358.